PL-TR-91-2117

IONOSPHERIC AND MAGNETOSPHERIC PROCESSES

Tom Chang

Massachusetts Institute of Technology
Center for Space Research
Cambridge, MA 02139

17 May 1991

Final Report
28 February 1986-28 February 1991

APPROVED FOR PUBLIC RELEASE; DISTRIBUTION UNLIMITED

PHILLIPS LABORATORY
AIR FORCE SYSTEMS COMMAND
HANSCOM AIR FORCE BASE, MASSACHUSETTS 01731-5000

This technical report has been reviewed and is approved for publication.

(Signature)
BAMANDAS BASU
Contract Manager

(Signature)
DAVID N. ANDERSON
Branch Chief

(Signature)
ROBERT A. SKRIVANEK
Division Director

This document has been reviewed by the ESD Public Affairs Office (PA) and is releasable to the National Technical Information Service (NTIS).

Qualified requestors may obtain additional copies from the Defense Technical Information Center. All others should apply to the National Technical Information Service.

If your address has changed, or if you wish to be removed from the mailing list, or if the addressee is no longer employed by your organization, please notify PL/IMA, Hanscom AFB, MA 01731-5000. This will assist us in maintaining a current mailing list.

Do not return copies of this report unless contractual obligations or notices on a specific document requires that it be returned.

REPORT DOCUMENTATION PAGE

1a. REPORT SECURITY CLASSIFICATION UNCLASSIFIED	1b. RESTRICTIVE MARKINGS N/A
2a. SECURITY CLASSIFICATION AUTHORITY N/A	3. DISTRIBUTION/AVAILABILITY OF REPORT APPROVED FOR PUBLIC RELEASE: UNLIMITED DISTRIBUTION
2b. DECLASSIFICATION/DOWNGRADING SCHEDULE N/A	
4. PERFORMING ORGANIZATION REPORT NUMBER(S)	5. MONITORING ORGANIZATION REPORT NUMBER(S) PL-TR-91-2117
6a. NAME OF PERFORMING ORGANIZATION Massachusetts Institute of Technology 6b. OFFICE SYMBOL (If applicable)	7a. NAME OF MONITORING ORGANIZATION Phillips Laboratory
6c. ADDRESS (City, State, and ZIP Code) Cambridge, MA 02139	7b. ADDRESS (City, State, and ZIP Code) Hanscom AFB, MA 01731-5000
8a. NAME OF FUNDING/SPONSORING ORGANIZATION 8b. OFFICE SYMBOL (If applicable)	9. PROCUREMENT INSTRUMENT IDENTIFICATION NUMBER F19628-86-K-0005
8c. ADDRESS (City, State, and ZIP Code)	10. SOURCE OF FUNDING NUMBERS

PROGRAM ELEMENT NO.	PROJECT NO.	TASK NO.	WORK UNIT ACCESSION NO
61102F	2310	G6	DA

11. TITLE (Include Security Classification)

Ionospheric and Magnetospheric Processes (unclassified)

12. PERSONAL AUTHOR(S)

Tom Chang

13a. TYPE OF REPORT	13b. TIME COVERED	14. DATE OF REPORT (Year, Month, Day)	15. PAGE COUNT
Final	FROM 2/28/86 TO 2/28/91	5/17/91	108

16. SUPPLEMENTARY NOTATION

17. COSATI CODES			18. SUBJECT TERMS (Continue on reverse if necessary and identify by block number)
FIELD	GROUP	SUB-GROUP	Ion Conics, beam-plasma interactions, turbulent heating, counterstreaming electrons, auroral zone

19. ABSTRACT (Continue on reverse if necessary and identify by block number)

Results of a five-year study of a variety of kinetic plasma processes in the ionosphere and magnetosphere are described. Specific topics discussed in detail include: (1) The formation of ion conics due to electromagnetic ion cyclotron and/or lower hybrid turbulence. (2) Auroral beam-plasma interactions and VLF turbulence. (3) Heating of charged particles in the ionosphere and magnetosphere due to strong plasma turbulence. (4) Formation of counterstreaming electron distributions along auroral field lines. and (5) Double layer formation along discrete auroral field lines. A complete listing of published papers and books during the years 1986-1991 are also included.

20. DISTRIBUTION/AVAILABILITY OF ABSTRACT ☐ UNCLASSIFIED/UNLIMITED ☒ SAME AS RPT ☐ DTIC USERS	21. ABSTRACT SECURITY CLASSIFICATION unclassified
22a. NAME OF RESPONSIBLE INDIVIDUAL Bamandas Basu	22b. TELEPHONE (Include Area Code) 617 377-5121 22c. OFFICE SYMBOL PL/LIS

TABLE OF CONTENTS

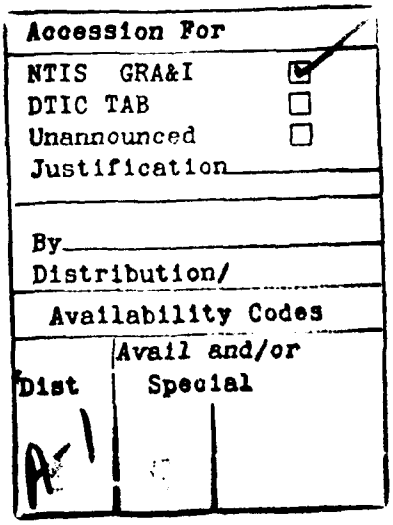

1. SYNOPSIS OF CONTRACT ACTIVITIES

During the past five contract years, we have completed all the milestones outlined in our original program. These include the study of (i) the generation of ion conics of ionospheric origin, (ii) nonlinear wave propagations resulting from auroral electron beam-plasma interactions, (iii) turbulent heating of charged particles in the ionosphere and magnetosphere due to wave-particle interactions, and (iv) the evolution of counterstreaming electrons in the auroral zone.

During this contract period, we published a total of 30 scientific papers addressing the various states of plasma turbulence and associated stochastic heating processes of charged particles in the geoplasma environment. Members of the MIT group engaged in the research of ionospheric-magnetospheric processes have been invited by numerous international/national conferences and scientific institutions to deliver invited and review lectures on the scientific findings contained in these papers.

The close proximity between MIT and the Geophysics Directorate, Phillips Laboratory, USAF has allowed direct personal exchanges and collaborations in several interesting research interactions. These included visits by and discussions with Drs. J.R. Jasperse, J.M. Retterer, M. Heinemann, Su. Basu and others. In addition, our research efforts have been enhanced considerably by periodic visits of a number of established scholars across the nation and from abroad. Our contributions in the study of the turbulence and heating processes in the ionosphere and magnetosphere were particularly influenced by Professor Paul Kintner of the Cornell University, Drs. William Peterson and Dave Klumpar of the Lockheed Palo Alto Research Laboratory, Dr. Mats Andre of the Swedish Space Institute, Dr. Hannu Koskinen of the Finish Meteorlogical Institute, Dr. Dave Winningham of the Southwest Research Institute, Dr. Roger Arnoldy of the University of New Hampshire, Dr. Noah Hershkowitz of the University of

Wisconsin, Dr. C.T. Dum of the Max-Planck Institute in Extraterrestrial Physics, and Dr. Don Gurnett of the University of Iowa.

Five scientific symposia on the "Physics of Space Plasmas", four Cambridge Workshops on various topics of geoplasma physics, and a Chapman Conference on Ion Acceleration in the Ionosphere and Magnetosphere were organized during the period. These activities resulted in the publication of six books based on the scientific presentations at these conferences.

The content of this report is organized as follows. In Sections 2-5, we discuss in detail the major contributions of our research activities. In Section 6, a complete listing of the scientific publications of the MIT group during the past five years is provided. A listing of the titles of the books of the published proceedings is given in Section 7.

2. PARTICLE ACCELERATION BY ELECTROMAGNETIC ION CYCLOTRON TURBULENCE

G. B. Crew and Tom Chang
MIT Center for Space Research, Cambridge, MA 02139

ABSTRACT

Low frequency electromagnetic turbulence is proving to be an important source of energy for the acceleration of ions in various regions of the Earth's magnetosphere. In particular it has been shown to account for some of the energetic oxygen conics found in the auroral regions, and a convincing case is being built for its role in the cusp/cleft region of the magnetosphere. The transfer of energy from the waves to the particles is efficiently accomplished through ion cyclotron resonance with the left-hand polarized component of the turbulence, and the result of the interaction is a heating of the particle distribution. In this tutorial review, we shall present a general theoretical treatment of ion cyclotron resonance heating in a weakly inhomogeneous magnetic geometry and then proceed to examine the formation of auroral ion conics in somewhat greater detail. For the auroral case, the properties of the electric field spectral density and the Earth's dipolar magnetic field allow the introduction of a similarity transformation which results in a considerable simplification of the analysis for the altitude-asymptotic form of the conic distribution. The merit of this approach is that it makes it possible to directly compare the theory with observations, and the agreement is found to be excellent.

I. INTRODUCTION

This is a tutorial review of the theoretical progress that has been made towards an understanding of the energetic ion populations found within the Earth's ionosphere–magnetosphere system which are generically referred to as ion conics. In fact, there is such a wide variety of ion conic observations as well as viable theoretical mechanisms to explain them that it is not possible to do them justice within the bounds of an hour's talk or an article of this length. Thus we shall here restrict our attention to a class of these phenomena where the energization in accomplished through an ion cyclotron resonance interaction with electromagnetic plasma turbulence.

We are concerned, then, with a resonant wave–particle interaction which results in a real heating of the ion population, which we term an ion cyclotron resonance heated conic, or simply ICRH conic for short. Such distributions are termed conics because of the distribution of ions in their velocity space: loosely speaking, they lie on a cone whose axis is aligned with the mag. tic field direction. Of course, there are a wide variety of ways in

which the ions may be so distributed, accounting for the veritable zoo of conic observations. By the same token any theory which purports to explain the formation of conics will produce some characteristic form for the velocity distribution. The point of the term ICRH conic is that these are events where theory and observation appear to be talking about the same thing, namely, a conic due to ion cyclotron resonance heating, and the term is used to distinguish such events from others which must have some other explanation.

Conics were first reported [1] more than a decade ago, and have since been found over a wide range of altitudes within the Earth's auroral zone (see, *e.g.* the observational reviews by Klumpar [2] and Burch [3]). Conics are important because they provide a means for ionospheric ions to escape the Earth's gravitational field and consequently constitute a major component of an ionospheric contribution to magnetospheric plasma [4–8].

They are also interesting to study because the ion energization can be over several orders of magnitude and generally appears to be accomplished through wave–particle interaction or other *bona fide* plasma processes (see, *e.g.* the theoretical reviews by Lysak [9] and Chang *et al.* [10]). Aside from the mechanisms to be discussed in this paper, considerable attention has been directed both towards wave–particle interaction processes as well as other possibilities. The former include interactions with current-driven electrostatic ion cyclotron waves [11–16], and lower hybrid waves [17–21] which are excited by the energetic precipitating auroral electron beam. Another possibility that has received some attention is energization through double layers [22–24].

The present work on energization through interaction with electromagnetic low frequency turbulence was motivated by a conic event [25] which did not seem to have been caused by any of these mechanisms. That is, the required waves were not observed, and the conic was well equatorward of the auroral electron beam/discrete auroral (or boundary plasma sheet) region where they would be expected. Rather, the conic was observed throughout a broad region above the diffuse aurora which maps to the central plasma sheet (CPS) of the magnetosphere [25]. On the other hand, there was an intense background of low frequency electromagnetic turbulence as is commonly observed [26], and Chang *et al.* [27] considered the possibility that ions might be energized in much the same fashion as heating in the ion cyclotron range of frequencies (ICRF) has been used for years in the fusion community. (ICRH has also been shown to be an important mechanism in the Earth's ring current; see *e.g.*, the review by Gendrin [28].) That is, some remote agency would be responsible for the generation of electromagnetic waves which would propagate to lower altitudes and result in the observed ion energization. Indeed, not only did the initial estimates demonstrate the viability of this scenario, but a subsequent numerical simulation [29] found that the mechanism produced a distribution of ions remarkably like the observed conics.

Moreover, the heating mechanism works for other events as well. Additional auroral events [30] have also been shown [31] to be explicable as ICRH conics. There are also conic events in the cusp/cleft where ICRF heating is probably responsible for the observed energization of ions [32–34]. In view of these exciting developments, this seems an appropriate time to review our understanding of the subject and look to future discoveries.

We begin in the next section with a primer on the conic formation process in general and describe the basic components which make an ICRH conic in particular. Section III describes a number of theoretical techniques that have been brought to bear on this problem and describes the type of results obtained. These results are then compared with the experimental observations, leading into a brief discussion which concludes the paper.

II. CONIC FORMATION PRIMER

It is clear that there are many ways to make a conic. To discuss the conic formation process in its most general terms, we offer Fig. 1, which schematically indicates the various components which may play a role. At the bottom of the diagram we have indicated a source population of cold ions. These are the raw materials for the conic: typically an ambient, cold, isotropic Maxwellian plasma with temperatures of at most a few eV. Under the influence of various agents, this population will evolve through space and time to eventually be observed as an energetic conic population broadly characterized by an energy of tens to thousands of eV, a perpendicular temperature in excess of parallel temperature, and of course a conic-like pitch angle distribution.

This evolution is controlled by two types of interactions: *e.g.*, wave–particle interactions which are responsible for the energization or heating of the ion population, and adiabatic interactions which rearrange the ions in their phase space in various ways, but neither add nor remove energy. We have already mentioned several wave–particle interaction processes in the Introduction; the adiabatic forces include effects due to the geomagnetic field and the large-scale DC electric fields found in the magnetosphere. The relative contributions of these two types of interactions, together with the underlying geometry, determine the morphology of the conic which is ultimately observed. The wide variety of conic observations is largely due to the details lying behind Fig. 1.

Aside from questions concerning these two classes of interactions are questions that are in some sense secondary concerning the origin of the wave turbulence or the adiabatic forces. For the former, this can include the identification of a free energy source, the manner of its transformation into wave activity, and its possible propagation to the region of the wave–particle interactic There can also be troublesome questions of self-consistency when one extends the analysis beyond the simple linear instability phase.

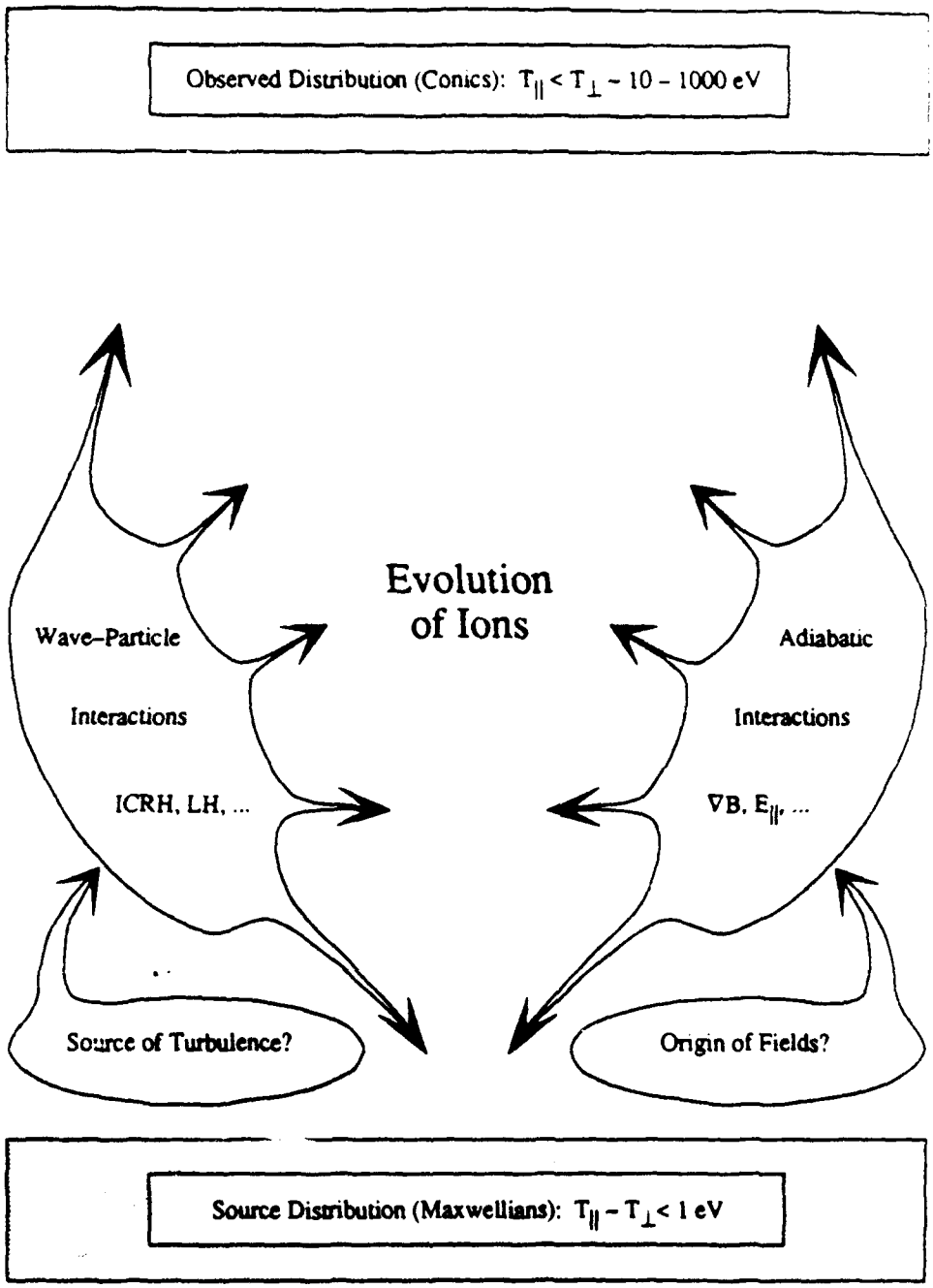

Figure 1. A schematic diagram of the conic formation process whereby low energy ionospheric plasma is energized through wave particle interactions to magnetospheric energetics. The variety of conic formed is determined by both the type of wave turbulence participating, as well as the various adiabatic forces which also may play a role.

Some progress has been made on this question for the ICRH conics: a plausible origin for the wave turbulence has been identified in the anisotropy of the particle distributions in the ring current [35, 36]. The waves then propagate to lower altitudes where they interact with the ions to form conics.

The adiabatic forces are usually determined by the placement of the conic formation process within some larger setting: the Earth's dipolar magnetic geometry and the large-scale potentials of the auroral acceleration region and the polar cap are determined by processes which are indifferent to conics. In either case these secondary questions go considerably beyond the scope of this tutorial, so we shall not discuss them further.

A. Basic Physical Ingredients

1. Heating Rate. The first process to consider is the process responsible for the energization and heating of the conic. For ICRH conics this is, of course, the ion cyclotron resonance heating mechanism which we illustrate schematically in Fig. 2. Each ion of charge q and mass m_i finds itself adrift in a sea of low frequency electromagnetic turbulence. In general, this includes activity spanning a broad frequency range which at each frequency may be decomposed into three separate polarizations (left hand, right hand, and parallel to **B**). To most of this activity, the ion is oblivious. However, the ion is sensitive to components in the left-hand polarization at frequencies near to its cyclotron frequency. To see this, we need only integrate the left-hand components over some band $\Delta\omega$ in the vicinity of the ion cyclotron frequency Ω ($\equiv qB/m_i c$) to obtain an electric field $\mathbf{E}_L(t)$ of some magnitude and polarization, $\mathbf{E}_L(\Omega)(\Delta\omega)^{1/2}$, which for some brief time Δt, rotates at the same rate and in the same sense as the ion. This results in a secular change $\Delta\mathbf{v}_\perp$ in the ion's velocity vector $\mathbf{v}_\perp$ given by

$$m_i \Delta\mathbf{v}_\perp = q\,\mathbf{E}_L(t)\Delta t \ , \tag{1}$$

and a consequent change in perpendicular energy

$$\Delta W_\perp = \frac{1}{2}m_i(\mathbf{v}_\perp + \Delta\mathbf{v}_\perp) - \frac{1}{2}m_i|\mathbf{v}_\perp|^2 = m_i\,\mathbf{v}_\perp\cdot\Delta\mathbf{v}_\perp + \frac{1}{2}m_i|\Delta\mathbf{v}_\perp|^2 \ . \tag{2}$$

Of course for a population of ions, or alternatively for a random sequence of such interactions, the term linear in $\Delta\mathbf{v}_\perp$ averages out; we may use the last term to construct an effective heating rate:

$$\dot{W}_{\perp,res} \equiv \frac{\Delta W_\perp}{\Delta t} = \frac{q^2|\mathbf{E}_L(\Omega)|^2}{2m_i}\Delta\omega\Delta t \ . \tag{3}$$

The interaction time Δt is limited by the coherence time of the electric field spectrum; roughly speaking, $\Delta\omega\Delta t \approx 2\pi$. Thus the heating rate (3) is directly proportional to the electric field spectral energy density evaluated at the local

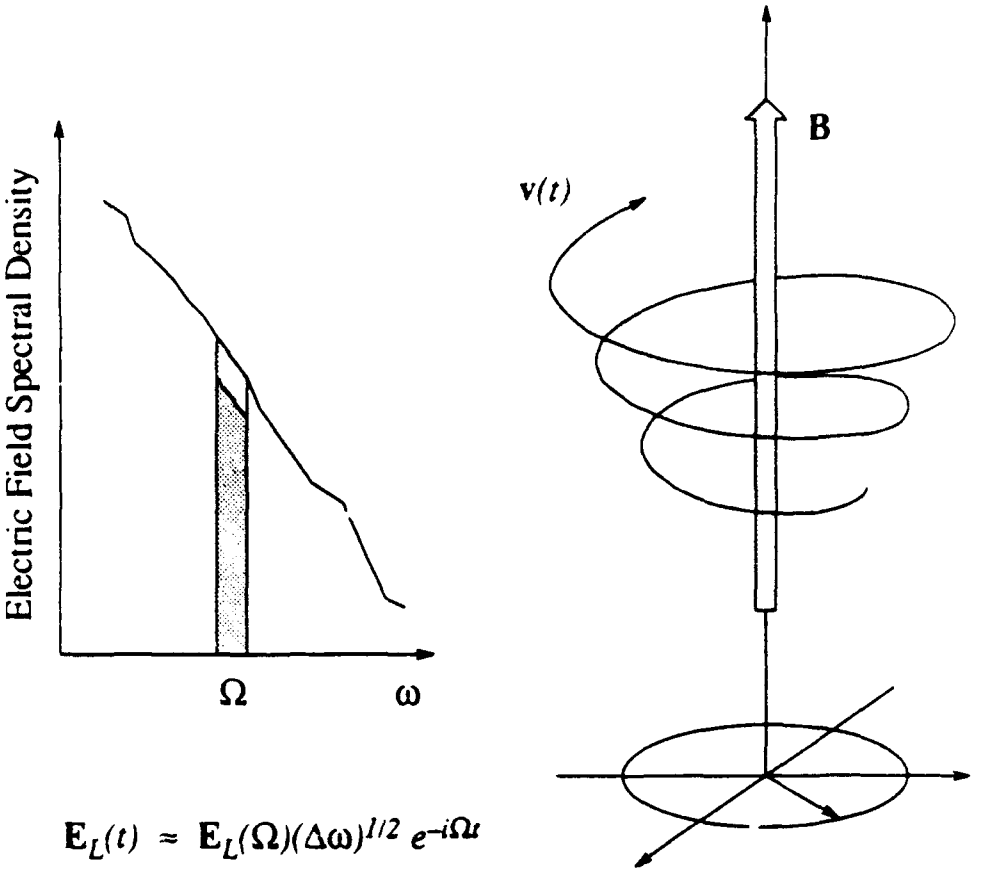

Figure 2. A schematic of the ion cyclotron resonance heating mechanism. The left-hand side of the diagram indicates a power-law spectrum (log scales) of electric field turbulence, a band near the cyclotron frequency Ω (shaded), and a small fraction with which the ions are resonant (shaded darker). This component appears to each ion as an electric field $E_L(t)$ which corotates with each ion and gradually increases its energy.

cyclotron frequency, Ω.

2. Diffusion. The preceding discussion of ICRH is rather heuristic (qualitatively correct; quantitatively inadequate); fortunately, a quantitatively correct description is readily available from the standard kinetic theory of wave–particle interactions. In this context, the interaction is completely described by a diffusion tensor, whose general form for interaction with electromagnetic waves has been worked out in some detail [37, 38]. In the space physics applications which interest us, we do not require such complexity (and indeed, the observational data set is not currently sufficiently complete to

merit it). For long wavelengths ($k_\perp v_\perp$, $k_\parallel v_\parallel \ll \Omega$), a much simpler calculation [39] results in a diffusion operator acting on the distribution function f of the form

$$\mathbf{D}[f] = \frac{1}{v_\perp}\frac{\partial}{\partial v_\perp}\left[v_\perp D_\perp \frac{\partial f}{\partial v_\perp}\right], \tag{4}$$

where

$$D_\perp = (\pi q^2/2m_i^2)\int_0^\infty d\omega\, |E_L|^2(\omega)\, \delta(\omega - k_\parallel v_\parallel - \Omega) \tag{5}$$

is the diffusion coefficient for ions of charge q and mass m_i expressed in terms of the electric field spectral density in left-hand polarized waves, $|E_L|^2$. Here the phase space velocity variable has been decomposed into components $v_\parallel$ and $v_\perp$, parallel and perpendicular to **B**, respectively, and we have retained only the most important term in expression (4).

The Doppler shift $k_\parallel v_\parallel$ in Eq. (5) may usefully be neglected: we have already taken $k_\parallel v_\parallel \ll \Omega$ and for minority species ions there is typically little observed structure in the electric field spectral density near Ω. Thus we may take

$$D_\perp \approx (\pi q^2/2m_i^2)|E_L|^2(\Omega)\,. \tag{6}$$

This results in the considerable simplification of having a velocity-independent diffusion coefficient.

There are a few other comments which should perhaps be made at this point concerning the applicability of formula (6). One is that this diffusion coefficient depends on the spectral density in the proper (*i.e.*, left-hand) polarization, rather than the total observed turbulence. As we shall see below, we must make some accommodation for the fact that the polarization is typically not determined by the observations. On the other hand, the main study of this turbulence [26] did find evidence for a characterization of the turbulence as at least partially electromagnetic, and of indefinite (though at times predominantly right-hand) polarization, implying that some $|E_L|^2$ is present as some fraction of the observed total.

A second point is that formula (6) represents an approximation required in part by our ignorance of many details of the actual wave spectrum. In particular, we are usually almost totally ignorant of the k-spectrum of the turbulence. For the plasma modes under consideration, inclusion of such information should it become available, would most probably result in corrections of at most order unity. That is the main physics and effects we discuss would still transpire, and quantitative results should still be valid to something like a factor of two.

Finally, it is our intention in this work to apply this heating mechanism only to minority species ions. For the high-altitude auroral and cusp regions, this means O^+ and possibly He^+, but probably not H^+ ions. The main reason

is that cold plasma wave theory does not allow waves at the majority species cyclotron frequency to propagate in a left-hand polarization, for precisely the same reasons that we propose such modes for ion heating. That is, such modes do not propagate because there are plenty of ions to resonate with them and sap them of energy. The situation is improved somewhat for minority species ions because they represent less of a drain. In particular, the "stop gap" in propagation is sufficiently narrow that the Doppler shift mentioned above shifts the resonance condition to neighboring, allowed wave modes. Of course, cold plasma theory is only an approximation, as is the infinite and homogeneous geometry it which it is derived. The inclusion of realistic effects change the picture somewhat. And of course, the observations typically show a structureless spectrum near the minority cyclotron frequency, arguing that we are reasonably safe with formula (6).

3. Mirror Force. At the same time that the ions are being heated, they are also subjected to a variety of adiabatic (*i.e.*, independent of heating) forces; the most important of these is usually the mirror force which arises from the Earth's geomagnetic field. One way to understand this force is to consider that in the absence of heating, each ion is constrained in its motion to preserve both its energy $m_i(v_\perp^2 + v_\parallel^2)/2$ and its magnetic moment $m_i v_\perp^2/B$. Thus as an ion drifts upwards toward regions of decreasing magnetic field its $v_\perp$ must decrease with B. However, it can only preserve its energy with a corresponding increase in $v_\parallel$. The result is a conversion of perpendicular energy into parallel energy. In the absence of heating, this would result in an upward moving, field-aligned population at high altitudes. However, if there is heating, the perpendicular energy will be replenished as it is converted into parallel energy—some form of conic distribution of ions then results as a compromise between these two effects. This is illustrated schematically in Fig. 3 which shows a portion of the ion velocity space. The effects of heating (horizontal arrows) and the mirror force (curved arrows) combine to produce a conic (closed contours).

Aside from it role in shaping the form of the ion distribution, the mirror force plays a secondary role which is crucial to the degree of energization which may take place. Since the mirror force accelerates ions along the magnetic field, the ions are induced to travel along the field line to higher altitudes, and most importantly, lower gyrofrequency. This means that cyclotron resonance successively brings the ions into interaction with waves of different frequencies; since each interaction is limited to some brief time Δt, the ions do not appreciably deplete any of the waves they encounter. That is, the feedback of the ions on the waves is an insignificant part of the story, and the process does not saturate in the usual sense of the term. The limits to ion energization are determined instead by geometry and the frequency extent of the spectrum.

4. Electric Fields. A second adiabatic force which can play a role in the conic formation process is large-scale electric fields. For example, in the

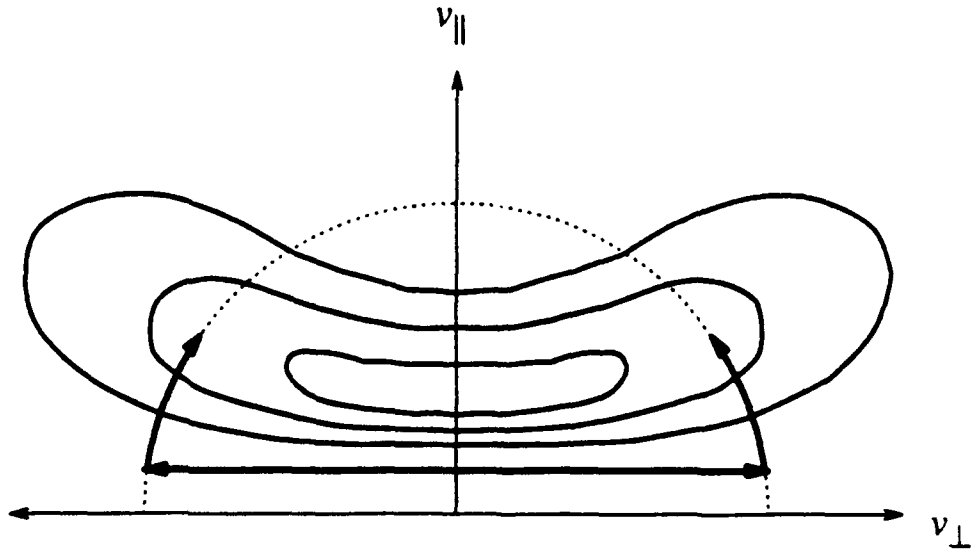

Figure 3. A cartoon to indicate the role played by the mirror force in shaping the conic distribution (closed contours). Ions diffuse to larger $v_{\perp}$ under the influence of the heating mechanism (horizontal arrows). As the ions drift to greater altitudes the mirror force directs ions to larger $v_{\parallel}$ at the expense of $v_{\perp}$ in order to conserve energy; the ions move on curves of constant energy (curved arrows on dotted line).

cusp there is a significant cross polar cap potential leading to a dawn-dusk electric field. In combination with the Earth's magnetic field this leads to a bulk plasma drift, $\mathbf{v}_E \equiv \mathbf{E} \times \mathbf{B}$, which we must include in order to properly follow the ions. No direct energization of ions results from this electric field, however.

Another possibility is the field-aligned potential drop such as is found in the discrete aurora. This results in an electric field $E_{\parallel}$ whose sense is to accelerate ions upward. Indeed, upward-directed ion beams rather than conics are indeed observed in the discrete aurora. Aside from the discrete aurora, however, evidence for such electric fields is not as conclusive, and as we shall see below, ICRH conics can be adequately formed with $E_{\parallel} \equiv 0$.

B. Kinetic equation

The ideas of the preceding section can be made considerably more precise by developing a kinetic model for the conic evolutionary process [29, 40–42]. Specifically, we are interested in obtaining the distribution function $f(t, \mathbf{r}, \mathbf{v})$ in the usual six-dimensional phase space of $\mathbf{r}$, $\mathbf{v}$. In principle, f is

given as a solution of a kinetic equation of the general form

$$\frac{\partial f}{\partial t} + \nabla \cdot \Gamma[f] = \mathbb{D}[f] \tag{7}$$

given suitable initial and boundary conditions. Here $\Gamma[f]$ is the phase space flux of ions due to adiabatic forces (convection, mirror force, *etc.*), and $\mathbb{D}[f]$ is the diffusion operator describing the heating process as discussed above. Without its right-hand side, Eq. (7) makes a statement of conservation of ions in phase space. With the inclusion of $\mathbb{D}$, this statement is modified to include the wave-induced diffusion of ions.

In practice, we seldom have enough information to merit a solution containing the complete dynamics of the ion evolution in its magnetospheric setting. Thus it behooves us to consider the process as more-or-less stationary, and neglect the time variable t. Thus we are more concerned with the boundary conditions on Eq. (7) rather than initial conditions.

In addition, typically one or more spatial coordinates are ignorable, and the remaining coordinate system is best aligned with respect to the magnetic field (*e.g.*, use l, the arc-length along, and some variable Λ across the magnetic field line). Additionally, both the evolution of the distribution and the measurement of the complete distribution take place on time scales longer than the gyroperiod, so it is most convenient to average Eq. (7) over this fastest timescale and work with a gyrophase average distribution $f(l, \Lambda, v_\parallel, v_\perp)$. The resulting equation for f is still rather complicated, and it is best to write it down as it applies to cusp and the auroral zone separately.

1. Cusp Conics. We consider the cusp case first, because it can be made sufficiently simple that it admits an exact solution of the kinetic equation. The typical observational geometry is illustrated in Fig. 4. In events of this type, the satellite crosses from a relatively quiet region where a cold ion population is observed into a region of intense, low frequency turbulence where a heated population is found. At the same time, there is a substantial $\mathbf{E} \times \mathbf{B}$ drift of ions from the quiet region into the turbulent region. In these cases, the use of the word "conic" is something of a misnomer to the purist, since the dominant pitch angle of the distribution is near 90°, suggesting that the mirror force does not play a major role, although there is component of drift along $\boldsymbol{B}$.

As a simple example to analyze, we can neglect everything but the $\mathbf{E} \times \mathbf{B}$ drift and the heating. In this limit, the kinetic equation (7) becomes

$$v_E \frac{\partial f}{\partial \Lambda} = \frac{1}{v_\perp} \frac{\partial}{\partial v_\perp} \left[v_\perp D_\perp \frac{\partial f}{\partial v_\perp} \right], \tag{8}$$

where v_E is the $\mathbf{E} \times \mathbf{B}$ drift speed, and $D_\perp$ was given above as expression (6). The remaining spatial variable Λ is designed to follow the motion of the ions as they drift across the magnetic field in the direction of increasing invariant latitude.

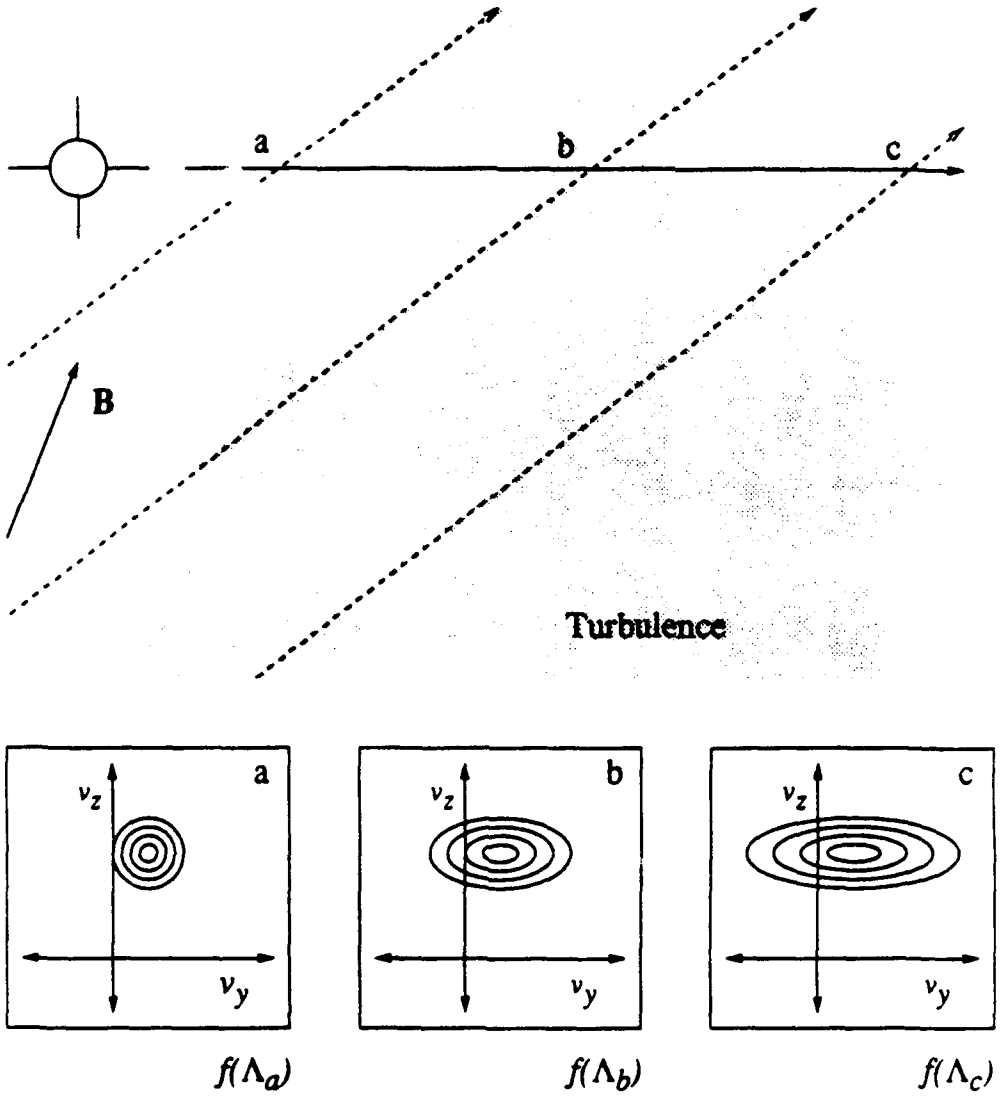

Figure 4. A cartoon illustrating the observational geometry typical of ion conic events in the cusp. Here the satellite drifts across the magnetic field from a relatively quiet region into a region of intense electromagnetic turbulence. The ions, drifting at some angle to the magnetic field (dashed lines), are successively encountered at points (a) unheated, (b) partially heated, and (c) significantly heated; contour plot sketches of the distribution function $f(\Lambda)$ in velocity space (v_z and v_y are parallel and perpendicular to B) at the corresponding coordinates Λ_a, Λ_b, and Λ_c appear in the lower part of the diagram.

If we introduce an effective "heating time" $t(\Lambda) \equiv D_\perp \Lambda / v_E$, we obtain a simple diffusion equation:

$$\frac{\partial f}{\partial t} = \frac{1}{v_\perp}\frac{\partial}{\partial v_\perp}\left[v_\perp \frac{\partial f}{\partial v_\perp}\right] . \tag{9}$$

The "initial condition" is in fact a boundary condition at the edge of the turbulent region which we identify by $\Lambda = 0$ for convenience. For simplicity, we require the ions to start at this point with a cold, source Maxwellian distribution, f_s, characterized by a thermal velocity v_t. It is then straightforward to obtain the distribution $f(\Lambda, v_\parallel, v_\perp)$ at all values of Λ:

$$f(\Lambda, v_\parallel, v_\perp) = \frac{n_i}{\pi^{3/2} v_t [v_t^2 + 4t(\Lambda)]} \exp\left[-\frac{v_\perp^2}{[v_t^2 + 4t(\Lambda)]} - \frac{v_\parallel^2}{v_t^2}\right] . \tag{10}$$

This solution is sketched in the lower portion of Fig. 4 and is simply a Maxwellian population with a temperature increasing linearly with Λ.

In practice, this simplified model is only valid near $\Lambda = 0$; away from the boundary, other effects begin to play a significant role. We shall not discuss the cusp conic events in any greater detail in the paper, largely since the topic has evolved considerably since the workshop [43, 44].

2. Auroral Conics. The kinetic equation in the main auroral zone is somewhat more complicated, mostly because the dominant drift of ions is up along the magnetic field rather than across it. The mirror force now plays a major role, consequently terms reflecting its effects must be retained. On the other hand, we can neglect terms arising from electric fields as these are now secondary effects. The resulting equation may be written in the conservative form [31]

$$\frac{\partial}{\partial l}\left[v_\parallel\left[\frac{f}{B}\right]\right] - \frac{\partial}{\partial v_\parallel}\left[-\left[\frac{v_\perp^2}{2B}\frac{dB}{dl}\right]\left[\frac{f}{B}\right]\right] + \frac{1}{v_\perp}\frac{\partial}{\partial v_\perp}\left[v_\perp\left[\frac{v_\perp v_\parallel}{2B}\frac{dB}{dl}\right]\left[\frac{f}{B}\right]\right] = \frac{1}{v_\perp}\frac{\partial}{\partial v_\perp}\left[v_\perp D_\perp \frac{\partial}{\partial v_\perp}\left[\frac{f}{B}\right]\right] . \tag{11}$$

This is a convective-diffusion equation for the density of ions per unit length of flux tube, f/B, in the coordinate space of $(l, v_\parallel, v_\perp)$. That is, the divergence of the flow of ions in phase space due to adiabatic effects is balanced by the divergence of the flow induced by the wave–particle interactions. The components of the former are the field-aligned convection ($v_\parallel$) and the parallel and perpendicular accelerations of the mirror force; the diffusive flow is proportional to the velocity-space gradient of f/B with coefficient $D_\perp$.

An additional complication implicit in Eq. (11) is the dependence of B and $D_\perp$ on l in a non-trivial fashion. To some extent we can simplify this by scaling the magnetic field with altitude roughly as l^{-3}. On the other hand, $D_\perp$

depends on l directly through the spectral density $|E_L|^2(\omega)$ found at each altitude, and indirectly though the value of the cyclotron frequency Ω at l. A simple way to deal with this is first, to neglect the direct dependence on l and use the spectrum observed at the satellite for all altitudes, and second, to approximate the observed spectrum as a power law with some spectral index α:

$$|E_L|^2(\omega) \quad \propto \quad \omega^{-\alpha} . \tag{12}$$

Then since the cyclotron frequency varies with the magnetic field

$$\Omega(l) \equiv (q/m_i c)B(l) \quad \propto \quad (l/l_o)^{-3} , \tag{13}$$

where we have used a convenient reference location l_o (*e.g.* at the satellite) to express the scaling, the diffusion coefficient varies with altitude as

$$D_\perp \simeq D_o(l/l_o)^{3\alpha} . \tag{14}$$

This model can be made slightly more general than these assumptions allow, provided we are willing to relax the meaning of α from being the observed spectral index to being the spectral index of the resonant turbulence (which spans the altitude range).

An additional complication is that the polarization of the turbulence is usually not determined by the observations. Typically, what is observed is a spectrum $|E_x|^2(\omega)$ based on the response of one antenna to the total (all polarizations) turbulence. Thus we introduce an observational form factor η which relates the turbulence reported to the fraction in the left-hand polarization: $|E_L|^2 \simeq \eta|E_x|^2$.

The situation is illustrated schematically in Fig. 5. Here we illustrate the evolution of the ions from low altitudes (bottom of the figure) to high altitudes within some flux tube. The boundary condition applied to Eq. (11) is that the low altitude population be characterized by ionospheric parameters—typically a cold Maxwellian. At any altitude l, the ions resonate with the turbulence at their local gyrofrequency, gain a bit of energy, convert some perpendicular energy into parallel energy, and drift to higher altitudes. This sequence is repeated at successively higher altitudes as the ions evolve into an energetic conic. We shall examine this scenario in greater detail in the next section as we discuss different techniques for extracting information from Eq. (11).

III. SOLUTION TECHNIQUES

In this section we shall discuss some of the different approaches which have succeeded in contributing to our understanding of ICRH conics. Each approach has its respective merits and limitations. In concert, however, we obtain a wealth of information.

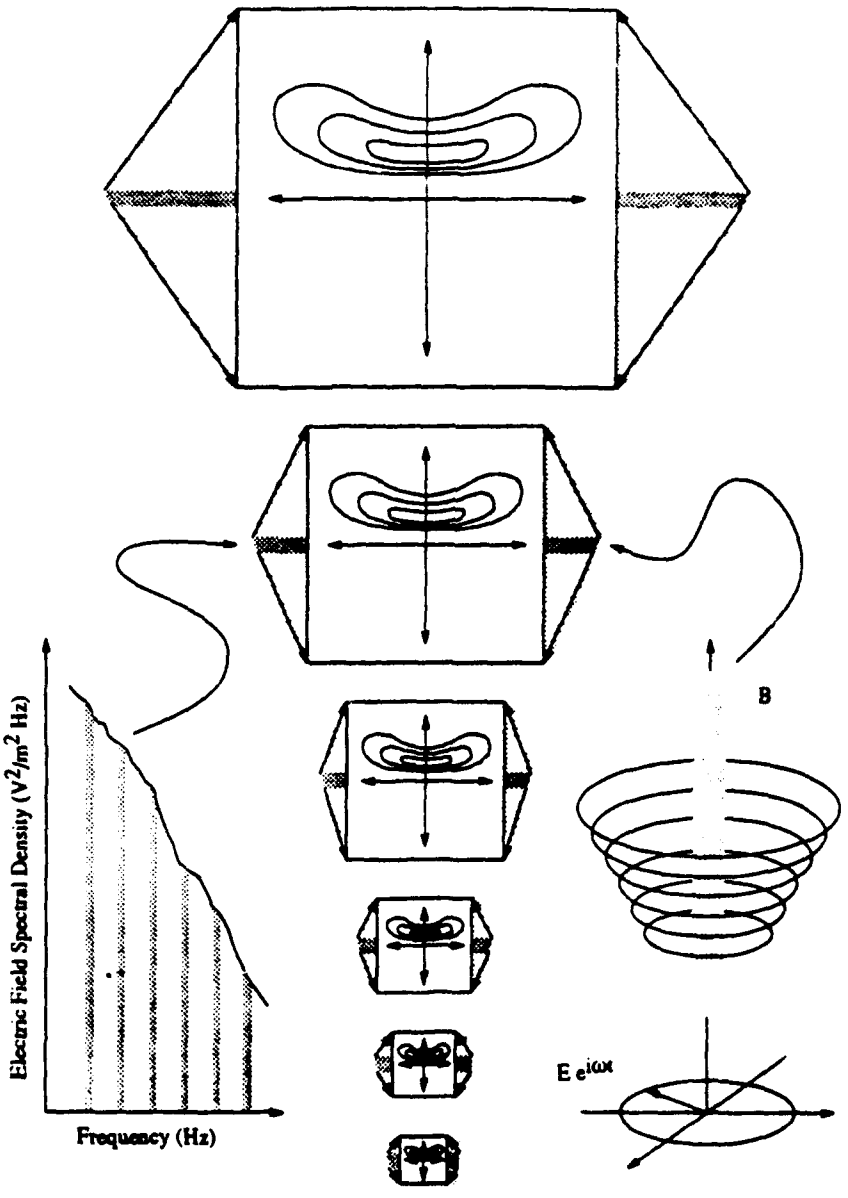

Figure 5. A cartoon of the evolution of ICRH conics confined to an auroral flux tube. Different portions of the electric field spectral density (shaded bands in plot at the left) interact with the ions at successive altitudes (wave–particle interaction cartoon at right) to produce a gradual evolution of the ion distribution function from cold distributions (at the center bottom) to hot, energetic distributions (at the center top). Following an initial relaxation (not shown, but somewhere below the figure), the form of the conic remains unchanged.

A. Numerical Solution

A fairly direct approach is look for a numerical solution of the problem, and this is readily obtained using the Monte Carlo solution technique [29], which was first applied to the formation of lower hybrid conics [45]. The idea here is to follow some number of "test" particles through their journey up the flux tube. The action of the wave turbulence is mimicked by the application of a sequence of random velocity kicks Δv which result in velocity space diffusion. An observed spectrum of turbulence may be invoked to determine the strength of the diffusion via Eq. (6); the principle uncertainties here are the fractional polarization parameter η and the exact form of the initial distribution.

This technique was applied to the conic event observed on the Dynamics Explorer 1 (DE-1) satellite with the High Altitude Plasma Instrument (HAPI) reported in Ref. [25]; the results are shown in Fig. 6 [29]. The simulation used a spectral index $\alpha = 1.7$ and intensity $|E_x|^2 = 1.2\times10^{-6}$ V^2/m^2Hz at f_{ci} ($\equiv\Omega/2\pi$) = 5.6 Hz, derived from the simultaneous DE-1 Plasma Wave Instrument (PWI) measurements. The mean particle calculations [27] indicated a value of $\eta \sim 1/8$ was appropriate. The temperature of the initial distribution was taken ~ 0.2 eV, which is appropriate for O^+ ions at 1.2 R_E geocentric. No field-aligned potential drop was required to produce the net upward drift of the conic.

One of the interesting results of the simulation (aside from the excellent agreement with the observations) is the insensitivity of the result to the initial distribution. Basically, the cooperative action of the diffusion and mirror forces is sufficiently strong to rapidly rearrange the initial form of f into that of a conic. Indeed, in the simulation, the ion distribution was recognizably a conic after only a several hundred km increase in altitude. Thereafter, the form of the distribution remained relatively fixed while becoming more energetic with increasing altitude. This sort of evolution was included in the sketch of the distributions in Fig. 5, is termed self-similar, and is discussed in the next subsection.

B. Similarity Regime

The essential point we shall exploit here is the fact that the high altitude conic observations are made in what can be termed a similarity regime where the conic evolution is self-similar. That is, the observations are made above the altitudes where the distribution is in the process of relaxing onto the conic shape and still retains some of its initial character. This gives us the freedom to ignore details of the initial (unknown) distribution f_s because they are irrelevant. The situation is entirely analogous to the process of striking a tuning fork to produce a tone. After a brief interval, one obtains the same tone independent of how the tuning fork was struck.

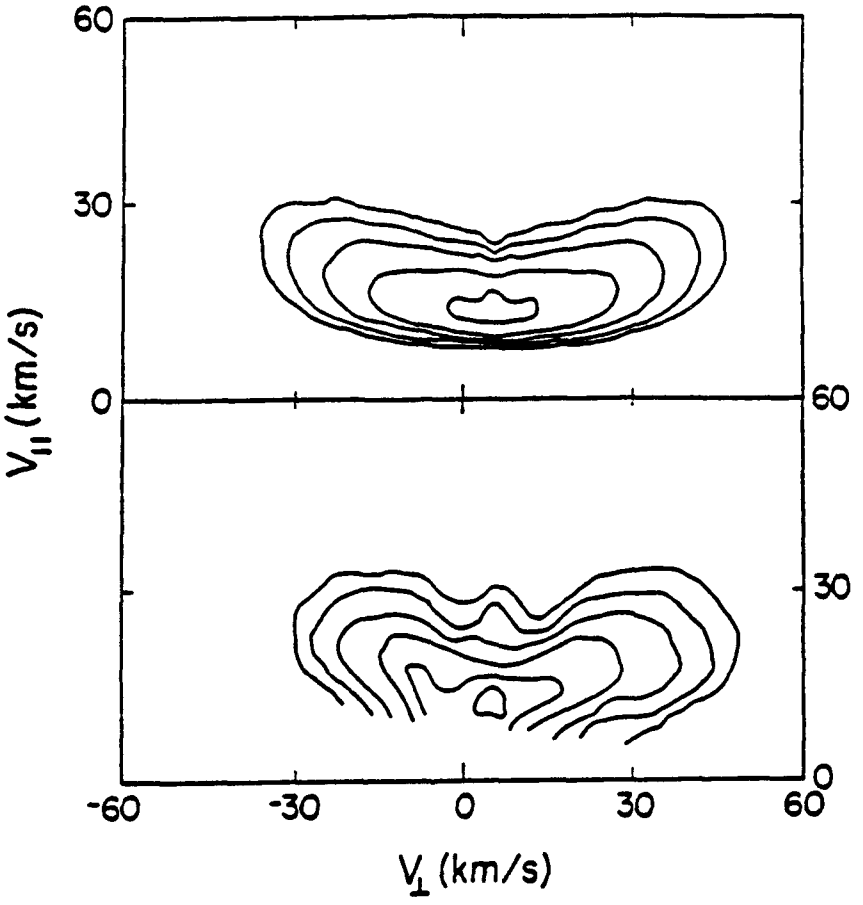

Figure 6. The top panel is the result of a Monte Carlo calculation for the oxygen-dominated conic which was observed on the DE-1 satellite with the HAPI instrument and is displayed in the bottom panel. The contours in both panels are uniformly spaced with an increment of 0.4 in the logarithm of the phase space density (from Ref. [29]).

1. Distribution Function. The physical basis for the similarity regime is that at each altitude throughout the evolution process the physical conditions are in some sense the same—the evolution of the distribution at any altitude is similar to the evolution at other altitudes. Formally, some of the physical quantities (B and $D_{\perp}$) vary as powers of (l/l_o), and it is possible to scale the rest in the same fashion, leaving the kinetic equation (11) invariant. One way to do this is to introduce new velocity variables x and y for the perpendicular and parallel components of velocity, respectively [41]:

$$x(v_\perp, l) \equiv (v_\perp / v_o)(l/l_o)^{-\sigma} , \tag{15a}$$

$$y(v_\parallel, l) \equiv (v_\parallel / v_o)(l/l_o)^{-\sigma} , \tag{15b}$$

and ask that the distribution function depend on velocity and l only through these variables, except perhaps for some overall factor of (l/l_o). The parameters σ and v_o give us two degrees of freedom with which to make this approach work. In fact, if we take

$$\sigma \equiv \frac{3\alpha + 1}{3} , \tag{16a}$$

$$v_o \equiv (D_o l_o)^{1/3} , \tag{16b}$$

we find that the shape of the conic is then given by a dimensionless distribution $F(x, y)$ related to $f(l, v_\parallel, v_\perp)$ by

$$f(l, v_\parallel, v_\perp) = n_i(l_o) v_o^{-3} F(x(v_\perp, l), y(v_\parallel, l)) (l/l_o)^{-(4\sigma+3)} . \tag{17}$$

Here the first two factors carry the dimensions of the distribution: $n_i(l_o)$ is the density of ions at the observation point, v_o plays the role of a characteristic thermal velocity, and the final factor ensures that ions are conserved in the flux tube. At any given altitude, the distribution $F(x, y)$ is the same as $f(l, v_\parallel, v_\perp)$ with the velocity scales relabeled according to Eqs. (15).

The equation which determines F may be usefully cast as a convective-diffusion equation for a density $N(x, y) \equiv x F(x, y)$:

$$\nabla \cdot (\mathbf{u} N) = \frac{\partial^2 N}{\partial x^2} , \tag{18}$$

where there is an imposed flow field

$$u_x \equiv \frac{1}{x} - \left[\frac{3}{2} + \sigma\right] x y , \tag{19a}$$

$$u_y \equiv \frac{3}{2} x^2 - \sigma y^2 . \tag{19b}$$

This flow results from the combined effects of the magnetic mirror force, the mean particle heating, and the scaling of velocities. The random component of the diffusion process is described by the right hand side of Eq. (18).

An important point to note concerning these equations is that they are parameterized only by σ. The parameter v_o enters only into the determination of the velocity scale and the dimensional factors. The situation is analogous to the characterization of a bi-Maxwellian distribution by a thermal velocity (v_t) and an anisotropy factor ($A \equiv T_\perp / T_\parallel$). The energy of the distribution is characterized by v_t, but its shape is completely described by the anisotropy factor A.

The Monte Carlo approach may be applied effectively to the solution of this equation [41]. The central idea is to treat Eq. (18) as the time-asymptotic limit of a Fokker–Planck equation. One may then launch a single particle (with essentially arbitrary initial conditions) and follow its evolution according to Langevin equations. The distribution $N(x, y)$ is then available as the time integral of the particle distribution divided by the duration of the simulation. From $N(x, y)$ we may construct $F(x, y)$ through division by x. This procedure is considerably more efficient than the more general Monte Carlo procedure discussed above, which must retain all of the details of the altitudinal evolution.

This procedure is illustrated for $\sigma = 2.53$ in Fig. 7. Several streamlines of the flow field $\mathbf{u}(x, y)$ are indicated in the left-hand panel of Fig. 7. The first thing to note is that the flow converges on a fixed point where $\mathbf{u} = 0$. This occurs at the point

$$x = \left[\frac{2\sigma}{3}\right]^{1/6}\left[\frac{3}{2} + \sigma\right]^{-1/3}, \tag{20a}$$

$$y = \left[\frac{2\sigma}{3}\right]^{-1/3}\left[\frac{3}{2} + \sigma\right]^{-1/3}. \tag{20b}$$

The convergence that this flow pattern exhibits is then balanced by the

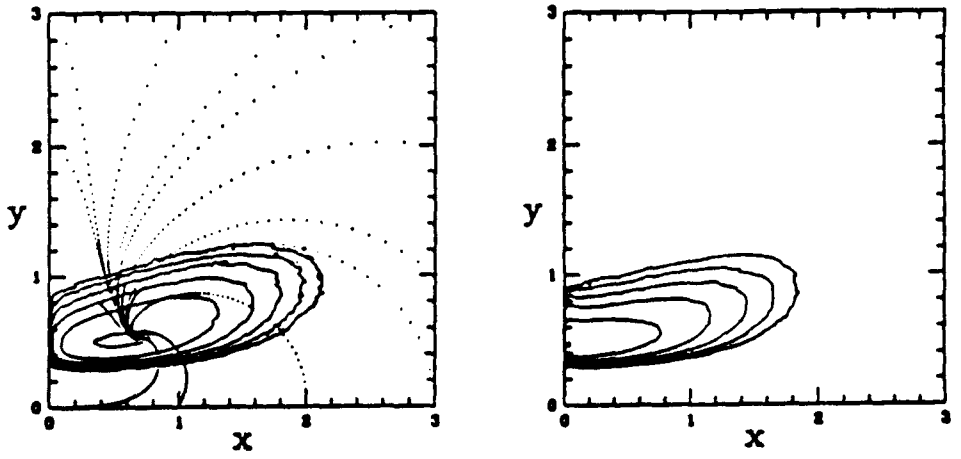

Figure 7. The left-hand panel shows the distribution $N(x, y)$ for $\sigma = 2.53$ obtained by integrating the Langevin equations for a particle in a flow field $\mathbf{u}(x, y)$, indicated by the dotted trajectories. The distribution $F(x, y)$ obtained from $N(x, y)$ appears in the right-hand panel. The contours in these plots are placed at half decades (from Ref. [41]).

diffusive action of the right-hand side of Eq. (18). Thus as the density tends to pile up at the fixed point, the action of this term is to spread out the pile into something of a mound. Although the diffusion acts only in the x direction, the flow pattern produces a spread, albeit smaller, in the y direction. This is seen in the form of the function $N(x, y)$ also included in the left-hand panel of Fig. 7. Division by x then skews the result to obtain the distribution $F(x, y)$. One can determine that $N(x \to 0, y)$ goes linearly to zero, with the result that F maximizes at $x = 0$. The resulting distribution $F(x, y)$ appears in the right-hand panel of Fig. 7.

We note that this distribution has all of the qualitative features of the observed conic. One feature of special note is the absense of ions at small $v_\parallel$ (*i.e.* we find $F(x, y \to 0) \to 0$ rapidly). This is the feature that invites explication in terms of a field-aligned potential [30], but here we clearly see how the feature arises without it: the flow $\mathbf{u}(x, y)$ sweeps particles away from the origin toward the fixed point, and there is no way for the ions to diffuse back to the origin.

2. Moments. Further progress can be made with the theory in the similarity regime. So far, we have concentrated on methods (albeit numerical) which may be used to obtain the distribution function. However, this function often contains more information that we need. In many situations, one is quite happy to make due with less information, and this is often expressed in terms of some fluid moments of the distribution:

$$< v_\perp^n v_\parallel^m > \equiv 2\pi \int_0^\infty v_\perp dv_\perp \int_0^\infty dv_\parallel \, v_\perp^n v_\parallel^m f(l, v_\parallel, v_\perp) . \tag{21}$$

Analogously, we may use the scalings (15) to obtain dimensionless variants $< x^n y^m >$. Typically, we are interested in a few of the lowest order moments, as these tell us the density, momentum, energy, and energy flux of the conic.

The usual road to the calculation of moments is to construct fluid equations from the kinetic equation (11). Unfortunately for our case, all this does is to generate an infinite hierarchy of equations with no obvious "equation of state" which may be used to correctly truncate the hierarchy. Applying the same procedure to the velocity-scaled equation for F is not of much more help as the result is a three term recursion relation among the moments of the distribution. Re-expressed in terms of the physical velocities, this relation is

$$\begin{aligned} 3m < v_\perp^{n+2} v_\parallel^{m-1} > - [n(3+2\sigma) + 2m\sigma] < v_\perp^n v_\parallel^{m+1} > \\ + 2n^2 v_o^3 < v_\perp^{n-2} v_\parallel^m > = 0 . \end{aligned} \tag{22}$$

Unfortunately, the solution to this relation has infinitely many free parameters (*e.g.*, $< v_\perp^n >$ and $< v_\parallel^m >$ with integers $n > 0$ even and $m > 0$). Nevertheless, it turns out that it is possible to obtain these moments of the distribution directly via a path integral technique [42].

The details would take us considerably beyond the scope of this paper. However, the basic idea is that a probability density functional P is available to assign relative probabilities to any path $\Psi(t)$ the ion might take in obeying the Langevin equations for a single particle which may be derived from the kinetic equation (18). An example of such a path is the one actually taken by the single particle we followed in constructing Fig. 7. There are infinitely many such paths, and their relative probability $\Psi(t)$ can be expressed as a functional of position (x, y) and conjugate momenta (p_x, p_y) components of the path $\Psi(t)$,

$$P[\Psi] = \exp\{ i \int dt [p_x(u_x - \dot{x}) + p_y(u_y - \dot{y}) + i p_x^2 x] \} . \qquad (23)$$

Arbitrary moments $M(\Psi)$ of the distribution may then be constructed as weighted path integrals:

$$< M(\Psi) > = \frac{\int D\Psi \, M(\Psi) \, P[\Psi]}{\int D\Psi \, P[\Psi]} . \qquad (24)$$

It turns out that evaluation of these moments is practical via a Feynman diagram perturbation expansion technique. The unperturbed system corresponds to an ion oscillating about the fixed point of the flow **u**. The effective perturbation parameter is the relaxation time for the ion to return to this fixed point; this time decreases with increasing σ. It is then practical to obtain arbitrary moments of the conic by algebraic means.

Results of the calculation for the parallel ($n_i v_o^2 < x^0 y^2 >$) and perpendicular ($n_i v_o^2 < x^2 y^0 >$) energy densities, and the parallel ($n_i v_o^3 < x^0 y^3 >$) and perpendicular ($n_i v_o^3 < x^2 y^1 >$) energy flux densities are shown in Fig. 8. While the parallel quantities vary with σ by over an order of magnitude for the range plotted, the perpendicular quantities are relatively insensitive to σ. This is due to the fact that smaller values of σ correspond to effectively larger parallel drifts, while at the same time the relative strength of the diffusion is roughly independent of σ. The solid points (•) correspond to numerical solutions of the kinetic equation (18). The zeroth and first order of the perturbation expansion are indicated by dashed (---) and solid (—) lines, respectively.

A number of features are worthy of note. One is the fact that the expansion improves with increasing σ. This is due to the fact that at large σ particles are more rapidly swept into the sink of the flow **u**. The result is a comparatively tighter conic. Conversely, as σ decreases, the turbulence is able to better scatter the ions against this flow, resulting in a greater dispersal of ions in phase space—a distribution that might appear to be a "heated beam" rather than a conic.

A final point to note is that the results are not terribly sensitive to σ. One could interpret this to mean that formation of a conic is relatively

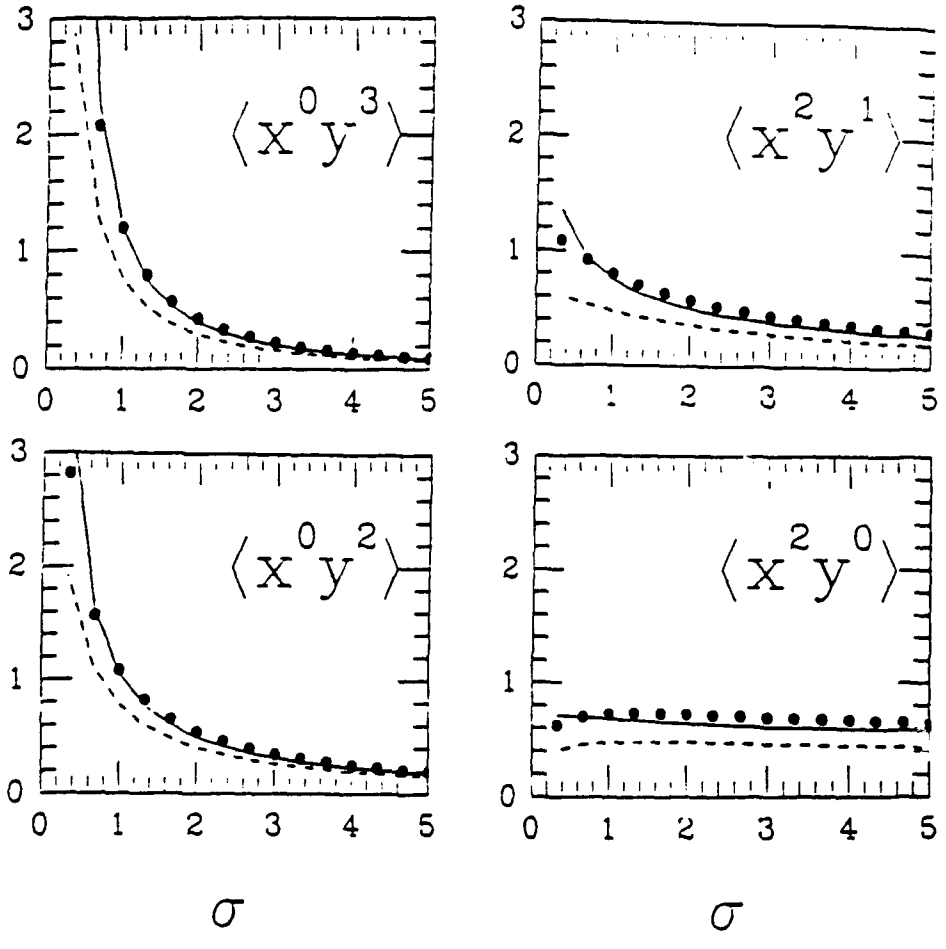

Figure 8: Results of the path integral calculation for the parallel ($n_i v_o^2 < x^0 y^2 >$) and perpendicular ($n_i v_o^2 < x^2 y^0 >$) energy densities, and the parallel ($n_i v_o^3 < x^0 y^3 >$) and perpendicular ($n_i v_o^3 < x^2 y^1 >$) energy flux densities. The solid points (•) correspond to numerical similarity regime solutions. The dashed (---) and solid (—) lines are the result of the zeroth and first order of perturbation theory, respectively (from Ref. [31]).

insensitive to the spectral index of the applied turbulence. Alternatively, a determination of the spectral index from the moments of the conic distribution is not likely to be an accurate procedure. On the other hand, the moments nevertheless contain substantial information concerning the particle distribution and indeed could be used to categorize particle observations, *e.g.*, as an extension of the current use of densities, drifts and temperatures.

IV. THEORY MEETS OBSERVATIONS

With the preceding theoretical discussion behind us, we are now in a position to consider how well the theory meets the observations. In fact, we shall see that the agreement is rather good. To date, three conic observations have been given a detailed examination within the context of this theory [29, 31]. An overview of these events appears in Table I. These events were observed with the DE-1 satellite within the (diffuse) auroral zone. A gross characterization of each event may be made with the energies $W_{\perp,\parallel} \equiv m_i v_{\perp,\parallel}^2/2$. Comparable values for each event are also obtained from the wave data using the heuristic theory [27].

Table I. Three O^+ ICRH conic events observed with the Dynamics Explorer 1 satellite (from Ref. [31]).

	81288‡	81318†	82061‡	
Year	1981	1981	1982	
Day	Oct. 15	Nov. 14	Mar. 2	
UT	2046	2346	1743	h min
l_o	4.28	2.0	4.52	R_E
IL	73.7	60.0	66.7	°
MLT	811	1911	000	h min
Kp§	3–	5	5+	
f_{ci}	0.67	5.6	0.43	Hz
$\lvert E_x\rvert^2(f_{ci})$	$\sim 1.5\times10^{-5}$	$\sim 1.2\times10^{-6}$	$\sim 8.8\times10^{-6}$	$V^2m^{-2}Hz^{-1}$
n_o	~ 0.3	~ 10	~ 1.4	cm^{-3}
$W_\perp$	~ 1020	~ 40	~ 240	eV
$W_\parallel$	~ 850	~ 30	~ 190	eV

‡Cf. Ref. [30]; †Cf. Ref. [25]; §from Refs. [46–48].

Here we shall review only the first event (day 81288) in detail [31]. This event has received a fair amount of attention in the literature, beginning with its initial publication [30], where the form of the distribution was taken to be suggestive of a two-stage acceleration process. The bulk parallel drift of the conic was supposed to be the result of passing a heated distribution through a field-aligned potential drop. Subsequent explanations for the distribution were offered [49, 50] in which the necessary acceleration arose out of the transport of ions across the polar cap. However, as we have seen in the HAPI event (Fig. 6, and Ref. [29]), this apparent parallel acceleration arises naturally out of the wave–particle interaction process, and indeed no parallel electric field is required. Indeed, Temerin [51] showed that this effective

parallel acceleration arises from any diffusive acceleration process occurring over a wide altitude range in the Earth's magnetic geometry and was the first to apply such an argument to the 81288 event. Indeed, preliminary work [52] demonstrated that the ICRH mechanism was viable. We review here some of the subsequent work [31] which supports the view that the event is most probably an ICRH conic.

A. Observations

1. Wave Data. As we have seen in the theoretical analysis, the characteristics of ICRH conics are completely determined by the two parameters σ and v_o. We therefore need to extract these parameters from the observational data.

Owing to the high altitude of the observations, the oxygen cyclotron frequency fell below the normal frequency range of the Low Frequency Correlator (LFC) of the Plasma Wave Instrument (PWI) [53] and it was necessary to obtain the electric field spectral density from the DC electric field portion of the instrument. The spectral information could then be obtained from a Fourier transform of each spin's worth (6 s) of data—in practice we obtained smoother spectra using the maximum entropy method (MEM) which has been shown to do a better job representing spectra of the power-law type [54].

A detailed examination of the DC wave forms [31] also suggested that the left and right wave polarizations were dominant over the parallel polarization. Thus in using the approximation $|E_L|^2 \approx \eta|E_x|^2$ we note that unpolarized turbulence ($|E_L|^2 \sim |E_R|^2$) corresponds to $\eta \sim 2$.

The electric field data for the event is presented in Fig. 9. Here the spectra is plotted in a time series format, using a combination contour/halftone representation. What is immediately obvious from the figure is that the peak of wave activity occurs near the center of the figure ($\sim$ UT 2046:40 $\approx$ UT 74800 s). This is in some respects analogous to the sequence observed in the energy-time spectra of the EICS data (left-hand side of the top panel Plate 1 of Ref. [30]).

With these spectra in hand, it is rather straightforward to compute the parameters σ and v_o. In fact, σ is determined from the spectral index (modulo uncertainties in the model) by Eq. (16a), and v_o is determined by the electric field spectral density at the resonant frequency via Eqs. (6) and (16b); in SI units we have

$$v_o \equiv 38.52 \left[\frac{l_o}{1\ R_E}\right]^{1/3} \left[\frac{\eta|E_x|^2(f_{ci})}{10^{-6}\ V^2m^{-2}Hz^{-1}}\right]^{1/3} \text{(km/s)} \qquad (25)$$

where $f_{ci} \equiv \Omega(l_o)/2\pi$ is the local local cyclotron frequency in Hz.

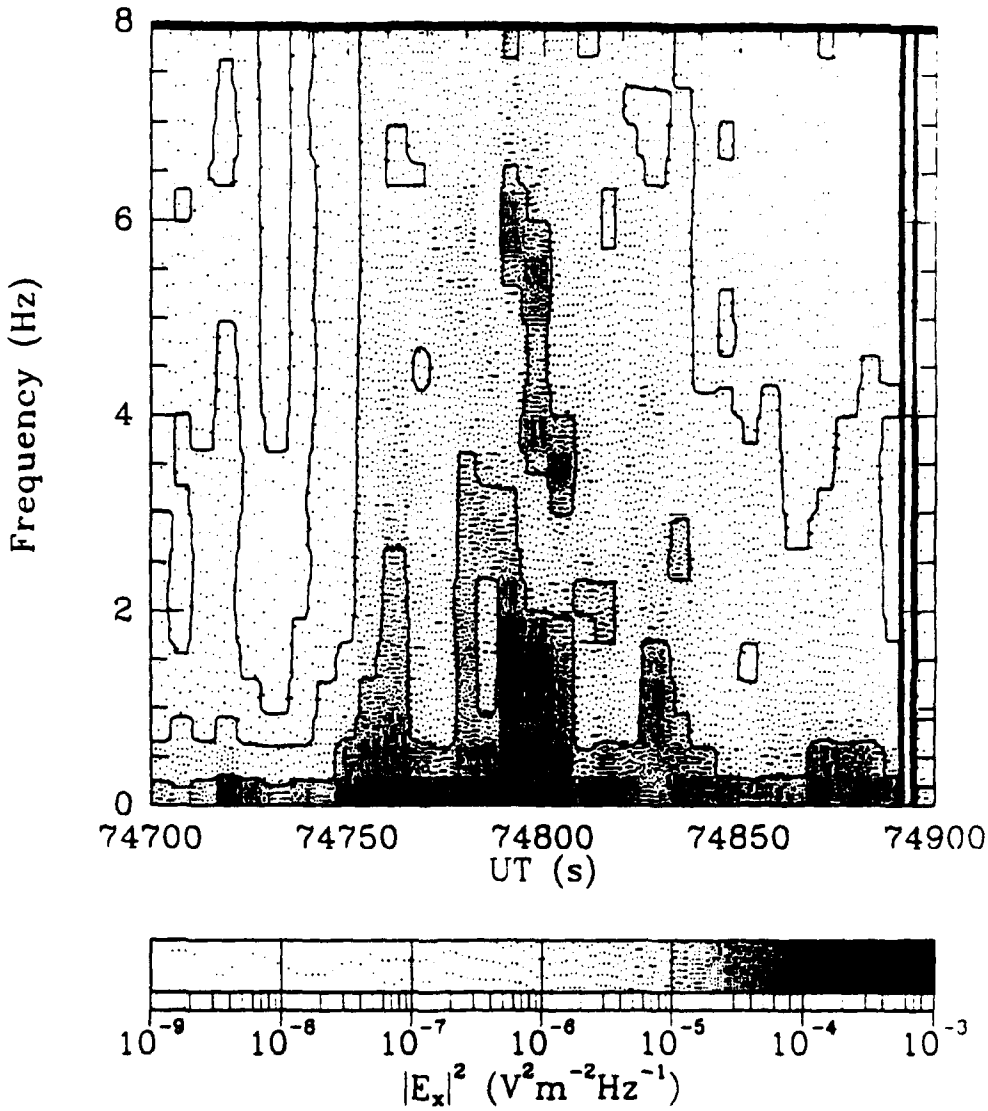

Figure 9. Electric field spectral density based on the DE-1 PWI DC data plotted as a function of UT on day 81288. A contour/halftone format is used, where the contours are logarithmically spaced by decades, and the darker regions correspond to the greater spectral density. The vertical lines near UT 74900 s result from a data gap (from Ref. [31]).

2. Particle Data. The 81288 conic is sufficiently energetic to be well resolved by the Energetic Ion Composition Spectrometer (EICS) [55] instrument in the "FAST" mode in which it was operating. In order to construct a distribution function, each individual measurement (tested for significance

against the noise background) was used to provide an estimate of f_o within ranges of pitch angle and velocity as determined by the angular and energy acceptances of the instrument together with the duration of the measurement. Over time, values of f_o become available for a set of points distributed on a plane in velocity space determined by the satellite rotation axis. Assuming a reasonably continuous distribution, values anywhere on the plane may be obtained through interpolation or simply reference to the nearest measured value. In the FAST mode, alternate 6 s satellite spin periods are devoted to different ion species and different (interleaved) energy acceptance ranges. Thus, a partial energy scan is available after 6 s, while 18 s are required for a complete energy scan of one species.

However, a transformation from this plane of measurement to the space of parallel and perpendicular velocity components is still required. Given the relative drift between the satellite frame and the plasma frame (where it is assumed to be gyrotropic), the required transformation is easily constructed. For the events considered, the plane of measurement nearly includes the field-aligned direction, so each half of this plane spans most of the $(v_\perp, v_\parallel)$ space. There are thus a variety of ways to use the data to construct $f_o(v_\perp, v_\parallel)$: the differences between them may be taken as an uncertainty of the determination of f_o, given the statistics of the measurements and other assumptions about the plasma conditions which may be only approximately satisfied.

Table II. Moment relations that determine the parameters σ and v_o.

n	m	$(\cdots)\,\sigma$	−	$(\cdots)\,v_o^3$	=	$(\cdots)$
0	1	$(2\langle v_\parallel^2\rangle)\,\sigma$	−	$(0)\,v_o^3$	=	$(3\langle v_\perp^2\rangle)$
2	0	$(4\langle v_\perp^2 v_\parallel\rangle)\,\sigma$	−	$(8\langle 1\rangle)\,v_o^3$	=	$(-6\langle v_\perp^2 v_\parallel\rangle)$
2	1	$(6\langle v_\perp^2 v_\parallel^2\rangle)\,\sigma$	−	$(8\langle v_\parallel\rangle)\,v_o^3$	=	$(3\langle v_\perp^4\rangle - 6\langle v_\perp^2 v_\parallel^2\rangle)$

We determine σ and v_o from the EICS observation of f_o using the recursion relation (22) as illustrated in Table II. In particular, we note that each instance of the recursion relation (22) presents us with a linear relation in these parameters. Any two of these relations may be solved to yield their values, but we would not expect different pairs to result in the same values unless f_o is truly an ICRH conic and all the approximations are applicable. In practice, we obtain σ and v_o from a least squares fit to the three relations given in Table II. Some appreciation of the relative error involved may be obtained by considering the spread of the solutions to these relations taken pairwise.

B. Comparison

1. Distribution Functions. We first address the extent to which the conic observed is consistent with the form predicted by theory. We would expect to see the most energetic, and therefore best resolved, conic near the peak of the event determined from the wave activity (UT 74800 s from Fig. 9). In order to reduce the level of noise in the data, an average of three complete energy scans (UT 74794–74836 s) is presented in Fig. 10.

For comparison with the numerical solutions for $F(x, y)$, we compute the moments of this distribution, finding a density $n_i(l_o) \simeq 0.3$ cm^{-3}, $v_o \simeq 162 \pm 5$ km/s, and $\sigma \simeq 2.76 \pm 0.2$. Thus (in round figures) we apply a velocity scale $v_o = 160$ km/s to the numerical solution obtained with $\sigma = 8/3$ and present the result in Fig. 11. Allowing for the artifacts of the data acquisition and reduction (*e.g.*, the "boxes" in Fig. 9 which correspond to the individual data points), the agreement between Figs. 9 and 10 is remarkable: both distributions peak near $v_\parallel \sim 80$ km/s as $v_\perp \to 0$, and the $v_\perp$ extent of the contours is comparable. There are several measurements in the observational plot (*e.g.*, for $v_\perp \sim 220$–300 km/s) which have no counterpart in the theoretical distribution; these are probably part of an unrelated oxygen population.

2. Moments. We next turn to the time series of the observations. This is most conveniently presented in terms of v_o and σ which may be determined separately from each instrument, and which are presented in Figs. 12 and 13. Indeed, an important reason for using these parameters is that the observations of each instrument may be independently reduced to these parameters, thereby testing the theory which says they should produce similar results.

The determination of v_o and σ with the EICS observations can be made on a spin by spin basis. Two six-second spin periods separated by a spin period (or a total of 18 seconds) are required to construct a complete O^+ energy distribution which includes left and right halves; thus Fig. 12 expresses the results obtained by various ways in order to express some of the uncertainties inherent in this calculation. In particular, there are dotted and dashed lines, which correspond to the right and left halves of the conic, respectively, and these traces are doubled because there are two ways to pair adjacent spins. The sum of the left and right halves is plotted as points (squares and triangles denoting the pairing of spins), with vertical error bars based on the uncertainty in the determination of v_o and σ as described above and horizontal error bars indicating the interval of measurement (18 s).

An immediate impression from Fig. 12 is that the determination of σ is not nearly as precise as that of v_o. This shows up in the error bars as well as the general scatter of the data points. The primary explanation for this is the fact that although σ determines the shape of the conic, its control is somewhat subtle. While there is considerable qualitative difference between a

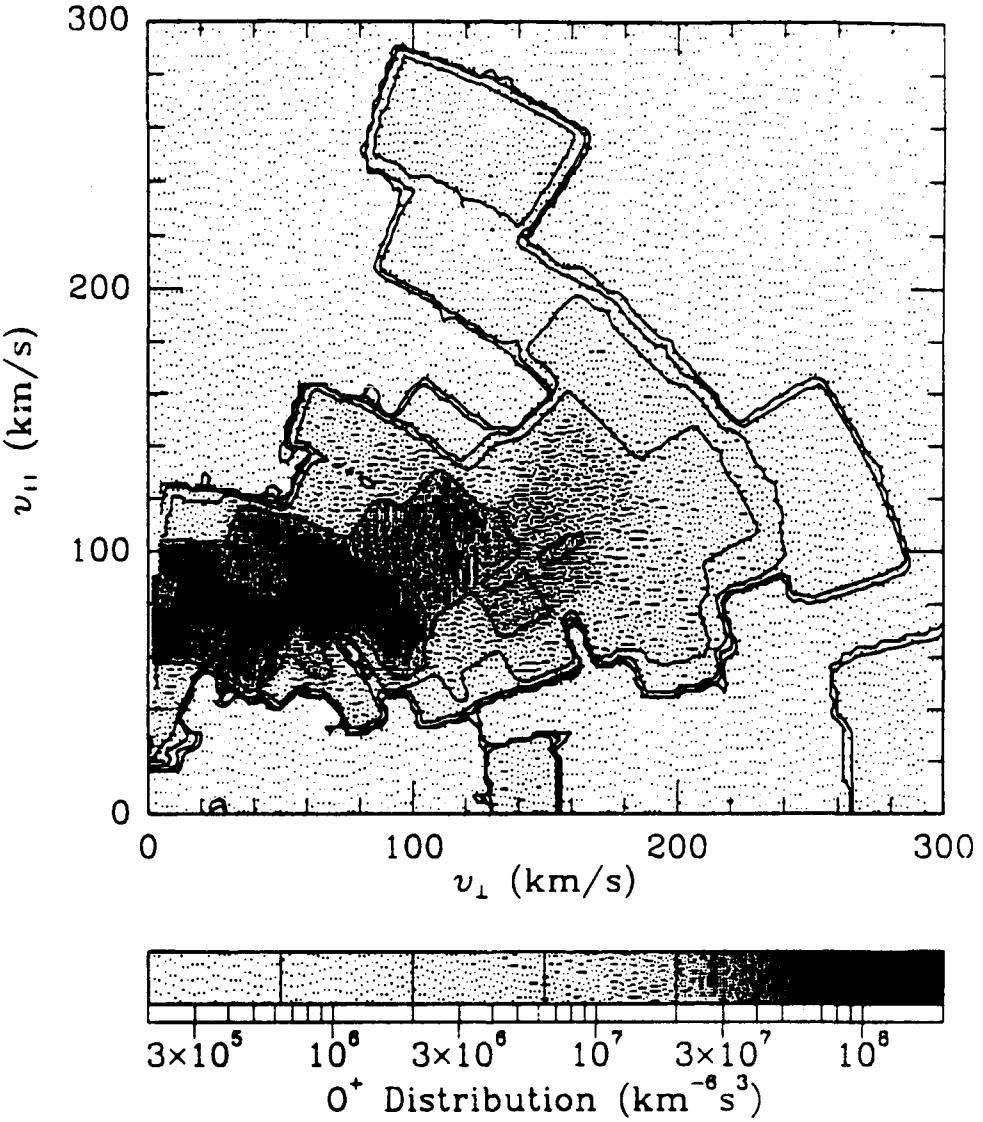

Figure 10. Conic distribution $f_o(v_\perp, v_\parallel)$ constructed from four spins of DE-1 EICS data near UT 74800 s on day 81288. Contours are placed at half decades, and the darker regions denote the greatest phase space density (from Ref. [31]).

conic with $\sigma = 0$ and $\sigma = 1$, there is little difference between $\sigma = 2$ and $\sigma = 5$. An excellent way to see this is via the path integral results (Fig. 8) which show a general insensitivity of the moments to σ values beyond 2.

Another observation to be made from Fig. 12 is that the error bars for times before UT 74780 s are qualitatively larger than those after this time. One may interpret this as a suggestion from the data that the observed

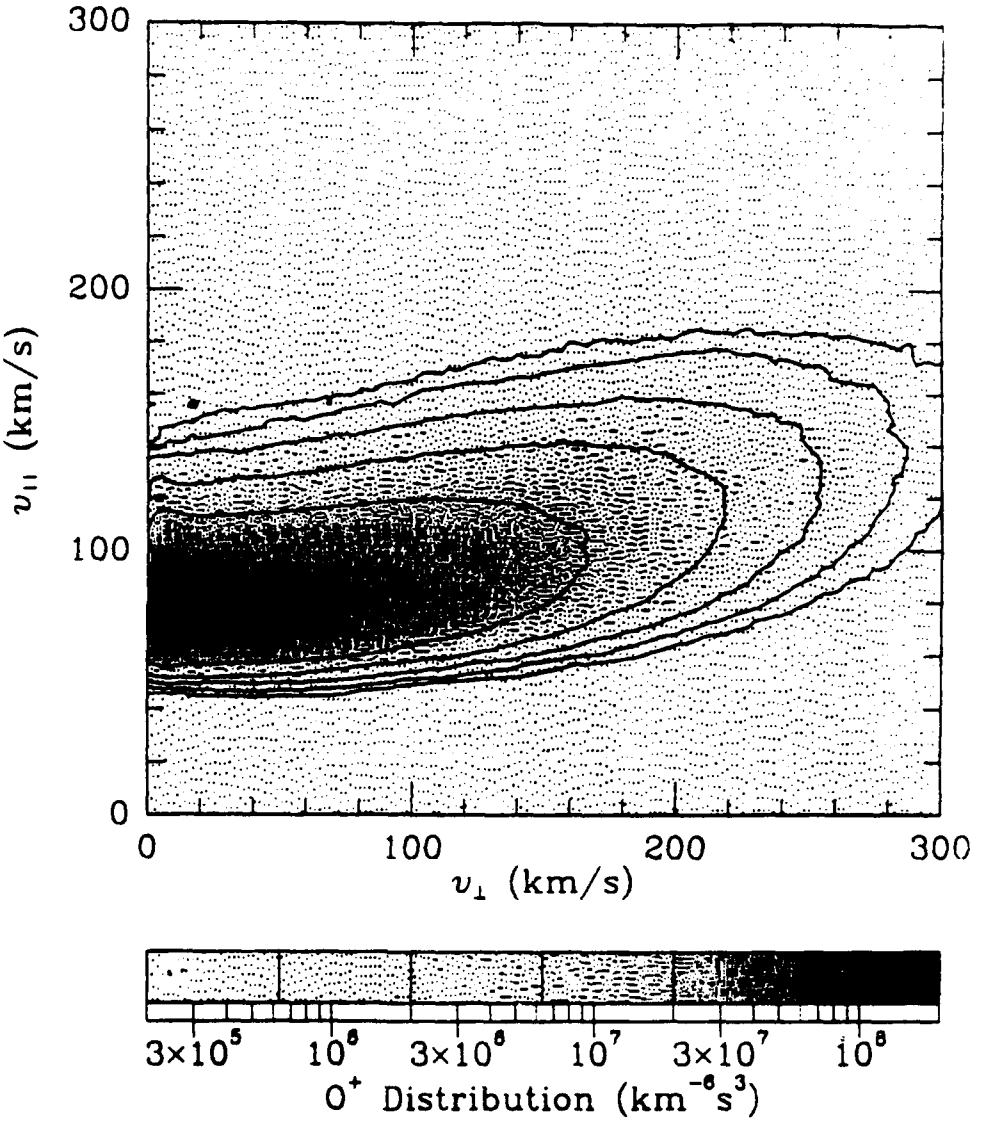

Figure 11. Conic distribution $f_o(v_\perp, v_\parallel)$ constructed from $F(x, y)$ with $\sigma = 8/3$ and a velocity scale of $v_o = 160$ km/s. The representation is identical to that of Fig. 10 (from Ref. [31]).

distribution here is far from an "ideal" conic. Indeed, examination of the detailed distributions at this time show a contamination with a quite obviously unrelated, energetic O^+ population.

The spectra obtained from the PWI DC data were averaged over three spins to provide a time resolution comparable to the particle data; low time resolution (32 s) PWI LFC data were also used for comparison. Either way,

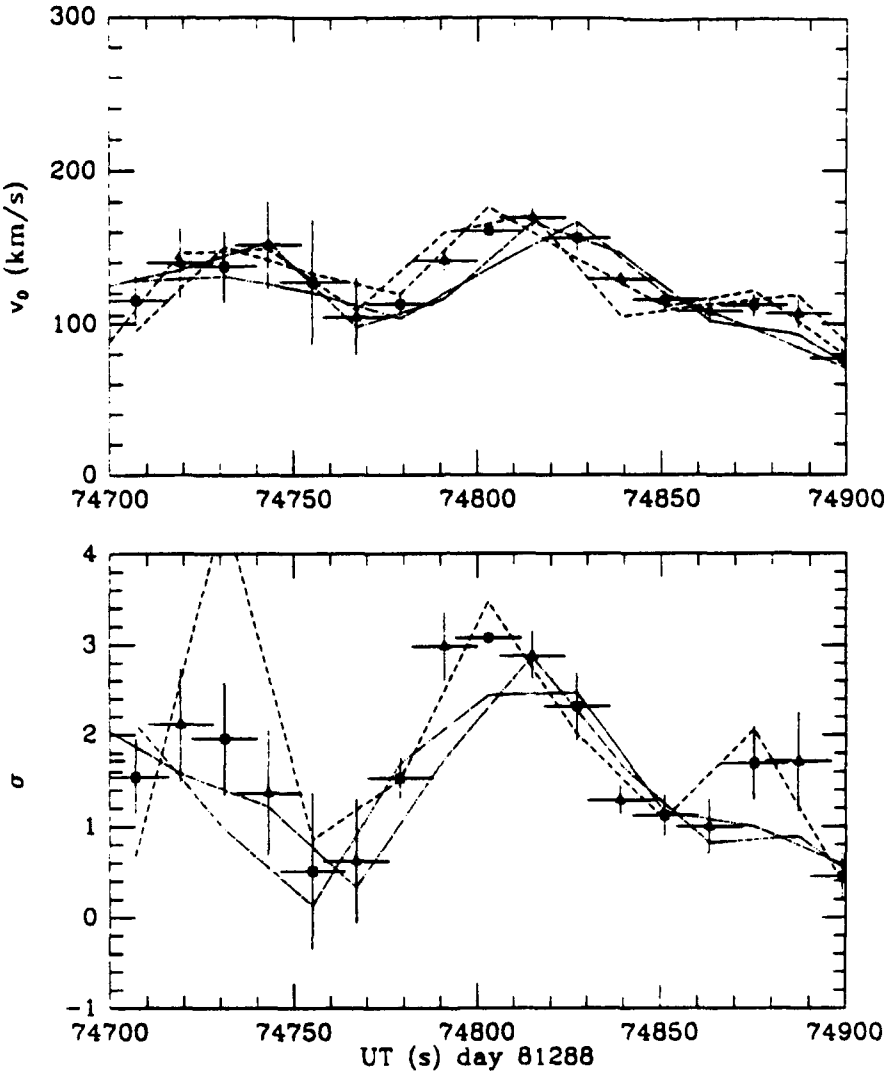

Figure 12. Time series of v_o and σ on day 81288 based on DE-1 EICS observations. In each panel, the dotted and dashed lines correspond to the right and left halves of the conic, and the solid points with error bars correspond to their average. Squares and triangles distinguish the two ways in which pairs of spins may be composed to construct a complete energy scan; these two ways are undifferentiated for the lines (from Ref. [31]).

a v_o and σ time series is then directly obtained from Eqs. (25) and 16. Because the polarization is undetermined, we have presented v_o values corresponding to a range of $\eta^{1/3}$: 1.0, 0.8, 0.6, and 0.4 for the DC data, and 0.8 and 0.6 for the LFC data. These last two values correspond to between

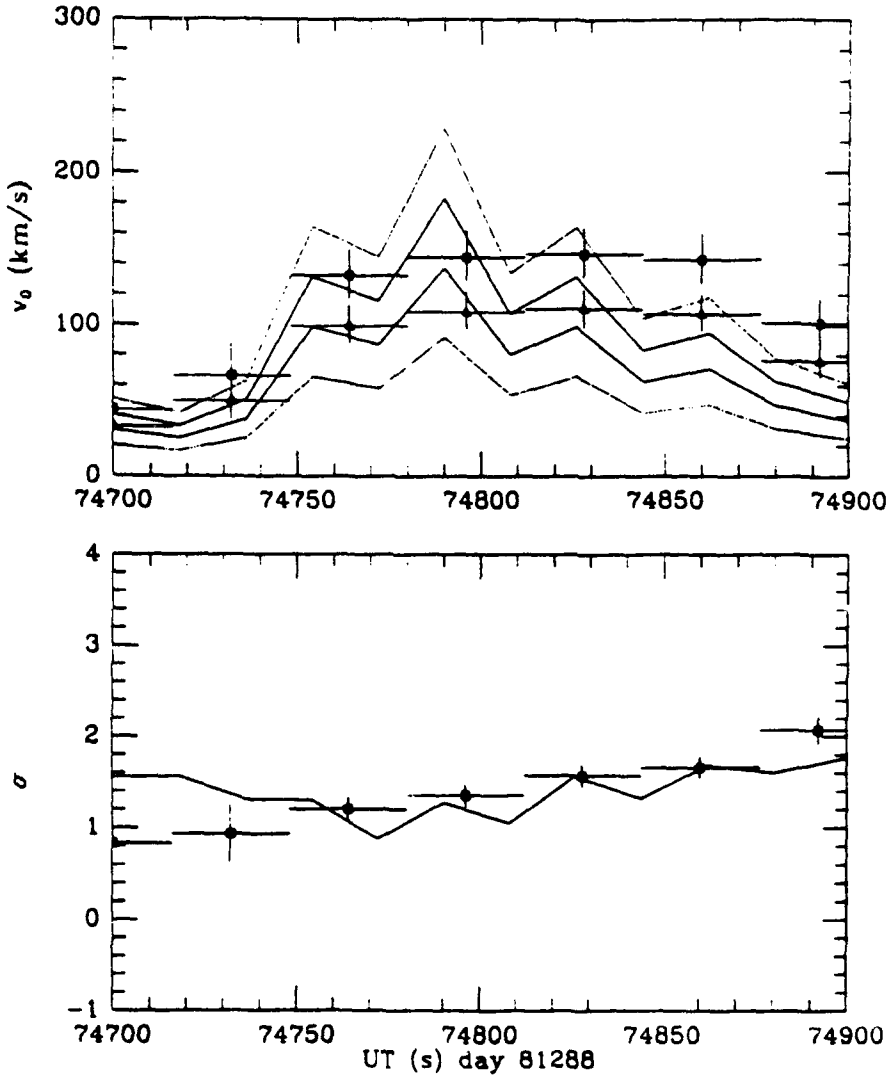

Figure 13. Time series of v_o and σ on day 81288 based on PWI observations. In each panel, the lines correspond to power-law fits of the DC data and the open points to power-law fits of the LFC data. The multiplicity of v_o values comes from the use of different values of $\eta^{1/3}$: 1.0 (dotted), 0.8 (solid, squares), 0.6 (solid, triangles), 0.4 (dotted; from Ref. [31]).

13% and 5% of the total electric field spectral density being left hand polarized. We note that the general trend of the event is consistent with Fig. 12, and that the DC and LFC data are in general agreement. The DC spectra at this timescale (18 s) are somewhat more dynamic than the LFC data, which have a lower time resolution (32 s). There appears to be some trend for the

LFC data to provide somewhat more energetic values of ν_o; on the other hand, at these altitudes, the lowest LFC frequency band lies at 1.78 Hz, requiring an extrapolation down to the local oxygen cyclotron frequency. At these time scales, the spectral slope appears to be fairly constant over the displayed interval: $1 \leq \alpha \leq 2$; and it is consistent between DC and LFC.

In comparing particles (Fig. 12) with waves (Fig. 13), we note that the ν_o presentations are in reasonable agreement, presenting the same general trend of a climax for the event near UT 74800 s. A value of η in the range $0.2 \leq \eta \leq 0.5$ would provide reasonably good agreement between the two sets of observations. The situation for σ is perhaps not as conclusive. However, as we remarked above, its determination from the EICS data is not likely to be well constrained, particularly for $\sigma \geq 2$. To some extent the larger values of σ near UT 74800 s may be an aliasing of the increases in ν_o at that time.

To briefly summarize the results obtained for this event [31], there appears to be a rather clear correlation between the ν_o parameter determined separately from EICS and PWI. The situation for σ is not as simple. On the one hand, the agreement appears to be much worse. On the other hand, the disagreement is largely due to the variation of σ as determined from the ion data, and as we have pointed out above, there are a number of reasons not to expect σ to be accurately computed from the ion data. Thus, given the agreement for ν_o we should be inclined to forgive the σ variation of the ions in an assessment of the validity of the theory as formulated.

Of course, some of the assumptions which we have made in order to constrain the theory and simplify the comparison of the two instruments might be the source of some of the discrepancy. For example, implicit in the assumption that $|E_L|^2 - \eta|E_x|^2$ is the assumption that the frequency dependence of $|E_L|^2$ is the same power law as $|E_x|^2$. More generally, we could take $|E_L|^2(f_{ci}) \sim \eta|E_x|^2(f_{ci})$ but assign different spectral indices α_L and α_x to their frequency dependence. Then for the same values of η, it is easy to reconcile $\alpha_L \geq \alpha_x$ with the observations, and it is rather difficult to have $\alpha_L \leq \alpha_x$. Since the σ parameter relevant to the conic is $\alpha_L + 1/3$, we would then expect the PWI data to provide a lower bound for the value of σ computed from the EICS data, and this is entirely consistent with the σ plots in Figs. 12 and 13.

Why this might be the case (*i.e.*, $\alpha_L \neq \alpha_x$) is another question. In the theory, the wave power at higher frequencies is used to provide heating at lower altitudes. Thus in a model for the event where the wave power is generated at high altitudes and is propagating downward, there would be some reflection of the waves which would tend to make the high altitude observations somewhat more energetic than those at lower altitudes. There is indeed some suggestion (Fig. 9 of Ref. [26]) that the higher frequencies are less energetic at lower altitudes that at higher ones. Thus, even if the turbulence

was unpolarized, since we construct a model of the turbulence on the flux tube based on the high altitude observations, we must have $\alpha_L \geq \alpha_x$.

Another significant assumption which affects the analysis is the assumption of a quasi-steady evolution process. As indicated above, this assumption was made mostly in order to simplify the analysis; but at the same time, observations by a single satellite do not provide sufficient information to include these effects. Qualitatively, we still expect to see conics; quantitatively, we would expect some corrections. For the two events we have presented, the wave activity could be characterized by a temporal turn-on, turn-off sequence. Taking causality into consideration, we would then expect to see the peak of wave activity precede that of the conic energy. Indeed, an allowance of ~ 20 s on day 81288 substantially improves the correlation of the v_o plots appearing in Figs. 12 and 13.

V. SUMMARY

In this paper we have discussed the ion cyclotron resonance heating mechanism as it applies to the understanding of conic events. We have approached this understanding from a number of levels, starting with the basic physical ideas and working our way up through kinetic theory and ultimately on to a comparison with the observations. Thus we have seen how to estimate the zeroth order effects with a simple ion heating rate; we have discussed how to formulate the problem exactly with a kinetic equation for the distribution f; we have considered a number of analytic and numeric approaches for determining f; we have seen how the auroral conics are best viewed in the context of a similarity regime determined by parameters σ and v_o; and we have seen that these results are consistent with the auroral observations in as much detail as the observations permit. For the cusp conics, the work of comparison is still in progress, but the results to date [32–34] are quite promising.

Of course, the reader is reminded that one should not conclude from this work that all conics are ICRH conics—we have not considered here any evidence which detracts from the viability of other conic generation mechanisms given the proper ionospheric/magnetospheric setting. Indeed, many of the low-altitude rocket observations of energetic conics [56–59] are probably not ICRH conics (or at least not as we have discussed them here). However, future conics discovered in the presence of an intense, low-frequency, electromagnetic turbulence should be seriously considered as ICRH conics.

There are, of course, many questions which arise in the course of this work. These include the application of ICRH to other domains in space plasmas, majority species heating, the ultimate origins of the low-frequency turbulence, possible correlations of conic generation with substorm activity, and other questions [31]. There are also observational uncertainties due to the limitations of the current generation of instruments/satellites which hopefully

will be cured in future missions. (See for example the discussion in this volume on the FAST mission [60].) As is the rule, one can expect that more questions will continue to be raised and that the conic story is far from over.

REFERENCES

[1] R.D. Sharp, R.G. Johnson, and E.G. Shelley, Observation of an ionospheric acceleration mechanism producing energetic (keV) ions primarily normal to the geomagnetic field direction, J. Geophys. Res., **82**, pp. 3324–3328 (1977).

[2] D.M. Klumpar, A digest and comprehensive bibliography on transverse auroral ion acceleration, in *Ion Acceleration in the Magnetosphere and Ionosphere*, Geophysical Monograph Series, Vol. 38, Tom Chang, M.K. Hudson, J.R. Jasperse, R.G. Johnson, P.M. Kintner, M. Schulz and G.B. Crew, eds., pp. 389–398 (American Geophysical Union, Washington D.C., 1986).

[3] J.L. Burch, Energetic particles and currents: results from Dynamics Explorer, Rev. Geophys., **26**, pp. 215–228 (1988).

[4] E.G. Shelley, W.K. Peterson, A.G. Ghielmetti, and J. Geiss, The polar ionosphere as a source of energetic magnetospheric plasma, Geophys. Res. Lett., **9**, pp. 941–944 (1982).

[5] A.W. Yau, B.A. Whalen, W.K. Peterson, and E.G. Shelley, Distribution of upflowing ionospheric ions in the high-altitude polar cap and auroral ionosphere, J. Geophys. Res., **89**, pp. 5507–5522 (1984).

[6] E.G. Shelley, Magnetospheric energetic ions of terrestrial origin from the Earth's ionosphere, Adv. Space Res., **6**, pp. 121–132 (1987).

[7] C.R. Chappell, The terrestrial plasma source: a new perspective in solar-terrestrial processes from Dynamics Explorer, Rev. Geophys., **26**, pp. 229–248 (1988).

[8] A.W. Yau, W.K. Peterson, and E.G. Shelley, Quantitative parametrization of energetic ionospheric ion outflow, in *Modeling Magnetospheric*

Plasma, Geophysical Monograph Series, Vol. 44, T.E. Moore and J.H. Waite, Jr., eds., pp. 211–217 (American Geophysical Union, Washington, D.C., 1988).

[9] R. L. Lysak, in *Ion Acceleration in the Magnetosphere and Ionosphere*, Geophysical Monograph Series, Vol. 38, T. Chang, M. K. Hudson, J. R. Jasperse, R. G. Johnson, P. M. Kintner, M. Schulz, and G. B. Crew, eds., pp. 261–270 (American Geophysical Union, Washington, D.C., 1986).

[10] T. Chang, G.B. Crew, and J.M. Retterer, Electromagnetic tornadoes in space: ion conics along auroral field lines generated by lower hybrid waves and electromagnetic turbulence in the ion cyclotron range of frequencies, Computer Physics Communications, **49**, pp. 61–74 (1988).

[11] E. Ungstrup, D.M. Klumpar, and W.J. Heikkila, Heating of ions to superthermal energies in the topside ionosphere by electrostatic ion cyclotron waves, J. Geophys. Res., **84**, pp. 4289–4296 (1979).

[12] R.L. Lysak, M.K. Hudson, and M. Temerin, Ion heating by strong electrostatic ion cyclotron turbulence, J. Geophys. Res., **85**, pp. 678–686 (1980).

[13] K. Papadopoulos, J.D. Gaffey, and P.J. Palmadesso, Stochastic acceleration of large M/Q ions by hydrogen cyclotron waves in the magnetosphere, Geophys. Res. Lett., **7**, pp. 1014–1017 (1980).

[14] P.B. Dusenbury and L.R. Lyons, Generation of ion conic distributions by upgoing ionospheric electrons, J. Geophys. Res., **86**, pp. 7627–7638 (1981).

[15] N. Singh, R.W. Schunk, and J.J. Sojka, Energization of ionospheric ions by electrostatic hydrogen waves. Geophys. Res. Lett., **8**, p. 1249 (1981).

[16] M. Ashour-Abdalla and H. Okuda, Turbulent heating of heavy ions on auroral field lines, J. Geophys. Res., **89**, pp. 2235–2250 (1984), and references therein.

[17] T. Chang and B. Coppi, Lower hybrid acceleration and ion evolution in the suprauroral region, Geophys. Res. Lett., **8**, pp. 1253–1256 (1981).

[18] G.B. Crew and T. Chang, Asymptotic theory of ion conic distributions, Phys. Fluids, **28**, pp. 2382–2394 (1985).

[19] I. Roth and M.K. Hudson, Lower hybrid heating of ionospheric ions due to ion ring distributions in the cusp, J. Geophys. Res., **90**, pp. 4191–4203 (1985).

[20] J.M. Retterer, T. Chang, and J.R. Jasperse, Ion acceleration by lower hybrid waves in the suprauroral region, J. Geophys. Res., **91**, pp. 1609–1618 (1986).

[21] J.M. Retterer, T. Chang, and J.R. Jasperse, Particle acceleration by intense auroral VLF turbulence, in *Physics of Space Plasmas (1989)*, SPI Conference Proceedings and Reprint Series, No. 9, T. Chang, G. B. Crew, and J. R. Jasperse, eds., p. 119 (Scientific Publishers, Inc.,

Cambridge, Mass., 1990), and references therein.

[22] W. Lennartsson, On the consequences of the interaction between the auroral plasma and the geomagnetic field, Planet. Space Sci., **28**, p. 135 (1980).

[23] J. E. Borovsky, The production of ion conics by oblique double layers, J. Geophys. Res., **89**, p. 2251 (1984).

[24] M. E. Greenspan, Effects of oblique double layers on upgoing ion pitch angle and gyrophase, J. Geophys. Res., **89**, p. 2842 (1984).

[25] J.D. Winningham and J. Burch, Observation of large scale ion conic generation with DE-1, in *Physics of Space Plasmas (1982–4)*, SPI Conference Proceedings and Reprint Series, No. 5, J. Belcher, H. Bridge, T. Chang, B. Coppi, and J.R. Jasperse, eds., pp. 137–158 (Scientific Publishers, Inc., Cambridge, MA, 1984).

[26] D.A. Gurnett, R.L. Huff, J.D. Menietti, J.L. Burch, J.D. Winningham, and S.D. Shawhan, Correlated low-frequency electric and magnetic noise along the auroral field lines, J. Geophys. Res., **89**, pp. 8971–8986 (1984).

[27] T. Chang, G.B. Crew, N. Hershkowitz, J.R. Jasperse, J.M. Retterer, and J.D. Winningham, Transverse acceleration of oxygen ions by electromagnetic ion cyclotron resonance with broad band left-hand polarized waves, Geophys. Res. Lett., **13**, pp. 636–639 (1986).

[28] R. Gendrin, Wave Particle interactions as an energy transfer mechanism between different particle species, Space Sci. Rev., **34**, pp. 271–287 (1983).

[29] J.M. Retterer, T. Chang, G.B. Crew, J.R. Jasperse, and J.D. Winningham, Monte Carlo modeling of ionospheric oxygen acceleration by cyclotron resonance with broad-band electromagnetic turbulence, Phys. Rev. Lett., **59**, pp. 148–151 (1987).

[30] D.M. Klumpar, W.K. Peterson, and E.G. Shelley, Direct evidence for two-stage (bimodal) acceleration of ionospheric ions, J. Geophys. Res., **89**, pp. 10779–10787 (1984).

[31] G. B. Crew, Tom Chang, J. M. Retterer, W. K. Peterson, D. A. Gurnett, and R. L. Huff, Ion cyclotron resonance heated conics: theory and observations, J. Geophys. Res., **95** (1990), in press.

[32] M. André, H. Koskinen, L. Matson, and R. Erlandson, Local transverse ion energization in and near the polar cusp, Geophys. Res. Lett., **15**, pp. 107–110 (1988).

[33] W.K. Peterson, M. André, G.B. Crew, A.M. Persoon, M.J. Engebretson, C.J. Pollock, and M. Temerin, Heating of thermal ions near the equatorward boundary of the mid-altitude polar cleft, in *Electromagnetic Coupling in the Polar Clefts and Caps*, NATO ASI Series C: Mathematical and Physical Sciences, Vol. 278, P.E. Sandhold and A. Egeland, eds., pp. 103–113 (Kluwer Academic Publishers, Dordrecht, 1989).

[34] M. André, G.B. Crew, W.K. Peterson, A.M. Persoon, C.J. Pollock, and M.J. Engebretson, Heating of ion conics in the cusp/cleft, in *Physics of Space Plasmas (1989)*, SPI Conference Proceedings and Reprint Series, No. 9, T. Chang, G. B. Crew, and J. R. Jasperse, eds., p. 203 (Scientific Publishers, Inc., Cambridge, Mass., 1990).

[35] Jay R. Johnson, Tom Chang, G. B. Crew, and Mats André, Equatorially generated ULF waves as a source for the turbulence associated with ion conics, Geophys. Res. Lett., **16**, pp. 1469–1462 (1989).

[36] Jay R. Johnson, Tom Chang, G. B. Crew, and Mats André, Equatorially generated ULF waves as a source for the turbulence associated with ion conics, in *Physics of Space Plasmas (1989)*, SPI Conference Proceedings and Reprint Series, No. 9, Tom Chang, G. B. Crew and J. R. Jasperse, eds., p. 433 (Scientific Publishers, Inc., Cambridge, MA, 1990).

[37] C.F. Kennel and F. Engelmann, Velocity space diffusion from weak plasma turbulence in a magnetic field, Phys. Fluids, **9**, p. 2377 (1966).

[38] D.G. Swanson, *Plasma Waves* (Academic Press, Boston, 1989), p. 296.

[39] R.Z. Sagdeev and A.A. Galeev, *Nonlinear plasma theory* (W.A. Benjamin, Inc., New York, 1969), pp. 54–55.

[40] G.B. Crew and T. Chang, Asymptotic theory of ion conic distributions, Phys. Fluids, **28**, pp. 2382–2394 (1985).

[41] G.B. Crew and T. Chang, Kinetic treatment of oxygen conic formation in the central plasma sheet by broadband waves, in *Modeling Magnetospheric Plasma*, Geophysical Monograph Series, Vol. 44, T. Moore and J.H. Waite, eds., pp. 159–163 (American Geophysical Union, Washington, D.C., 1988).

[42] G. B. Crew and T. Chang, Path integral formulation of ion heating, Phys. Fluids, **31**, pp. 3425–3439 (1988).

[43] G.B. Crew, M. André, and W.K. Peterson, Ion cyclotron resonance heating in the cusp/cleft, Bull. Am. Phys. Soc., **34**, p. 2009 (1989).

[44] M. André, G. B. Crew, W. K. Peterson, A. M. Persoon, C. J. Pollock, and M. J. Engebretson, Ion heating by broadband low-frequency waves in the cusp/cleft, in preparation for J. Geophys. Res.

[45] J.M. Retterer, T. Chang, and J.R. Jasperse, Ion acceleration in the suprauroral region: a Monte Carlo model, Geophys. Res. Lett., **10**, pp. 583–586 (1983).

[46] H.E. Coffey, Geomagnetic and solar data, J. Geophys. Res., **87**, p. 926 (1982).

[47] H.E. Coffey, Geomagnetic and solar data, J. Geophys. Res., **87**, p. 1733 (1982).

[48] H.E. Coffey, Geomagnetic and solar data, J. Geophys. Res., **87**, p. 5310 (1982).

[49] J.L. Horwitz, Velocity filter mechanism for ion bowl distributions (bimodal conics), J. Geophys. Res., **91**, pp. 4513–4523 (1986).

[50] J.B. Cladis, Parallel acceleration and transport of ions from polar ionosphere to plasma sheet, Geophys. Res. Lett., **13**, pp. 893–896 (1986).

[51] M. Temerin, Evidence for a large bulk ion conic heating region , Geophys. Res. Lett., **13**, pp. 1059–1062 (1986).

[52] J.M. Retterer, T. Chang, G.B. Crew, J.R. Jasperse, and J.D. Winningham, Monte Carlo modeling of oxygen ion conic acceleration by cyclotron resonance with broadband electromagnetic turbulence, in *Physics of Space Plasmas (1985–7)*, SPI Conference Proceedings and Reprint Series, No. 6, Tom Chang, J. Belcher, J. R. Jasperse and G. B. Crew, eds., pp. 97–111 (Scientific Publishers, Inc., Cambridge, MA, 1987).

[53] S.D. Shawhan, D.A. Gurnett, D.L. Odem, R.A. Helliwell, and C.G. Park, The plasma wave and quasi-static electric field instrument (PWI) for Dynamics Explorer-A, Space Sci. Instrum., **5**, pp. 535–550 (1981).

[54] P.F. Fougere, On the accuracy of spectrum analysis of red noise processes using maximum entropy and periodogram methods: simulation studies and application to geophysical data, J. Geophys. Res., **90**, pp. 4355–4366 (1985).

[55] E.G. Shelley, D.A. Simpson, T.C. Sanders, E. Hertzberg, H. Balsiger, and A. Ghielmetti, The energetic ion composition spectrometer (EICS) for the Dynamics Explorer-A, Space Sci. Instr., **5**, pp. 443–454 (1981).

[56] B.A. Whalen, W. Bernstein, and D.W. Daly, Low altitude acceleration of ionospheric ions, Geophys. Res. Lett., **5**, p. 55 (1978).

[57] A.W. Yau, B.A. Whalen, A.G. McNamara, P.J. Kellogg, and W. Bernstein, Particle and wave observations of low-altitude ionospheric ion acceleration events, J. Geophys. Res., **88**, pp. 341–355 (1983).

[58] P.M. Kintner, J. LaBelle, W. Scales, A.W. Yau, and B.A. Whalen, Observations of plasma waves within regions of perpendicular ion acceleration, Geophys. Res. Lett., **13**, pp. 1113–1116 (1986).

[59] P.M. Kintner, W. Scales, J. Vago, R. Arnoldy, G. Garbe, and T. Moore, Simultaneous observations of electrostatic oxygen cyclotron waves and ion conics, Geophys. Res. Lett., **16**, pp. 739–742 (1989).

[60] M.A. Temerin, C.W. Carlson, C.A. Cattell, R.E. Ergun, J.P. McFadden, F.S. Mozer, D.M. Klumpar, W.K. Peterson, E.G. Shelley, and R.C. Elphic, Wave–particle interactions on the FAST satellite, in *Physics of Space Plasmas (1989)*, SPI Conference Proceedings and Reprint Series, No. 9, T. Chang, G. B. Crew, and J. R. Jasperse, eds., p. 343 (Scientific Publishers, Inc., Cambridge, Mass., 1990).

3. PARTICLE ACCELERATION BY INTENSE AURORAL VLF TURBULENCE

John M. Retterer[1]
Air Force Geophysics Laboratory, Bedford, MA 01731

Tom Chang
Center for Space Research, MIT, Cambridge, MA 02139

J. R. Jasperse[1]
Air Force Geophysics Laboratory, Bedford, MA 01731

ABSTRACT

Broadband turbulence in the lower-hybrid to plasma frequency range is found in a variety of forms in the suprauroral region, most notably as auroral hiss and VLF saucers. When the turbulence is intense, it is observed to be associated with ion conics (ions heated transverse to the geomagnetic field) and "counter-streaming" electron fluxes (heated in both directions parallel to the field). This tutorial will begin with a review of the dispersion and propagation characteristics of whistler resonance-cone waves, which comprise the turbulence, and go on to discuss the theories for the excitation of the turbulence. Plasma simulation and mesoscale (Monte Carlo) simulation techniques will be used to illustrate the interaction of the ambient plasma with the turbulence. These calculations will demonstrate how this interaction results in transverse heating of the ions and parallel heating of the electrons of the plasma, leading to the formation of the observed heated and accelerated particle fluxes.

I. INTRODUCTION

Auroral hiss is a plasma-wave phenomenon commonly observed in the acceleration region above the Earth's auroral zone, associated with inverted-V electron precipitation [1]. The frequencies of these waves, extending from the lower-hybrid resonance up to the plasma frequency, fall in the VLF range. Their dispersion characteristics have led them to be identified with waves on the whistler resonance-cone plasma dispersion surface, which are excited by a plasma microinstability caused by the accelerated auroral electrons. The electric field intensities of these waves are occasionally large [2], and this turbulence has been observed to be correlated [3] with the energy flux of transversely accelerated ions observed in the topside ionosphere (see Ref. [4]

[1]Also: Research Affiliate, Center for Space Research, MIT

for a bibliography).

Above the ionosphere, these accelerated ions are observed in a form called an ion conic, because their pitch-angle distribution peaks at an oblique angle. A mechanism by which wave-particle interaction of ions with the intense turbulence near the lower-hybrid frequency leads to ion conic formation was suggested by Chang and Coppi [5]: first, the turbulence is excited in the ambient plasma of the suprauroral region by the accelerated auroral electrons. Wave-particle interaction of the ambient ion population with the turbulence near the lower-hybrid frequency then leads to ion acceleration nearly perpendicular to the field line, which is followed by the adiabatic folding of velocities as the ions mirror and travel up the field line, to create the conic velocity distribution.

Plasma simulations [6] have shown this mechanism to be effective not only for the transverse acceleration of ions, but also for the acceleration of the ambient electrons in the directions parallel to the geomagnetic field. The electron velocity distribution is found to have enhanced fluxes of energetic electrons in both directions with respect to the geomagnetic field, a form which is indeed observed in space in conjunction with ion conics: counter-streaming electrons [7].

The wave-particle interaction processes involved in the generation of the VLF turbulence and the acceleration of the ambient plasma are found to occur on spatial and temporal scales large compared to those which can be practically studied using self-consistent particle plasma simulation. To model ion conics, a larger-scale simulation model has been employed [8]. This model of global wave-particle interaction employs a Monte Carlo technique to follow the trajectories of many ions as they undergo the influences of wave-particle interaction and large-scale electric and magnetic fields in the suprauroral region. It has enjoyed considerable success in modeling the ion velocity distribution of ion conics formed in other regions by interaction with turbulence in the ion cyclotron frequency range [9; 10]. (See the review by Crew and Chang [11], for a discussion of this other form of ion conic.) Because the wave-particle interaction in this other case involves a simple frequency resonance, an empirical estimate of the rate of particle heating using the observed frequency spectrum of the turbulence directly is found to be satisfactory. In the case of interaction with VLF turbulence, on the other hand, the resonance requires the matching of velocities, and considerable uncertainty exists in using observed wave amplitudes to estimate the wave-particle interaction rate because the lack of wave-vector measurements prevents us from knowing the phase velocities of the waves. This problem has been addressed using models for the micro-physics of the local wave-particle interaction, based on a combination of observation and simulation results.

In this review, we will first touch on the wave dispersion and propagation characteristics and discuss the excitation mechanism of auroral hiss. The

local model for wave-particle interactions will be described and illustrated using simulation results and a simple nonlinear theory, which explains how the counter-streaming electrons and hot ion tails are produced. Finally, the application of the local results to the meso-scale model for ion conic formation in the suprauroral region will be discussed, using two examples to illustrate the method and the results achieved by the theory.

II. AURORAL HISS AND LOWER-HYBRID WAVES

The plasma waves that are observed in conjunction with ion conics and counter-streaming electrons are an intense form of an ionospheric plasma wave phenomenon known as auroral hiss. We begin here with a brief review of the literature of observations of auroral hiss and our theoretical understanding of the phenomenon.

From their first flights, polar-orbitting satellites carrying VLF radio receivers have measured a broad-band emission at high latitudes, ranging in frequency from the lower-hybrid-resonance frequency up through the whistler band [12; 13]. Correlation with particle spectrometer data [14] demonstrated the association between auroral-zone VLF hiss and intense fluxes of precipitating electrons in inverted-V events and suggested that the generation of the VLF modes occured through Landau resonance with the accelerated auroral electrons. Evaluation of the Poynting flux of these waves showed that the auroral hiss was indeed propagating towards the Earth along with the auroral electrons, and distinguished auroral hiss from a similar wave phenomenon, known as VLF saucers [15], whose Poynting flux at the same altitude was observed to flow away from the Earth. VLF saucers are located equatorward of the auroral hiss, and were not found to be correlated with energetic electron precipitation, implying that their source of free energy resided in some unobserved current carrier, possibly cold ionospheric electrons in the auroral return current region. VLF emissions have also been observed in conjunction with ~ 50 eV electron beams flowing away from the Earth in the cusp region [16]. The characteristic funnel-shaped dispersion of auroral hiss on a frequency-latitude spectrogram—that is, higher-frequency waves being more spread out latitudinally than lower-frequency waves—can be explained in terms of the propagation characteristics of whistler waves propagating near the resonance cone [1;15], which we will briefly describe below.

A. Dispersion Theory

To understand the plasma waves that make up auroral hiss, we can begin with the linear theory of a stable, cold, homogeneous plasma, and then make the necessary generalizations. In a cold magnetized plasma, the linear dispersion of electromagnetic waves is described by the following dispersion relation, using the notation of Stix [17]:

$$\tan^2\theta \equiv \frac{k_\perp^2}{k_\parallel^2} = \frac{-P(n^2-R)(n^2-L)}{(Sn^2-RL)(n^2-P)}, \tag{1}$$

where $n = kc/\omega$ is the index of refraction, θ is the angle of the wave vector $\boldsymbol{k}$ with respect to the background magnetic field B, and

$$P \equiv 1 - \sum_s \frac{\omega_{ps}^2}{\omega^2}, \quad \begin{matrix} R \\ L \end{matrix} \equiv 1 - \sum_s \frac{\omega_{ps}^2}{\omega^2}\frac{\omega}{\omega \pm \Omega_s}, \tag{2}$$

$$S \equiv \frac{1}{2}(R+L) = 1 - \sum_s \frac{\omega_{ps}^2}{\omega^2 - \Omega_s^2},$$

where ω_{ps} is the plasma frequency and Ω_s the gyro frequency of species s. We isolate the relevant root of this equation for whistler resonance-cone waves by considering the resonance limit, in which n approaches infinity. In this case, $\tan^2\theta = -P/S$, and with the ordering appropriate for VLF waves, $\Omega_i^2 << \omega^2 << \Omega_e^2$, we find the root

$$\omega^2 = \omega_{LH}^2 \equiv \frac{\omega_{pi}^2 + \omega_{pe}^2\cos^2\theta}{1 + \omega_{pe}^2\sin^2\theta/\Omega_e^2} \tag{3}$$

where we have assumed that the plasma consists of electrons and one ion species, with plasma frequencies respectively ω_{pe} and ω_{pi}. We see that the mode has frequencies ranging from the lower hybrid resonance frequency

$$\omega_{LHR}^2 \equiv \frac{\omega_{pi}^2}{1 + \omega_{pe}^2/\Omega_e^2} \tag{4}$$

when $\boldsymbol{k}$ is perpendicular to B, up to the plasma frequency ω_p (where $\omega_p^2 = \omega_{pe}^2 + \omega_{pi}^2$) when $\boldsymbol{k}$ is parallel to B. (If we analysed the dispersion relation slightly more generally, we would find that the upper limit is the smaller of the plasma or electron gyro frequencies, but the ordering we have selected is the appropriate one for the auroral acceleration region, at altitudes of the order of 1 R_E, where ω_{pe}/Ω_e is small.)

These waves propagate near the whistler resonance cone, where to first approximation the waves are electrostatic in nature and the frequency of a mode depends only on the angle of propagation with respect to the magnetic field. When ω is independent of $|\boldsymbol{k}|$, the group velocity, which defines the direction and speed with which wave energy propagates, is perpendicular to $\boldsymbol{k}$. Waves with frequencies near ω_{LHR}, whose wave vectors are approximately perpendicular to B, have group velocities approximately parallel to B, while waves near the plasma frequency ω_p, have group velocities approximately perpendicular to B. Thus, in the auroral region where B is nearly vertical, higher frequency waves on the whistler resonance cone propagate further in latitude than lower-frequency waves from the same source,

explaining the funnel or saucer shape dispersion characteristics of VLF hiss observed by satellite. By tracing the paths of the low and high frequency portions of the observed spectrum back to where they intersect, the distance from the source of the hiss or saucer can be inferred [1,15], although the direction along B, whether above or below the spacecraft, cannot be determined from the dispersion alone. The filled-in funnel spectrum observed for auroral hiss presumably implies a source distributed along the geomagnetic field line, while the saucer spectrum, which is only outlined by the dispersion curve, implies a source which is confined in extent along B [15], although it can be extended in longitude [18].

The first generalization we must consider in preparation for our study of wave-particle interaction with these waves is the introduction of kinetic effects and the consequences of finite-temperature plasma particle species. The dielectric tensor for electromagnetic waves in a Maxwellian plasma can be found in many texts [19] and we will not reproduce it here. Instead, we can begin with the facts that the waves of interest are essentially electrostatic and within the frequency range $\Omega_i << \omega << \Omega_e$ to write a simpler dispersion relation. Because wave frequencies are larger than the ion gyrofrequency, to the first approximation we may use the unmagnetized susceptibility [19, p.56] for the ions. For the electrons, we can use the magnetized susceptibility [19, p.73], retaining from the sum over cyclotron resonances only the zeroth order term, making the strongly magnetized approximation for the electrons because the frequencies of interest are much smaller than the electron gyrofequency. The dispersion relation for electrostatic waves in a Maxwellian plasma is then

$$\varepsilon(\boldsymbol{k},\omega) = 1 + \sum_s \chi_s(\boldsymbol{k},\omega) = 0 \tag{5}$$

where the sum of susceptibilities is over all species in the plasma, or

$$\varepsilon(\boldsymbol{k},\omega) = 1 + \frac{\omega_{pe}^2}{\Omega_e^2} + \frac{\omega_{pe}^2}{k^2 v_{te}^2} W\left[\frac{\omega}{k_\parallel v_{te}}\right] + \frac{\omega_{pi}^2}{k^2 v_{ti}^2} W\left[\frac{\omega}{k v_{ti}}\right] \tag{6}$$

for the simple ion-electron plasma. In this expression, W is the plasma dispersion function as presented by Ichimaru [19, p.56], $k_\parallel$ is the component of $\boldsymbol{k}$ along B, and v_{ts} is the thermal velocity, $\sqrt{T_s/m_s}$. By introducing kinetic effects, we allow the possibility of damping or excitation of the waves by resonant wave-particle interaction. If we consider both kv_{ti} and $k_\parallel v_{te}$ to be small compared to the frequencies of interest, we can solve the dispersion relation, Eq.(6), using a perturbative approach. To zeroth order in these terms, we recover the solution, Eq.(3), except with the slight error that $\sin^2\theta$ is missing from the second term in the denominator. To first order in $(kv_{ti})^2$ and $(k_\parallel v_{te})^2$, ω^2 contains positive additional terms proportional to these factors, much like the thermal correction of the Langmuir mode dispersion. The imaginary part of the frequency can be calculated using the following

approximation, valid for small imaginary frequency

$$\gamma = \frac{-\mathrm{Im}\,\varepsilon}{\partial\,\mathrm{Re}\,\varepsilon/\partial\omega}, \tag{7}$$

where ε is evaluated using the real frequency. We will not write out this result until the next section, where we include the auroral electron beam population and the opportunity for positive growth rates and instability.

The introduction of the effects of magnetized ions changes the dispersion at short wavelengths for nearly perpendicular propagation. When the perpendicular wavelength becomes comparable to the ion gyroradius, $\rho_i = v_{ti}/\Omega_i$, the frequency plateau near the lower-hybrid resonance frequency which existed at longer wavelength begins to break up into the high-harmonic ion Bernstein modes around ω_{LH}, separated approximately by the ion gyrofrequency. The upper envelope of the group of Bernstein modes is still roughly described by the unmagnetized lower-hybrid frequency including the thermal correction. This phenomenon is illustrated well by the plasma dispersion surfaces presented by André [20], calculated numerically using the dispersion code WHAMP [21]. The damping effect of magnetized ions was demonstrated in calculations by Gorney *et al.*[22] who showed that damping of auroral hiss by energetic ions, i.e., ion conics themselves, can produce observable absorption lines in the hiss spectrum at multiples of the ion gyrofrequency.

B. Resonance-Cone Plasma Wave Instability

With the association of auroral hiss with energetic electron precipitation in inverted-V events came the recognition [14] that a kinetic instability of the plasma containing both the accelerated auroral electrons and a ambient population of electron plus ion species could excite the waves through the Landau resonance with the auroral electrons, $\omega = k_{\parallel} u_{b\parallel}$, where $u_{b\parallel}$ is the velocity of the auroral electrons along the geomagnetic field. We first consider simple modeling using Maxwellians for all plasma species, and then discuss more detailed modeling that can be performed.

The effect of the DC electric field within the inverted-V potential structure in the direction of the geomagnetic field is to accelerate the plasma sheet electron population of the magnetosphere along the magnetic field lines toward the Earth [2;23]. The resulting plasma below the potential drop is a mixture of the hot, drifting auroral electron component and the much cooler ambient plasma of ionospheric origin. (In addition, electron components of intermediate energies, due to atmospheric backscatter and energy degradation of the auroral electrons, wave-particle interaction processes, etc., are also present; we will mention their effects later.) This situation gives rise to a beam-plasma instability of the bump-on-tail form which can excite the whistler resonance-cone waves of auroral hiss.

The simple, electrostatic linear theory will be our first introduction to this instability [5;24]. In addition to the ambient electron and ion species, modeled as Maxwellians of equal temperature ($T_i = T_e \sim 1$ eV), the unstable plasma contains the energetic electrons accelerated through the field-aligned potential drop. This species is modeled as a warm Maxwellian distribution, drifting parallel to the magnetic field with velocity $u_{b\parallel}$ such that the drift kinetic energy is ≥ 1 keV and its temperature is a few hundred eV. The density of the beam population is small—typically, less than 10^{-2} times the ambient density. To incorporate the beam population into the dielectric function of the electron-ion plasma, we add its susceptibility

$$\frac{\omega_{pb}^2}{k^2 v_{tb}^2} W\left(\frac{\omega - k_\parallel u_{b\parallel}}{k_\parallel v_{tb}} \right) \tag{8}$$

to Eq.(6). If the beam density is small enough, its effect on the real frequency of the resonance-cone mode is small. When we examine the imaginary component of the frequency, describing the growth or damping of the wave, we obtain

$$\gamma = \omega \left(\frac{\pi}{8}\right)^{1/2} \left[\frac{\omega_{pb}^2}{k^2 v_{tb}^2} \frac{(k_\parallel u_{b\parallel} - \omega)}{k_\parallel v_{tb}} \exp\left(-\frac{1}{2} \frac{(\omega - k_\parallel u_{b\parallel})^2}{k_\parallel^2 v_{tb}^2} \right) \right. \tag{9}$$

$$\left. - \frac{\omega_{pe}^2}{k^2 v_{te}^2} \frac{\omega}{k_\parallel v_{te}} \exp\left(-\frac{1}{2} \frac{\omega^2}{k_\parallel^2 v_{te}^2} \right) - \frac{\omega_{pi}^2}{k^2 v_{ti}^2} \frac{\omega}{k v_{ti}} \exp\left(-\frac{1}{2} \frac{\omega^2}{k^2 v_{ti}^2} \right) \right]$$

where ω is the real frequency of the wave, Eq.(3). We see that γ, the imaginary part of the frequency, can be positive, implying exponential growth of the waves, when the first term, due to the auroral beam population, is positive and is larger than the damping contributions from the ambient plasma electrons and ions, described by the second and third terms. Typically, this can happen for phase velocities $u_{b\parallel} - \eta v_{tb} < \omega/k_\parallel < u_{b\parallel}$, where η is a small factor.

The plasma of the auroral ionosphere, however, is not a cold Maxwellian, and the presence of a warm secondary population of electrons can strongly affect the instability by acting to damp the waves [25]. The study of the stability of the auroral plasma must be done using an empirical specification of the electron velocity distribution. A useful technique employed by Lotko and Maggs [25] is to fit an observed distribution with a sum of Maxwellians of different densities, temperatures, and drifts; this allows us to use the well-understood and accurately tabulated Maxwellian plasma dispersion function to analyze a more general plasma. An additional refinement is to calculate the solution of the complete electromagnetic dispersion relation. This must necessarily be done numerically, for which we use the WHAMP code of K. Ronnmark, kindly provided to us by M. André. Fig.

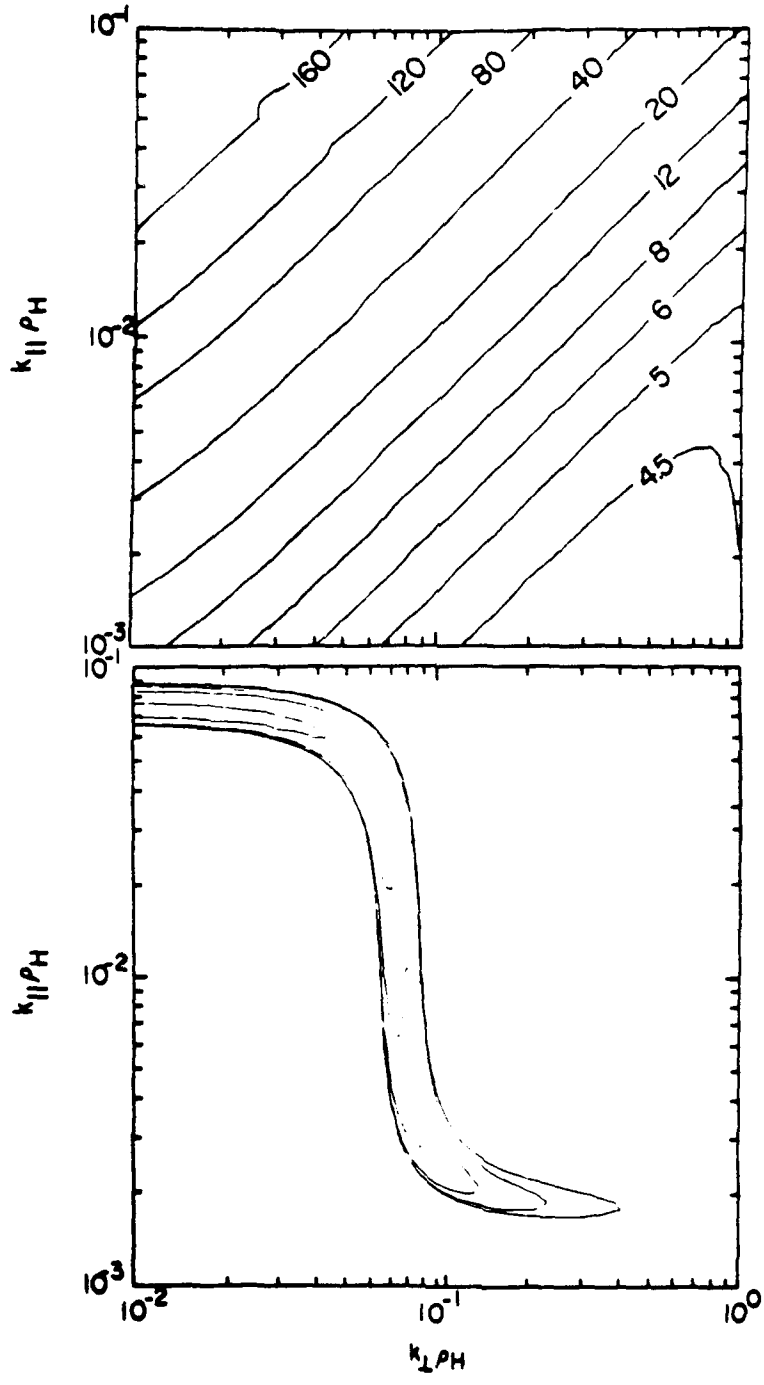

Figure 1. Linear calculation of resonance-cone frequency and growth rate. The top panel presents the real part of the frequency as a function of $k_\perp$ and $k_\parallel$ using contours, while the lower panel presents the imaginary part or growth rate.

1 presents the results of the instability calculation at an altitude of a few thousand kilometers, using a representative combination of plasma populations: a cool ionospheric electron component of density 130 cm^{-3} and a temperature of 1 eV; a combination of three warm electron components to represent an approximate power law flux, $j \sim E^{-1}$, between 10 eV and 1000 eV, with a total density of about 1.6; the auroral electron component of density 0.05, temperature 100 eV, drifting with an energy of 4000 eV; and finally a cool proton component of temperature 1 eV. The top panel gives the real part of the frequency plotted using contours of constant frequency as a function of $k_{\parallel}\rho_i$ and $k_{\perp}\rho_i$. The contours are labeled with the corresponding frequencies, expressed as a multiple of the ion gyrofrequency. The straight-line nature of the contours in the center of the plot shows the essential dependence of the frequency on the angle of propagation, as discussed in the previous subsection. Near parallel propagation we see the plasma-frequency plateau ($\omega_p = 180\Omega_i$), with a slight frequency perturbation due to the instability. Near perpendicular propagation, we find the lower-hybrid plateau ($\omega_{LHR} = 4.2\Omega_i$), modified by the thermal correction near the border of the figure. In the lower panel, the contours of positive growth rate as a fraction of the ion gyrofrequency are spaced logarithmically, two per decade from 0.001 for the outermost contour up to 1.0 at the peak. The growth rate contours approximately follow lines of constant $\omega/k_{\parallel}$, due to the Landau resonance that excites the instability. (We see this by noting the horizontal contours in the two frequency plateau regions, and the vertical contours in the intermediate region.) From the larger growth rates at higher frequency, one might infer that the spectrum of auroral hiss should be dominated by emissions near the plasma frequency. That this is not the case is due to the fact that the instability is a convective one, which in the auroral-arc geometry has great consequences for the form of the auroral hiss spectrum.

C. Convective Saturation and the Auroral Hiss Spectrum

The geometry of an auroral arc implies that the source of free energy for the excitation of auroral hiss is narrowly confined in latitude, but can be extended along the geomagnetic field line, following the trajectories of the accelerated auroral electrons. In addition to the structure of the electron beam, the background plasma in the vicinity of auroral arcs is often structured, too; characteristically, a field-aligned density depletion or cavity is observed, oriented along the auroral field lines [26]. This structure affects the propagation of the resonance-cone waves excited within the arc, and can affect the resonant absorption of the waves by the ambient plasma.

The consequences of the geometry of the precipitation region and the propagation of the auroral-hiss waves through the inhomogeneous ionosphere were pointed out by Maggs [27; 28]. Waves near the electron plasma frequency, with wave vectors nearly aligned with the geomagnetic field, have

group velocities nearly perpendicular to the field line and so can propagate quickly out of the auroral arc, limiting their amplitude. The group velocities of waves near the lower hybrid frequency, on the other hand, are directed nearly along the magnetic field line, allowing these waves to stay in resonance longer and possibly grow to amplitudes at which nonlinear effects are important for saturation. Using a ray-tracing calculation, Maggs showed that many of the features of the auroral hiss spectrum could be explained by the convective beam amplification of incoherent whistler radiation as it propagates through the inhomogeneous ionosphere.

The basic assumption of the ray-trajectory method is that the wavelength must be short compared to the distance over which the refractive index changes appreciably [17]. In a time-independent medium where the geometrical-optic assumption above applies, the path along which the energy of a stable wave propagates is described by the set of equations

$$\frac{d\boldsymbol{x}}{dt} = -\frac{\partial\varepsilon/\partial\boldsymbol{k}}{\partial\varepsilon/\partial\omega} = \frac{\partial\omega}{\partial\boldsymbol{k}} = \boldsymbol{v}_g\,, \qquad \frac{d\boldsymbol{k}}{dt} = \frac{\partial\varepsilon/\partial\boldsymbol{x}}{\partial\varepsilon/\partial\omega} \tag{10}$$

[17]. Here the first equation describes the path through space-time whose tangent is the group velocity of the wave, while the second equation describes the change in the wave vector which is necessary so that the dispersion relation for a locally homogeneous plasma, $\varepsilon(\boldsymbol{k},\omega,\boldsymbol{x})=0$, is satisfied everywhere along the ray path for a wave whose frequency stays constant.

Let us consider the propagation of a resonance-cone wave excited at high altitude propagating toward the Earth in the auroral density cavity, with density gradients along the field line towards the Earth and transverse (in the latitudinal direction) in both directions away from the density minimum at the center of the cavity. As the wave propagates toward the Earth, the parallel component of its wave vector falls to keep the wave on the resonance-cone of the cold-plasma dispersion relation, until the local lower-hybrid resonance frequency has risen to meet the wave's frequency and $k_\parallel$ falls to zero. At this point the wave will be reflected, although the description of this process requires a full-wave treatment, because the assumptions of ray-tracing will have failed before this point, when the wave's wavelength became so long that the geometrical optics approximation was violated. Propagation in the transverse direction is marked by a tendency for the resonance-cone waves to be refracted towards high density, or out of the depleted-density cavity; as the waves propagate transversely into increasing density, $k_\perp$ increases until the resonance is reached where ω equals ω_{LHR}. At this point the wave will be absorbed. Again, because refractive characteristics of the medium are changing rapidly at this point, a full-wave treatment of propagation is needed to describe the situation accurately. The phenomena of absorption at the lower-hybrid resonance remain poorly understood; in addition to the need for a kinetic description, the multiple Bernstein-mode branches nearby in the dispersion relation make the description of possible linear mode conversion

processes a nightmare [29].

The transverse structure of the inhomogeneous electron beam in the auroral arc can cause the dielectric function to change rapidly in space, too, modifying the growth of the resonance-cone waves. One way is through the "de-tuning" of the Landau resonance caused by the shear in the magnetic-field geometry produced by the current generated by the auroral electron beam. A WKB analysis of the wave equation and its turning points [30], however, shows for the appropriate scales and parameters of the auroral arc situation that the excitation of resonance-cone waves there is little affected by non-local effects.

The waves excited by the auroral beam are subject to the influences of both the parallel and perpendicular density gradients, to differing degrees depending on their propagation directions and thus their frequencies. Fig. 2 illustrates four ray trajectories for waves of different frequencies. These four rays start with $k_\perp$ oriented along the arc, (in, say, the East-West direction), but due to the transverse density gradient acquire a component of $k_\perp$ perpendicular to the arc (the North-South direction), and begin propagating out of it. The highest frequency wave propagates transversely out of the auroral arc soonest because its group velocity is directed more nearly perpendicular to B. The ends of the trajectories are depicted with dashed lines to remind us that the geometrical-optic assumption of the calculation begins to fail in that portion of the trajectory. As a wave propagates along its path, its phase velocity changes, so it can fall into or out of resonance with the auroral beam, as well as be convected out of the auroral arc. When the amplitude of the auroral hiss is weak and does not perturb the plasma, Maggs [27] showed how to use ray-tracing calculations to predict the spectral density of the auroral hiss at a point in space for a given frequency. The calculation is performed by integrating along a ray path the whistler noise emitted at each point and amplified in its propagation along the path, and then summing over all ray paths passing through the observation point. The formula is

$$P(\omega, k_\parallel, s_{obs}) = \int E\, F \exp\left[2 \int_{s_{obs}}^{s'} \frac{\gamma}{v_g} ds''\right] ds' \qquad (11)$$

where E is the incoherent emission rate and F is a geometric factor resulting from the divergence of ray paths. In the exponential amplification factor, the growth rate γ is calculated using a detailed model of the auroral electron flux, while the group velocity v_g and the path s are calculated using a model for the plasma in the auroral region. In a series of studies, Maggs and Maggs and Lotko [31] have shown that the features of the observed auroral hiss spectrum can be explained by this model. The work culminated in a study [32] in which a detailed fit to an observed hiss spectrum was made using simultaneous rocket data for the electron flux. Because the plasma density

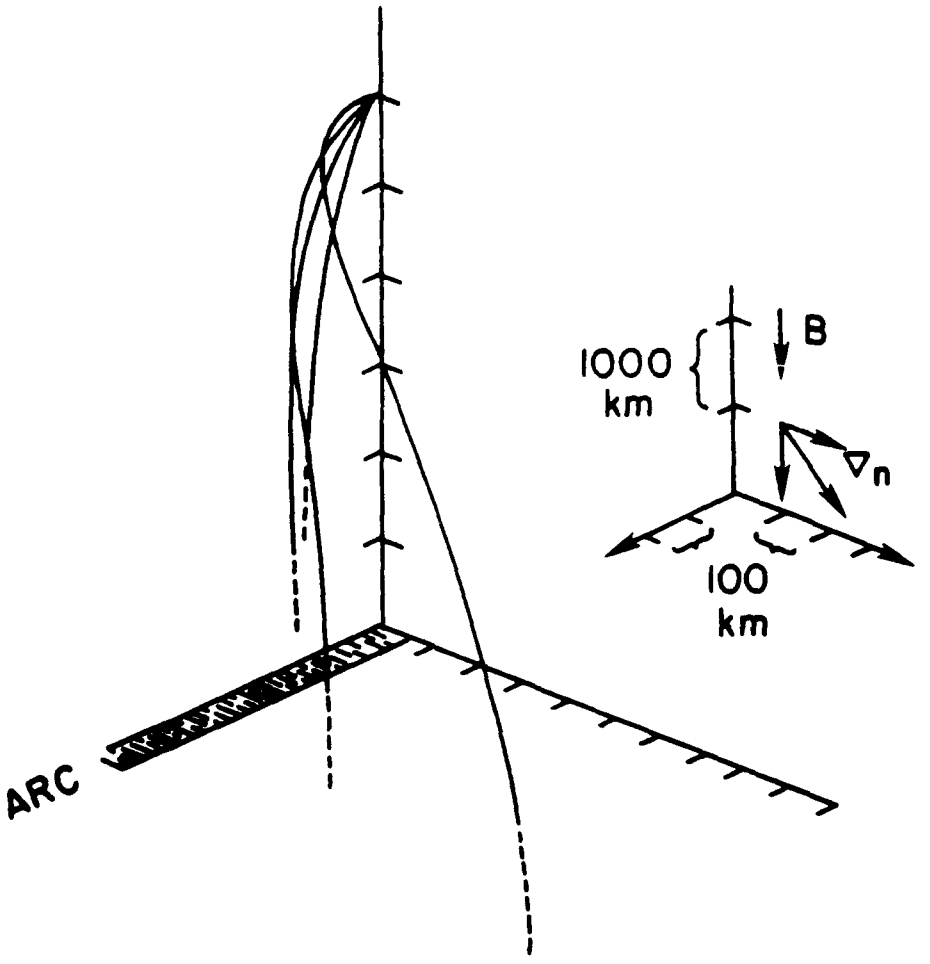

Figure 2. One view of a three-dimensional perspective plot of the trajectories of four resonance-cone waves, with frequencies of 0.1, 0.2, 0.4, and 0.7 of the plasma frequency at the altitude at which they were launched. The highest frequency mode is the one which propagates farthest from the arc. The scale of the plot and the orientation of the plasma density gradient are shown in the inset.

profile and composition cannot be measured along the entire length of any ray path, the plasma profile could not be specified by observation. It was found, however, that a reasonable choice for the plasma profile produced a theoretical hiss spectrum which agreed well with the observed spectrum, predicting both the frequency of the spectral peak at a few times ω_{LHR}, as well as the peak intensity and spectral shape.

It is expected that when the intensity of the hiss is high enough [33], quasilinear modification of the electron beam through wave-particle interaction with the hiss will become important. One way to address this problem is to formulate a set of equations describing the evolution of the parameters of a beam population subject to wave-particle interaction with the waves the beam excites as well as the other influences on the beam [34]. Another approach is to follow the evolution of a beam-plasma system self-consistently using a plasma simulation. We will follow the latter approach in the next section as we begin to explore the consequences of wave-particle interaction with intense auroral hiss.

III. LOCAL VELOCITY DIFFUSION THEORY

Let us first examine the wave-particle interaction process in the simpler situation of a homogeneous medium. With a basic understanding of the physics involved in the particle heating process, we will then turn in the next section to the treatment of ion heating in the more complicated geometry of the suprauroral region, in which auroral hiss turbulence, the inhomogeneous geomagnetic field, and possible parallel electric fields all play a role in determining the observed particle fluxes. In the presence of a turbulent electric field spectrum, the resonant (irreversible) effect on the ion velocity distribution function f is adequately described by a diffusion equation [35],

$$\frac{\partial f}{\partial t} = \frac{\partial}{\partial \boldsymbol{v}} \cdot \left[\boldsymbol{D} \cdot \frac{\partial f}{\partial \boldsymbol{v}} \right]. \tag{12}$$

The velocity diffusion tensor $\boldsymbol{D}$ depends on the spectral density of the electric-field turbulence as a function of frequency and wave-vector. If we specialize to the study of ion interactions, and use the unmagnetized trajectory approximation, we have

$$\boldsymbol{D} = \left[\frac{q}{m} \right]^2 \int \frac{d\omega}{2\pi} \int \frac{d^3k}{(2\pi)^3} \, \frac{\boldsymbol{kk}}{k^2} \, |E|^2(\boldsymbol{k},\omega) \, \pi \, \delta(\omega - \boldsymbol{k} \cdot \boldsymbol{v}) \tag{13}$$

where q and m are the ion charge and mass, ω is the frequency, $\boldsymbol{k}$ is the wave vector, and $|E|^2(\boldsymbol{k},\omega)$ is the spectral density of the magnitude of the electric field, which is assumed to be electrostatic in nature. Observations of auroral hiss tell us something about the electric-field spectral density which allows us to simplify this picture. The largest amplitudes of the fields are found at frequencies which are only a few times larger than the lower-hybrid resonance frequency, ω_{LHR}. The whistler resonance-cone dispersion relation tells us that the wave vectors of these waves are directed nearly perpendicular to the geomagnetic field. Thus, the largest contribution to the integral over the spectral density for $\boldsymbol{D}$ comes for the perpendicular component $D_\perp = \boldsymbol{k}_\perp \cdot \boldsymbol{D} \cdot \boldsymbol{k}_\perp / k^2$. This explains the essentially transverse heating of the ions

observed in ion conic events, and means that we can write the local evolution equation for the ion velocity distribution keeping only the perpendicular contribution

$$\frac{\partial f}{\partial t} = \frac{1}{v_\perp}\frac{\partial}{\partial v_\perp}\left[v_\perp D_\perp \frac{\partial f}{\partial v_\perp}\right] \tag{14}$$

where

$$D_\perp = \left[\frac{q}{m}\right]^2 \int \frac{d\omega}{2\pi} \int \frac{d^3k}{(2\pi)^3}\ \frac{k_\perp^2}{k^2}\ |E|^2(\boldsymbol{k},\omega)\ \pi\ \delta(\omega - \boldsymbol{k}\cdot\boldsymbol{v})\,. \tag{15}$$

Note the delta function in the integrand, imposing a resonance condition that states that the only waves which will cause ions of velocity v to diffuse in velocity are those waves for which the projection of the phase velocity in the direction of v equals the ion speed.

If we attempted to use an auroral-hiss spectrum predicted using local linear excitation, the resonance requirements would pose a great difficulty. The linear excitation of auroral hiss is achieved through a Landau resonance with the accelerated auroral electrons, whose velocities (corresponding to energies of 1 keV or more) serve to give us an estimate of the parallel phase velocities of the waves. By exciting oblique modes, whose wave vectors perpendicular to B are much larger than their parallel components, we reduce the transverse resonant velocity by a factor of the order of the square root of the mass ratio, $\omega/k = (\omega/k_\parallel)(k_\parallel/k) \simeq u_{b\parallel}\cos\theta$, but that is not enough. If we consider the phase velocities of linearly excited resonance-cone waves of frequency about twice ω_{LHR}, we find that they propagate at an angle given by $\cos^2\theta = 3m_e/m_i$. With an electron beam of energy 1 keV, this corresponds to an ion energy of 3 keV. There are very few ions of this energy in the undisturbed ionosphere, where the temperature is of the order of 1 eV. This difficulty is resolved when we recognize that a number of processes which act on the waves after their excitation tend to reduce their phase velocities. Propagation of the resonance-cone waves through a transverse density gradient toward the lower-hybrid resonance can reduce the phase velocities of the waves, as will linear mode conversion at the resonance, and there is also evidence (described below) for nonlinear mode-mode coupling processes which can effectively aid the ion acceleration process by generating short wavelength modes. To study the nonlinear evolution of the electron beam and the heating of the ambient plasma in a self-consistent way, we performed plasma simulations of the phenomena.

A. Plasma Simulations

To study the generation of the turbulence and the resulting ion and electron acceleration, we simulated the phenomena using an electrostatic particle model of the plasma [36]. The suprauroral situation beneath a field-aligned potential drop was modeled by allowing a weak, energetic (1 keV), warm (100 eV) electron beam traveling along the magnetic field to destabilize a cool (1 eV) electron-ion plasma. All species are represented initially as Maxwellian velocity distributions.

We begin with one-dimensional simulations [6], where we can study waves propagating at only one angle with respect to the magnetic field. To study the waves near the peak of the auroral hiss spectrum, we choose the angle of our simulation direction to be nearly perpendicular to $\boldsymbol{B}$, $\hat{\boldsymbol{k}} \cdot \hat{\boldsymbol{B}} = \cos\theta \sim \sqrt{m_e/m_i}$, allowing waves near the lower hybrid resonance frequency to be excited. (We of course cannot choose $\boldsymbol{k}$ to be exactly perpendicular to $\boldsymbol{B}$, or no coupling to the electron beam traveling along $\boldsymbol{B}$ would be possible.)

As in our analysis above, we treat the ions as unmagnetized in the simulation, although runs with magnetized ions showed basically the same results. For the electrons we employed the guiding-center drift approximation [37]. In a one-dimensional model, particle cross-field drifts are out of the plane of $\boldsymbol{k}$ and $\boldsymbol{B}$; in this case an electron's guiding-center velocity in the $\boldsymbol{k}$ direction is simply the projection in that direction of its velocity along $\boldsymbol{B}$, if the small polarization drift is neglected. With this approximation, the acceleration of a guiding center in the $\boldsymbol{k}$ direction is $q_e E(x,t)\cos^2\theta/m_e$, implying that the electron guiding center can be treated as a particle moving in the $\boldsymbol{k}$ direction with an effective inertia $m_e/\cos^2\theta$. At the angles of propagation of lower hydrid waves, the effective inertia of the electron guiding center is comparable to the ion mass, implying that electrons and ions will respond in similar ways to the waves, and incidently permitting realistic mass ratios to be used in the simulation.

As we follow the evolution of the plasma in the simulation, we first find the exponential growth of the waves linearly excited by the instability of the electron beam. Then as this instability saturates, the beam velocity distribution broadens and flattens as energy and momentum are transferred from it to the other species and the waves. The evolution of the fluctuation spectum is illustrated in Fig. 3. In this figure we have plotted $|E|^2(k)$ as a function of k at four times. The first snapshot, in the upper left, is taken during the stage of linear instability and shows the excitation of the waves in the narrow range of wave vectors of the linearly unstable modes. The next snapshot, in the upper right, shows the spectrum just prior to saturation, with a higher amplitude and slightly broader range of k. From this concentration in a relatively small region of k space, we subsequently see the wave energy redistribute itself throughout k space in the following two snapshots on the bottom of the

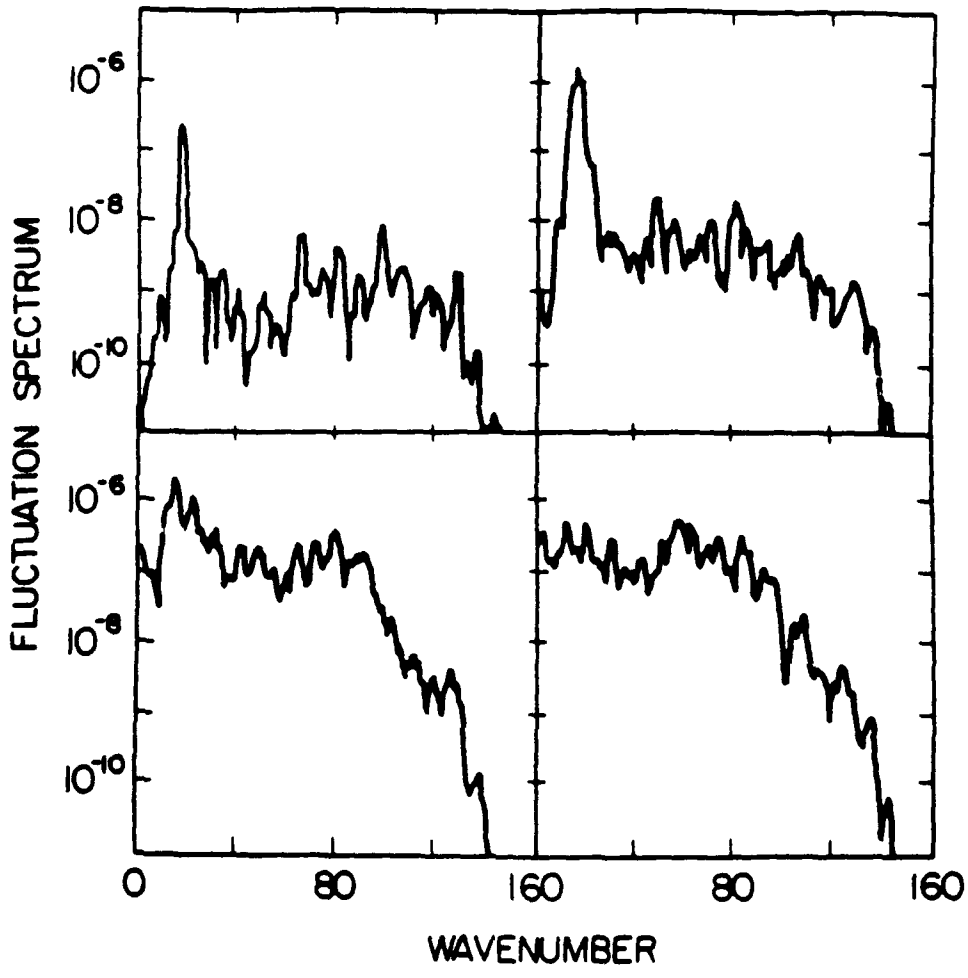

Figure 3. The wave spectrum in a 1-d simulation. In each panel the spectral density of the electric field is plotted as a function of wave vector at a fixed time, in sequence first from left to right, then from top to bottom. The wave vectors are expressed as a multiple of the fundamental wave vector of the simulation length.

figure, through the action of mode-coupling processes. The results at the end is an approximately steady-state spectrum which at smaller k take the Rayleigh-Jeans form, $|E|^2(k) = \text{constant}$.

The evolution of the particle velocity distributions is illustrated in Figs. 4 and 5. Fig. 4 shows two snapshots of the electron distribution of parallel velocities, one showing the initial velocity distribution and the other showing the distribution following saturation of the instability. The ambient (cool) electrons and the beam electrons are shown as separate distributions, although of course for stability analyses, etc., it is the sum of the two for the total

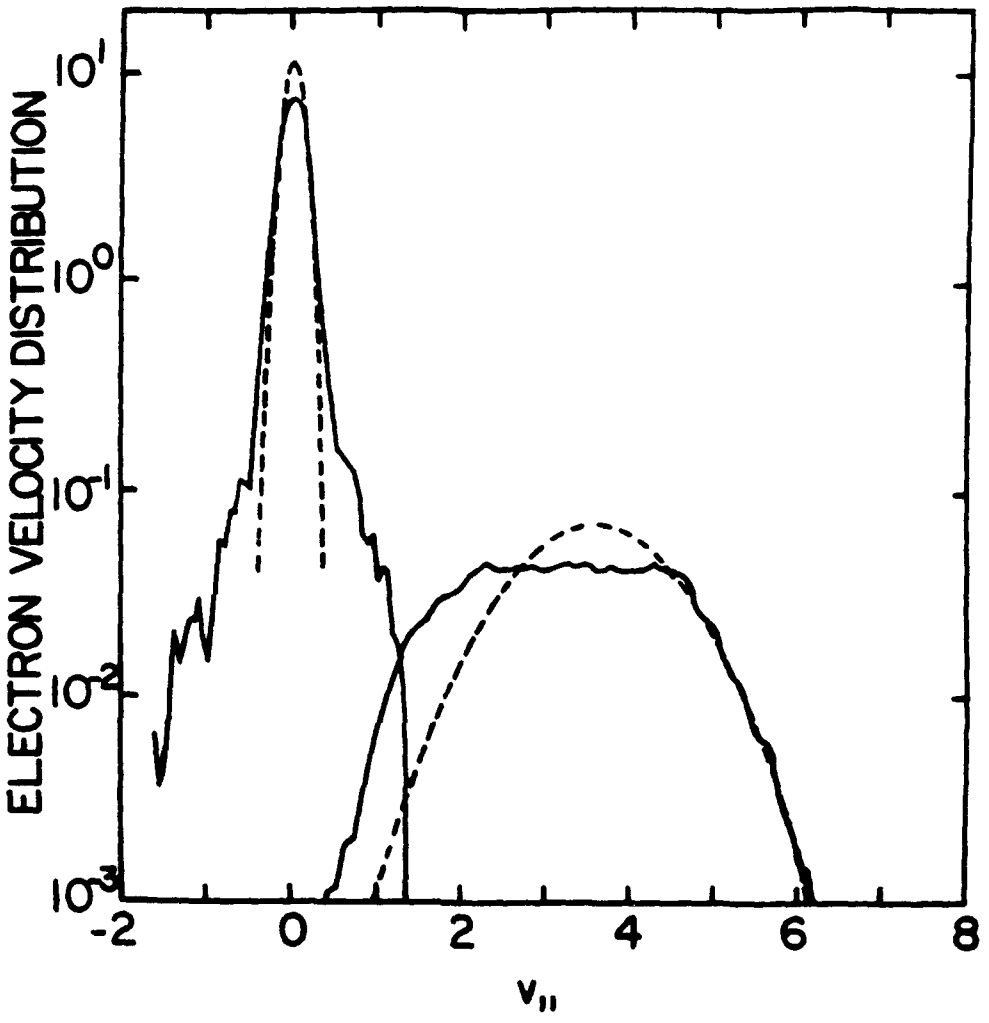

Figure 4. Electron parallel-velocity distribution in a 1-d simulation. The dashed curves give the initial distributions of the ambient and beam electron populations, while the solid curves give the distributions following the end of the simulation.

distribution which is relevant. The figure shows the plateau formation on the unstable beam distribution, but more interestingly, we see that the ambient electrons have been heated in both directions with respect to the magnetic field. The acceleration of electrons in the direction of the beam is not unexpected, because if produced by a resonant interaction with waves, then this heating was produced by waves traveling in the same direction as the beam, just as the waves that are linearly excited by the beam are. It is more surprising that nearly as many electrons were accelerated in the opposite direction, by waves that are traveling in the direction opposite to the beam. Evidence of such parallel acceleration of electrons in the suprauroral region can be

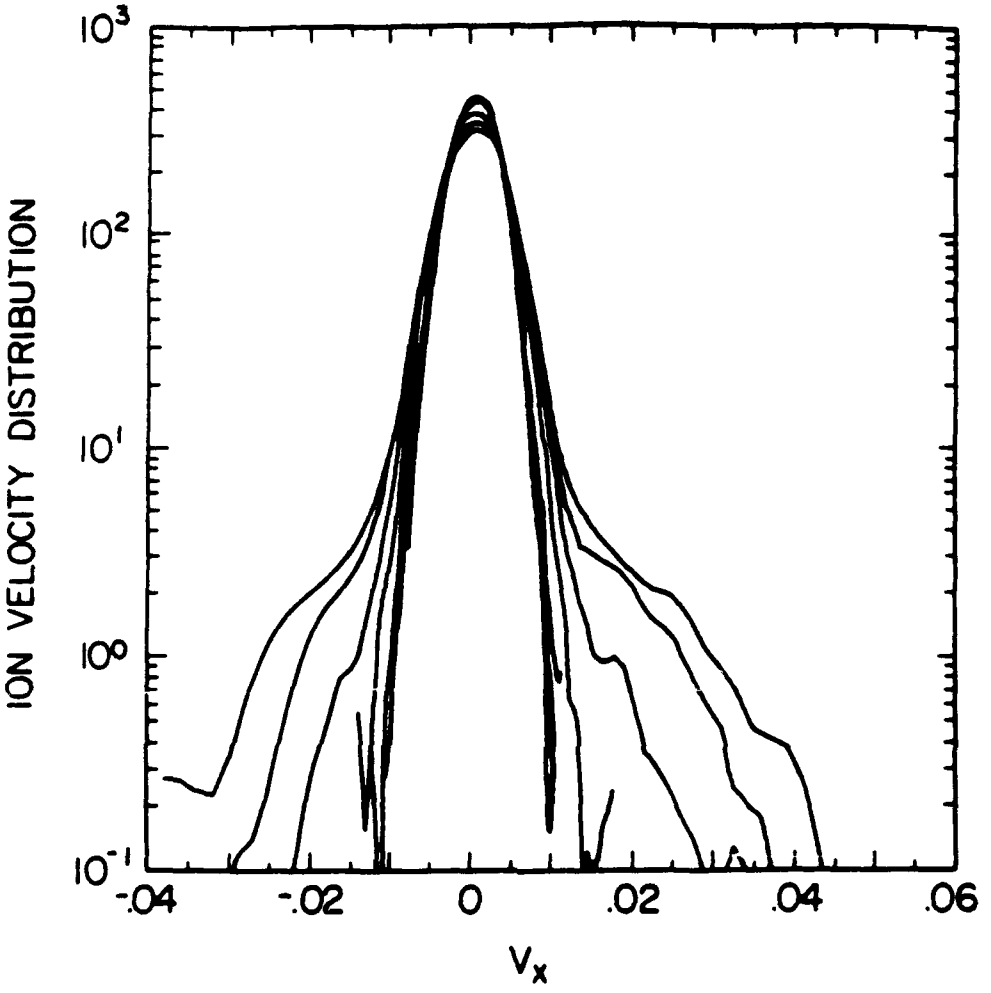

Figure 5. The ion velocity distribution in a 1-d simulation. The multiple curves give the ion velocity distribution at successive times throughout the simulation, showing the formation of the high-velocity tails.

found in the satellite observations of counter-streaming electrons [7], those of type 1, in which there is no indication of acceleration by a steady parallel electric field. An analysis of the magnitude of the phase velocities needed to resonantly interact with the ambient electrons, like the earlier one for the ambient ions, shows that the linearly excited waves would have phase velocities too high to affect the ambient electrons. From these two observations we infer that the nonlinear process we noted in the evolution of the wave spectrum is also aiding the electron acceleration. Fig. 5 shows us that the ion velocity distributions undergoes the formation of similar high-energy tails. Because the ions are unmagnetized, they are accelerated in the direction of

the simulation electric fields, nearly perpendicular to B. In this simulation, where $\cos^2\theta = m_e/m_i$, the ambient electrons and ions are heated by equal amounts.

In the interest of simplicity, this first set of simulations [6] were one-dimensional simulations, in which the waves could propagate in only one direction with respect to the ambient magnetic field. A number of interesting phenomena, however, can be realized only in higher dimension, where a range of propagation angles can be studied simultaneously. For example, both the real frequency and the convective linear growth rates of waves on the whistler resonance-cone dispersion surface are a function of the angle of propagation with respect to the magnetic field. Mode-coupling processes cannot be studied in complete generality in one dimension, because wave vectors are there constrained to be aligned in the same direction. Finally, because electrons and ions interact with different efficiencies to waves of different frequencies, an estimation of the relative effectiveness of electron and ion acceleration requires a simulation in which waves of an appropriate range of frequencies can be excited.

To address these questions, a series of two-dimensional simulations were performed [38]. Full electron dynamics were employed and the ions were treated as magnetized particles, although to compress the dynamical range of frequencies in the simulation a smaller than actual mass ratio was necessary. (For the lightest ions the ratio m_i/m_e was 25.) An angular cutoff was used to simulate the effect of the preferential convective saturation of the parallel propagating modes. It was found that a broadband frequency spectrum, spanning the allowed range of resonance-cone modes, was excited. The nature of the electron and ion acceleration, however, was not qualitatively changed. Figs. 6 and 7 show the electron and ion velocity distributions from a two-dimensional simulation run. A high energy tail in the direction perpendicular to the magnetic field is observed on the ion velocity distribution plotted as a function of energy, while the ambient electrons are heated with the counter-streaming tails as in the one-dimensional simulations. The amount of heating of the two ambient populations did depend on the choice of the resonance-cone angles permitted in the simulation, but because a range of resonance-cone modes were always excited in the two-dimensional simulations, the amount of heating was less sensitively dependent on the angle of propagation than it would have been in a one-dimensional simulation.

In one set of simulations a mixture of ions species was included, using both light ions representing the hydrogen of the ionosphere, and heavy ions representing oxygen. It was found that the heating of the heavier species was negligible. This can be understood as a consequence of the velocity dependent resonance condition for interaction with the waves. The waves are excited at very high phase velocities by the electron beam, and then are subject to mode-coupling processes that reduce their phase velocities. These processes continue until the phase velocities of the waves are sufficiently

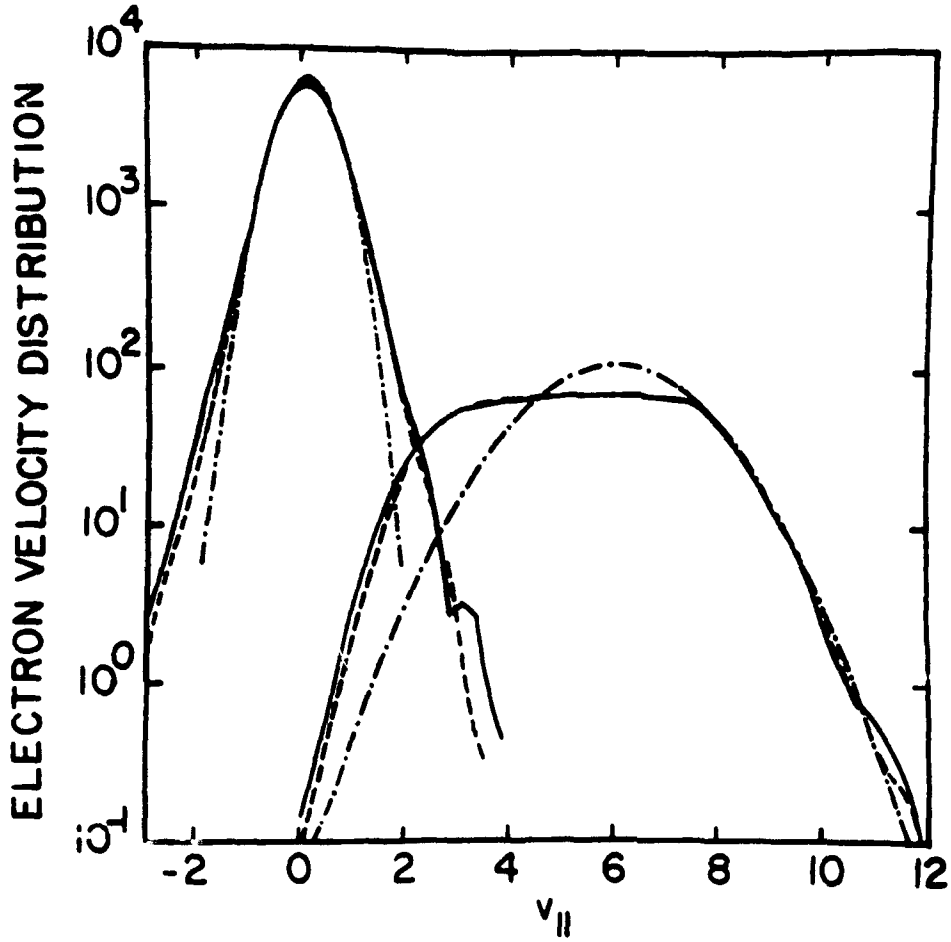

Figure 6. Electron velocity distribution in the 2-d simulation. The dot-dash curves give the initial parallel velocity distributions of the ambient and beam electron populations, while the dashed and solid curves give the distributions at two times near the end of the simulation run.

degraded that the cool ambient plasma species can begin to interact with them. The species of particles with the largest velocities will be able to interact with the waves first. By absorbing the wave energy, this first ion species prevents the waves from undergoing further degradation in phase velocity and isolates the species with smaller velocities, namely species with heavier masses, from interaction with the waves.

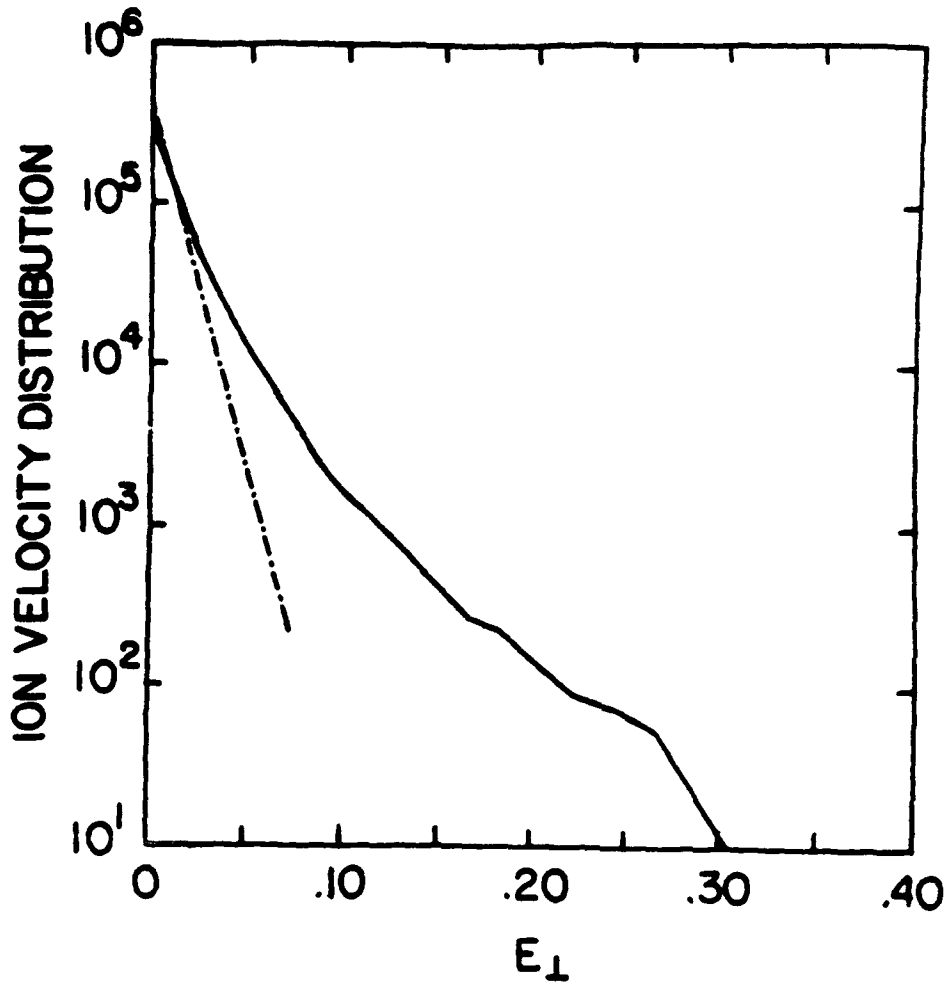

Figure 7. Ion velocity distribution in the 2-d simulation. The dot-dash line gives the initial velocity distribution (a Maxwellian) of the ion population as a function of the perpendicular energy per unit mass, while the solid curve give the distributions near the end of the simulation run.

B. Nonlinear Theory

It is a common observation that in plasma simulations, with their full treatment of nonlinear plasma phenomena, many plasma waves are excited which linear theory would predict to be damped or only weakly growing. Interaction of ions and electrons with such modes at low phase velocities can produce the energetic tails found on the their velocity distributions. One of the first nonlinear processes to act as waves begin to grow in the plasma

involves the coupling of only three (or four) waves. In weak turbulence theory [35] the coupling of three waves requires that the waves satisfy the resonance conditions

$$\omega_0 = \omega_1 + \omega_2 \tag{16}$$

$$\boldsymbol{k}_0 = \boldsymbol{k}_1 + \boldsymbol{k}_2 \tag{17}$$

where $(\omega_0,\boldsymbol{k}_0)$ are the frequency and wave vector of a parent wave, and $(\omega_1,\boldsymbol{k}_1)$ and $(\omega_2,\boldsymbol{k}_2)$ are the corresponding quantities for the two waves into which the parent wave decays. Let us suppose that the parent wave is a lower hybrid wave linearly excited by the electron beam instability. If the sideband wave $(\omega_1,\boldsymbol{k}_1)$ is another lower hybrid wave, then to satisfy the resonance conditions the beat wave $(\omega_2,\boldsymbol{k}_2)$ must be of very low frequency, of the order of the difference in thermal corrections to the frequencies of the two lower hybrid waves. The beat mode may be either a heavily damped acoustic quasimode or the near-zero frequency oscillating two-stream instability [39]. The phase velocities of the sideband modes are (if all three wave vectors are aligned and allowance is made for the two sign possibilities for $\boldsymbol{k}_2$)

$$\frac{\omega_1}{k_1} = \frac{\omega_0 \pm \omega_2}{k_0 \pm k_2} \approx \frac{\omega_0}{k_0 \pm k_2} = \pm\frac{\omega_0}{k_2} \tag{18}$$

If $k_2 \gg k_0$ then ω_1/k_1 can be much smaller than the phase velocity of the parent wave, ω_0/k_0, allowing resonant interaction with the ions and ambient electrons. Note that sidebands can be excited with phase velocities of both signs with nearly equal magnitudes, accounting for the symmetry of the hot tails on the velocity distributions.

A dispersion relation for this nonlinear process can be derived. Details can be found in Ref. [6] and references therein. From this dispersion relation, the wave-amplitude threshold for the decay process can be calculated, as well as the rate of the process when the amplitude of the parent wave exceeds this threshold. Such an analysis of lower hybrid parametric decay under suprauroral conditions has been performed by Koskinen [40]. He reports that decay through nonresonant quasimodes is one of the dominant processes, although other decay routes, such as decay into a lower hybrid mode and an ion Bernstein mode, are possible. He found that the threshold of wave amplitude for decay may be only a few millivolts per meter or smaller, insuring that this mode coupling process can be effective in the suprauroral region.

Visualizing the nonlinear evolution of the plasma wave spectrum in terms of parametric decay processes is a good way to describe the initial stages of the evolution, but as soon as the sideband modes have grown to appreciable magnitude, they too will be susceptible to decay, and a more general approach is necessary. In addition, to verify our interpretation of the simulatio. results we would like to be able to calculate the evolution of the

turbulent spectrum and its effect on the particle populations.

A nonlinear kinetic equation that describes the evolution of the wave spectrum subject to mode coupling effects has been derived. We refer to Ref. [6] for the details of the derivation, but the essence of the calculation can be summarized by saying that we begin with the warm fluid equations for the electron and ion plasma species (for simplicity, since the lower hybrid waves are supported in that approximation). Assuming that the electric field and other quantities consist of separate components oscillating at the lower hybrid and acoustic frequencies, we retain only the dominant nonlinear terms and derive an equation describing the time variation of the amplitude of the lower-hybrid field component. In one dimension, the result is

$$\frac{\partial \tilde{E}}{\partial t} - \frac{i}{2} C_d \frac{\partial^2 \tilde{E}}{\partial x^2} - i\, C_c |\tilde{E}|^2 \tilde{E} = 0 \tag{19}$$

where $\tilde{E}(x,t)$ is the amplitude of the electric field oscillating at ω_{LH}, assumed to vary slowly with time. The spectral density at ω_{LH} is proportional to $|\tilde{E}|^2$. C_c and C_d are coefficients for the coupling and dispersion processes, respectively, expressed in terms of plasma frequencies, temperatures, charges, and masses of the species of the plasma. It is of the same form as the nonlinear Schroedinger equation derived to describe Langmuir turbulence [41]. Perhaps the most fascinating results of the nonlinear Schroedinger equation are the solitary wave solutions (for the envelope of the lower hybrid waves in this case) which it supports. In one dimension, and in the absence of dissipation, these sharply peaked wave packets propagate without alteration because the nonlinear refraction balances the effects of dispersion. With Landau damping present, the formation of solitary waves through the modulational instability of an intense lower hybrid wave is interrupted when the wave energy has spread to wave vectors large enough to become susceptible to damping. To be able to describe the effects of such dissipation on the waves, as well as the resulting effects on the particles, we introduce kinetic effects into the model, following Thomson *et al.*[42]. To introduce Landau damping into the wave equation, we Fourier transform spatially and add the linear dissipative term.

$$\frac{\partial \tilde{E}_k}{\partial t} = \gamma_L(k)\tilde{E}_k - \frac{i}{2} C_d k^2 \tilde{E}_k + i\, C_c \sum_{k',k''} \tilde{E}_{k'} \tilde{E}^*_{k''} \tilde{E}_{k+k''-k'} \tag{20}$$

where the linear damping or growth rate is given by the quasilinear expression

$$\gamma_L(k) = \frac{\pi}{2} \omega_{LH} \sum_s \frac{\omega_{ps}^2}{k^2} \frac{\partial f_s}{\partial v}\Big|_{v=\omega(k)/k} . \tag{21}$$

The effect of the wave-particle interaction on the particles is described by the resonant quasilinear diffusion equation

$$\frac{\partial f_s}{\partial t} = \frac{\partial}{\partial v}\left[D_s \frac{\partial f_s}{\partial v}\right] \tag{22}$$

where in one dimension the velocity diffusion coefficient is

$$D_s(v) = \left[\frac{q_s}{m_s}\right]^2 \int \frac{dk}{2\pi} |\tilde{E}_k|^2 \pi \delta(\omega(k) - k\,v) \quad . \tag{23}$$

The set of equations, Eqs.(20) and (22), with Eqs.(21) and (23), comprise our theoretical model, a generalization of the quasilinear equations to include the effects of mode coupling. We use this set of equations now to study the saturation of the bump-on-tail instability that excites the intense long-wavelength lower hybrid modes. The calculation begins with initial conditions corresponding to those with which we started the one-dimensional particle simulations, and the equations are integrated forward in time to study the evolution of the system. Fig.8 compares the evolution of the total lower hybrid wave energy in the one-d simulation and in the theoretical model. The dashed curve in the figure gives the evolution of the electrostatic energy in the simulation, while the solid curve gives the result from the theoretical model. We experimented with the model by removing the mode-coupling term from the equation; the dot-dash curve gives the results for the wave energy in this case. We see at initial times the exponential growth in energy associated with the linear instability. Once the threshold for mode-coupling processes has been exceeded, a turbulent steady-state in the waves is soon reached, while energy is transferred to the particle populations (although their energies are not shown here). The level of energy in the saturated state is very similar to the level observed in the simulation. In the solution without the mode-coupling term, on the other hand, the wave energy continues to grow, although the growth rate slows as the beam velocity distribution plateaus at the phase velocities of the fastest growing modes. Without the mode-coupling term, the energy transferred to the ambient particle populations is negligible.

The detailed ion velocity distribution in the mode coupling calculation shows the high velocity tails characteristic of the particle simulation. Fig. 9 shows a snapshot of the ion velocity distribution following the saturation of the instability, illustrating the formation of the tails. The solid curve gives the result from the theoretical model, while the dashed curve in the figure gives the comparable result from the particle simulation. We conclude from these comparisons that our theoretical model with mode-coupling does satisfactorily describe the phenomena observed in the particle simulations. While the simple quasilinear velocity diffusion model is adequate to describe the effect of the turbulence on the particles, a full nonlinear treatment is necessary to describe the evolution of the turbulence.

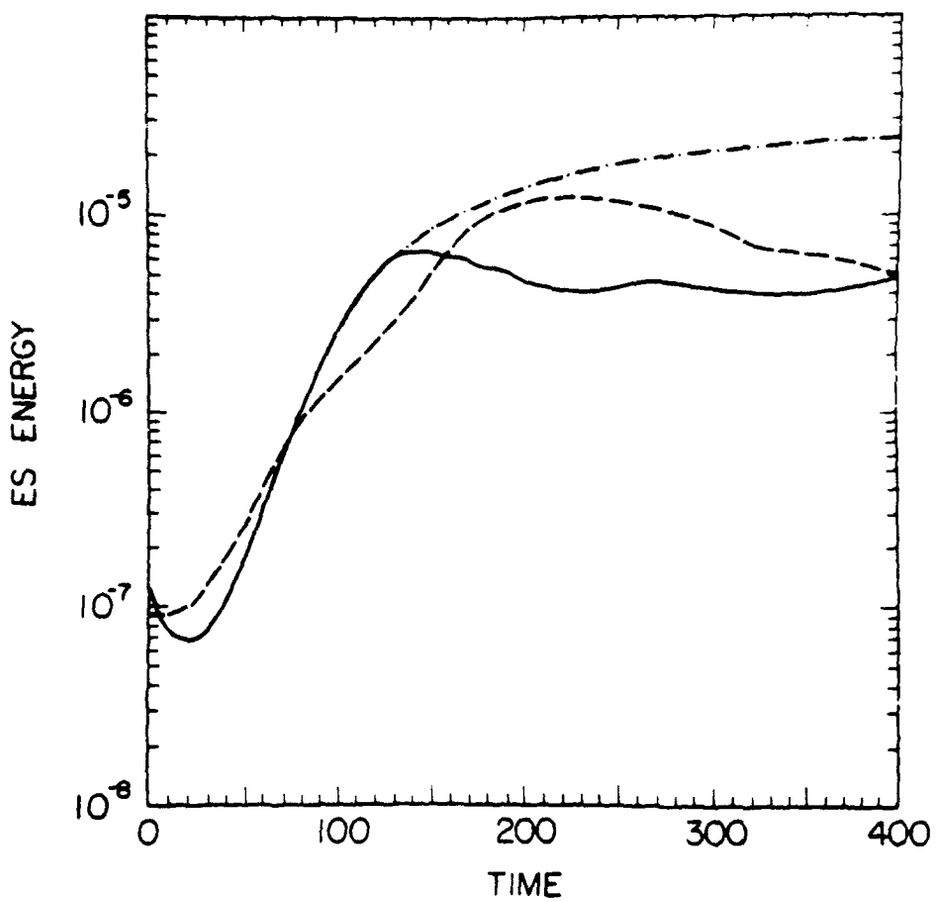

Figure 8. The energetics of the lower-hybrid waves in the theoretical model. The dashed curve gives as a function of time the electrostatic energy of the waves in a 1-d particle simulation run, while the solid curve gives the prediction of this quantity from our theoretical model. The dot-dash curve gives the theoretical result when the mode-coupling term is removed from the model. Time is in units of ω_{LH}^{-1}.

C. Diffusion Models

Although the simulation results can serve as a qualitative guide to the phenomena observed in space, the situation in the auroral region is more complicated than we can practically study using simulations. Important phenomena occur on a wider range of spatial and tempora! scales than self-consistent numerical models can accomodate simultaneously. For success in modeling the observations we must hope to extract from the simulations a

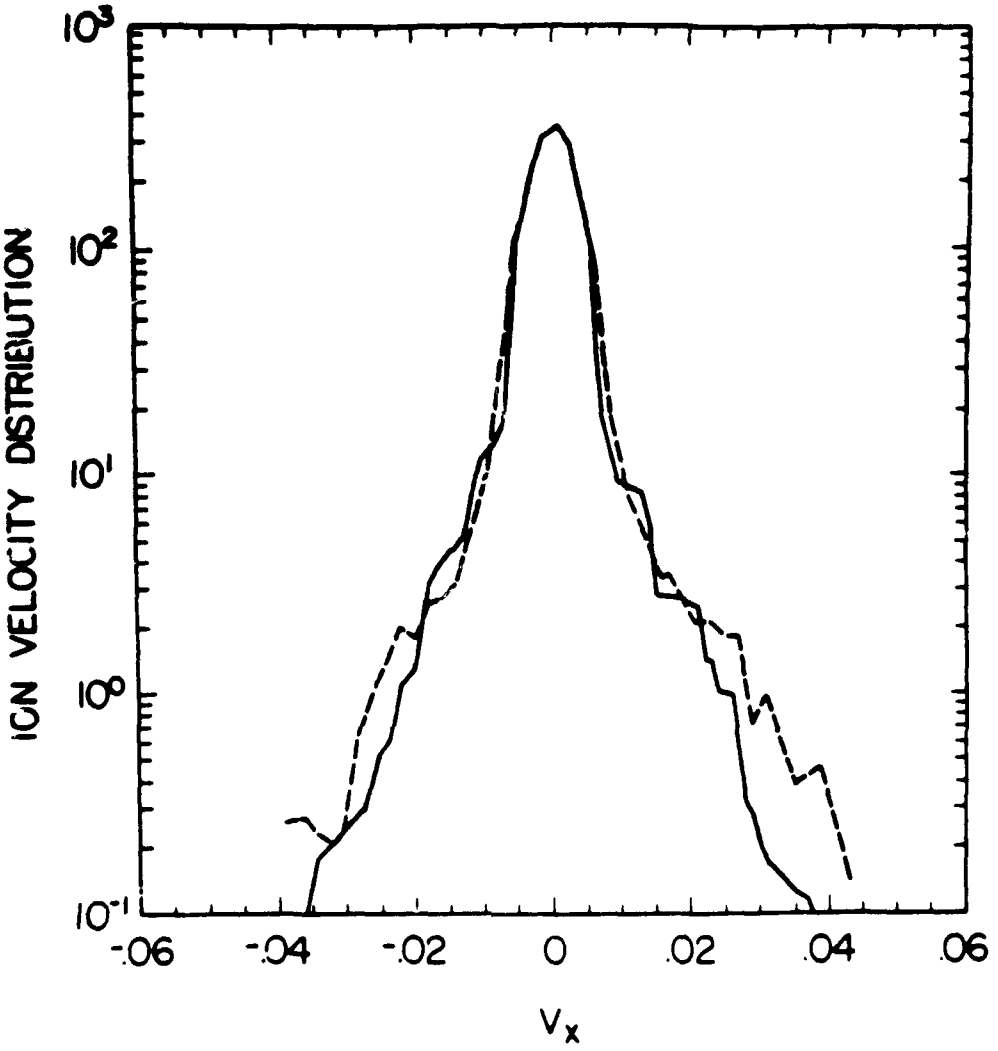

Figure 9. The ion velocity distribution in the theoretical model. The dashed curve gives the ion velocity distribution at the end of a particle simulation run, while the solid curve gives the theoretical prediction for the ion distribution.

description of the micro-physics of the wave-particle interaction, to incorporate into a model of the larger scale variations in the suprauroral region. For the heating of the ambient particle species, the model is the velocity diffusion equation, to which the simulations provide a model for the aspects of the spectral density of the electric fields which cannot be measured directly.

Because of the variety of circumstances to be found in the suprauroral region, we must also expect to employ wave observations in our specification

of particle heating rates to insure the applicability of our models. Satellites rarely measure wavevector information for the electric field spectral density: the observed spectral density of any component of the electric field is a function only of frequency (which unfortunately includes the possibility of aliasing of spatial structure if the spacecraft is moving through an inhomogeneous medium). Thus, if the satellite antenna system were equally responsive to all wavelengths, the spacecraft receiver would measure

$$\int \frac{d^3k}{(2\pi)^3} |E|^2(\boldsymbol{k},\omega) = |E|^2(\omega) \; . \tag{24}$$

One can obtain a rough order of magnitude of the transverse velocity diffusion rate by using the observed value of $|E|^2(\omega)$ at some frequency near the lower hybrid frequency in the order-of-magnitude evaluation of Eq.(15)

$$D_\perp \sim \left[\frac{q}{m}\right]^2 |E|^2(\omega) \tag{25}$$

and this is frequently all that can be done to estimate the diffusion rate. One cannot, however, describe the velocity dependence of $D_\perp$ using a description this crude, and the high-energy tail structure of the particle fluxes seen both in space and the simulations requires a velocity dependent diffusion rate. This is the point where our simulation results can suggest the form for a model of the unobservable wave vector specta of the resonance-cone waves.

To use the frequency-spectrum observations to estimate the velocity diffusion rate, let us first condense all our ignorance of the spectral density into one function, the distribution of spectral density with respect to the wave vector, given a specified frequency, $S(\boldsymbol{k} \mid \omega)$

$$|E|^2(\boldsymbol{k},\omega) = |E|^2(\omega) \; S(\boldsymbol{k} \mid \omega) \tag{26}$$

where

$$\int \frac{d^3k}{(2\pi)^3} S(\boldsymbol{k} \mid \omega) = 1 \; . \tag{27}$$

For frequencies near the lower hybrid frequency, we can write the most important functional dependence of S on $\boldsymbol{k}_\perp$

$$S(\boldsymbol{k} \mid \omega) = S_\perp(\boldsymbol{k}_\perp) S_\parallel(k_\parallel) \; . \tag{28}$$

Although in a turbulent plasma we cannot assume in general that the frequencies and wavevectors of the modes in the plasma satisfy a dispersion relation perfectly, for this application this assumption does not cause a great error, and we write

$$S_\parallel(k) = 2\pi\delta(k - k_{\parallel 0}) \tag{29}$$

where

$$k_{\|0} \equiv k_{\|}(k_\perp,\omega) = \pm\Lambda(\omega)\,k_\perp \tag{30}$$

$$\Lambda^2(\omega) = (1+\omega_{pe}^2/\Omega_e^2)\,\frac{\omega^2-\omega_{LHR}^2}{\omega_p^2-\omega^2} \quad . \tag{31}$$

Let us substitute these expressions into the formula for the transverse velocity diffusion rate

$$D_\perp = \frac{1}{2}\left[\frac{q}{m}\right]^2 \int\frac{d\omega}{2\pi}\,|E|^2(\omega)\int\frac{d^2k_\perp}{(2\pi)^2}\,\frac{(\boldsymbol{k}_\perp\cdot\hat{\boldsymbol{v}}_\perp)^2}{k^2}\,S_\perp(k_\perp)\,\delta(\omega-\boldsymbol{k}_\perp\cdot\boldsymbol{v}_\perp-k_{\|0}v_\|) \tag{32}$$

For waves near the lower hybrid frequency, $k_{\|0}$ is much less than $k_\perp$, and the resonance condition is essentially one on the perpendicular velocity. If we assume that $S_\perp(\boldsymbol{k}_\perp)$ is isotropic in the plane perpendicular to B, we can do one more integration of this expression, and we get

$$D_\perp = \frac{1}{2}\left[\frac{q}{m}\right]^2 \int\frac{d\omega}{2\pi}\,\frac{|E|^2(\omega)}{1+\Lambda^2}\,\frac{\omega^2}{v_\perp^2}\int_{\omega/v_\perp}^{\infty}\frac{dk_\perp}{2\pi k_\perp}\,\frac{S_\perp(k_\perp)}{(k_\perp^2v_\perp^2-\omega^2)^{1/2}} \quad . \tag{33}$$

To proceed further, we need a model for $S_\perp(k_\perp)$. Crew and Chang [43] suggested the following form, to describe the general situation where $S_\perp$ peaks near a wave vector k_o

$$S_\perp(k_\perp) \propto \frac{(k_\perp/k_o)^\mu}{1+(k_\perp/k_o)^\nu} \quad . \tag{34}$$

In this expression the free parameters are the wave vector k_o and the two spectral indices μ and ν. For the normalizing integral, Eq.(27) to be defined, we need $\nu>\mu+3$, and for $D_\perp$ to be nonsingular, $\mu>0$. This form, it turns out, fits the body of the wave vector spectra measured in the one-dimensional simulations quite well, and we will use it to parametrize the wave vector spectra to calculate the velocity diffusion rate. Crew and Chang [43] next showed that to a good approximation, the diffusion coeficient one obtains using this form has the following velocity dependence

$$D_\perp(v_\perp) \propto \frac{(v_\perp/v_o)^{\nu-\mu-3}}{1+\eta(\mu,\nu)\,(v_\perp/v_o)^{\nu-\mu}} \quad . \tag{35}$$

Here η is a numerical constant, dependent on μ and ν, and v_o is a characteristic velocity near which the diffusion rate is a maximum; if the frequency spectrum peaks near a frequency ω_o, then $k_o = \omega_o/v_o$. We expect that v_o is of the order of the perpendicular phase velocity of the waves excited by the auroral electron beam, or smaller if mode-coupling processes have been effective in transferring wave energy to shorter wavelength, lower phase-

velocity waves. At $v_\perp$ goes to zero, $D_\perp$ goes to zero as $v_\perp^{\nu-\mu-3}$; at velocities much larger than v_o, $D_\perp$ falls as $v_\perp^{-3}$.

The peaked nature of $D_\perp$ reflects the way in which wave-particle interaction leads to the formation of high-energy tails on the velocity distributions, rather than, say, simple bulk heating. Because $D_\perp$ falls to zero at small velocity, the bulk of the velocity distribution is unaffected by interaction with the waves. At higher velocity $D_\perp$ begins to become appreciable, and the diffusion process begins to affect particles in the distribution. Because there are initially more particles at lower velocity than at higher velocity, the net flux in velocity space is toward higher velocities, leading to the formation of high-energy tails. Crew and Chang [43] demonstrated this by developing an asymptotic method for analytically solving the velocity diffusion equation with the peaked diffusion coefficient and presenting the solutions.

IV. ION CONIC FORMATION

We must now consider how our local description of particle heating by wave-particle interaction with intense auroral hiss can be applied in the suprauroral region, where ion conics and counter-streaming electrons are observed in the vicinity of auroral arcs. The basic point of view for our studies of this problem is the test-particle approach, in which the motion and heating of particles are studied in specified global models of the geomagnetic field, the steady electric fields, and the spectral density of the turbulent fluctuating electric fields. The justification for this approach lies in the expectation that the perturbation caused by these particles will be small because the number of ionospheric ions and electrons which are affected by this turbulence will be small, being those particles which can meet the velocity resonance conditions for interaction. We will first outline the method of the model, and then go on to describe several applications.

In the absence of wave-particle interactions, the evolution along a goemagnetic field line of the ion velocity distribution, f, would be described by the Liouville equation [44]. If we use the guiding center approximation, the equation is the following:

$$\frac{df}{dt} \equiv \frac{\partial f}{\partial t} + v_\parallel \frac{\partial f}{\partial s} + \frac{1}{2B}\frac{dB}{ds}\left[-v_\perp^2 \frac{\partial f}{\partial v_\parallel} + v_\parallel v_\perp \frac{\partial f}{\partial v_\perp}\right] + \frac{q}{m} E_\parallel \frac{\partial f}{\partial v_\parallel} = 0 \quad (36)$$

where s is a coordinate denoting position along a geomagnetic field line, B is the magnitude of the geomagnetic field, and q and m are the charge and mass of an ion. We ignore possible cross-field drifts caused by a perpendicular electric field, $E_\perp$, and only retain the effects of a possible parallel field, $E_\parallel$. The ion motion is then constrained to lie along a field line. The ions move adiabatically, conserving their magnetic moment and energy in the static geomagnetic field and parallel electric field. The component of the

gravitational field that lies along B can easily be included together with the parallel electric field, although its effect is less important for the light hydrogen ions of this study than it would be for oxygen conics.

In the presence of a transverse heating process, the effect on the ions of their interaction with the turbulence is adequately described by a diffusion equation,

$$\frac{df}{dt} = \frac{1}{v_\perp}\frac{\partial}{\partial v_\perp}\left[v_\perp D_\perp \frac{\partial f}{\partial v_\perp}\right], \tag{37}$$

where the left-hand side of the equation contains the terms of the Liouville equation and $D_\perp$ is the quasilinear velocity diffusion rate perpendicular to the geomagnetic field obtained in the previous section.

A. The Mean-Particle Equations

Before solving the spatially dependent kinetic equations for the ion distribution function, it is useful to have an estimate of the relevant ranges of energy and pitch angle that will be important in the problem at hand. For such an analysis, a simple model described by the mean-particle equations can be derived from the terms in the kinetic equation. This pair of ordinary differential equations describe the evolution of the perpendicular and parallel energies of a typical particle within the ion distribution. The equations are

$$\frac{dW_\perp}{ds} = \frac{\dot{W}_{\perp turb}}{v_\parallel} + W_\perp \frac{d\ln B}{ds} \tag{38}$$

$$\frac{dW_\parallel}{ds} = -W_\perp \frac{d\ln B}{ds} + qE_\parallel \tag{39}$$

where $W_\parallel = \frac{1}{2}mv_\parallel^2$ and $W_\perp$ are the "typical" parallel and perpendicular energies, respectively. The perpendicular heating rate due to wave-particle interaction, $\dot{W}_{\perp turb}$, is estimated from the right-hand side of the kinetic equation. For example, if we assume that the velocity distribution is Maxwellian and that the diffusion rate $D_\perp$ is independent of velocity, then the appropriate moment of Eq.(14) gives the heating rate $2mD_\perp$. Chang and Coppi [5] used these equations to demonstrate that lower hybrid waves could be an effective heating mechanism for the production of ion conics.

B. The Monte Carlo Method

To predict the form of the distribution function, it is necessary to return to the kinetic equation and solve it in detail. Even in the simplest situation where a steady state solution is sought, the problem is a three dimensional one, with three independent variables position along the field line, perpendicular

velocity, and parallel velocity. In addition, the specified fields in a problem will not necessarily be found in forms that make the problem amenable to analysis. Test-particle simulation techniques offer a flexibile and robust way of attacking such complicated problems. We will solve the kinetic equation for the ion velocity distribution using a Monte Carlo model which was developed to investigate problems of this kind [8]. From an initial distribution in velocity and space, the calculation of the evolution of the distribution proceeds by following the trajectories of a large number of ions with time. Between the velocity perturbations caused by interaction with the waves, it is assumed that the ions travel in the static geomagnetic field with constant energy and magnetic moment.

The wave-particle interactions are taken into account by perturbing the ion velocities with random increments Δv in each small time step, Δt. To see how these perturbations affect the velocity distribution, consider the situation in which the steady fields are absent and the perturbations act alone. If $P_{\Delta t}(\Delta v)\, d^3\Delta v$ is the probability of a change of velocity Δv during a time interval Δt, then the effect of velocity perturbations over Δt on the distribution $f(v,t)$ is the convolution

$$f(v,t+\Delta t) = \int f(v-\Delta v,t) P_{\Delta t}(\Delta v)\, d^3\Delta v \tag{40}$$

If we perform the Fokker-Planck expansion of Eq.(40) for the limit that Δt goes to zero, we recover the local velocity diffusion equation, Eq.(12), if we choose $P_{\Delta t}(\Delta v)$ to be the gaussian distribution with moments

$$<\Delta v> = \nabla_v \cdot \mathbf{D}\, \Delta t \tag{41}$$

and

$$<\Delta v\, \Delta v> = 2\, \mathbf{D}\, \Delta t \ . \tag{42}$$

In the calculation, this probability distribution is sampled using random numbers. To simulate transverse velocity diffusion, the two components of Δv in the plane perpendicular to B are chosen to be gaussian random variables such that $<\Delta v_x> = (v_x/v_\perp)\, \Delta t\, dD_\perp/dv_\perp$, $<\Delta v_y> = (v_y/v_\perp)\, \Delta t\, dD_\perp/dv_\perp$, and $<\Delta v_x^2> = <\Delta v_y^2> = 2D_\perp \Delta t$. The vector Δv is added to the ion's transverse velocity assuming a random orientation with respect to the gyrophase.

Because we are studying the heating and acceleration of ions of ionospheric origin, the initial velocity distribution of the ions is chosen to be a Maxwellian distribution at a characteristic topside ionospheric temperature, 1 eV, and for simplicity we will generally start the particles all at one altitude. As ions pass the observation points, statistics on their velocities are accumulated to calculate the steady state ion velocity distribution at these points. The velocity distribution of the ions at their initial location s_o can be written

$$f(v_\perp, v_\parallel, s_o) = \frac{n_o}{\pi N} \sum_{i=1}^{N} \delta(v_\perp^2 - v_{\perp io}^2)\, \delta(v_\parallel - v_{\parallel io}) \tag{43}$$

where $v_{\perp io}$ and $v_{\parallel io}$ are the initial velocity components of an ion, chosen so that f equals the desired initial distribution, and the density of the N ions is normalized to n_o. After the ions have followed their trajectories to the point s, the velocity distribution at that point can be calculated. It is

$$f(v_\perp, v_\parallel, s) = \frac{n_o}{\pi N} \sum_{i=1}^{N} \frac{v_{\parallel io}}{v_{\parallel i}} \frac{B_s}{B_o} \delta(v_\perp^2 - v_{\perp i}^2)\, \delta(v_\parallel - v_{\parallel i}) \tag{44}$$

where $v_{\perp i}$ and $v_{\parallel i}$ are the components of the ion velocity at s. The weighting factor under the sum is a consequence of the invariance of the parallel particle flux $n(s)\langle v_\parallel(s)\rangle / B(s)$ in a steady state[43]. Physically, the weighting factor expresses two effects: $v_{\parallel io}/v_{\parallel i}$ describes the reduction in phase-space density that occurs when particles get spread out along a field line when $v_\parallel$ changes, while B_s/B_o describes the dilution due to the increasing flux-tube area as B decreases with increasing s. The detailed velocity distribution, Eq.(44), contains more information than we really need or want; the details are condensed by binning the distribution on a 32 by 32 grid in $v_\perp$-$v_\parallel$ space for plotting purposes. Binning according to the magnitude of $v_\perp$ introduces an additional weighting factor of $v_\perp$, which is divided out of the bin occupation numbers to give the phase-space densities which we will be presenting. Velocity moments can also be calculated from f.

C. High Altitude Ion Conic

The first application of the Monte Carlo model presented here will be an ion conic that was observed at high altitude by the S3-3 satellite on day 280, 1976, orbit 718. This conic has been described by Temerin *et al.* [2] and by Gorney *et al.* [22]. The conic is seen in conjunction with VLF hiss, as well as with evidence of parallel acceleration of electrons at energies of 1.6 - 5 keV above the satellite, which was at an altitude of 5700 km. The conic is folded up from perpendicular velocity by about 40°, implying that the region of peak transverse heating was at an altitude of about 3600 km; from the width of the conic it can be estimated that the region of enhanced transverse heating was about 700 km in extent along the field line. This means that virtually all of the transverse heating of the conic occurred at altitudes below the spacecraft, and that the observations at the satellite of the amplitude of the auroral hiss will be of little help in estimating the rate of ion heating. In this case what we can do by modeling the conic is to infer some of the characteristics of the turbulence which would be required to explain the remote heating, and then judge how well these characteristics fit our expectations for them.

To model the heating process, then, we must specify a model for the velocity diffusion rate as a function of perpendicular velocity and position along the field line. For the velocity dependence we choose the rational form given above, Eq.(35), while for the spatial variation, we choose a power law in geocentric distance. We do not make any claims about the uniqueness of this form; rather, one should conclude simply that it is a form that can produce conics with the observed shape. Altogether, the diffusion rate is written

$$D_\perp = \left[\frac{q}{m}\right]^2 S_{E0} \left[\frac{R_E + a_o}{R_E + a}\right]^\alpha \frac{\left[\max(v_\perp, v_{min})/v_o\right]^\beta}{1 + (v_\perp/v_o)^{\beta+3}} \qquad (45)$$

where S_{E0} is a reference value of the electric-field spectral density, R_E is the Earth's radius, a is an altitude, a_o is the reference altitude, α is the spatial power-law index, v_{min} is a perpendicular velocity below which $D_\perp$ is essentially constant with a small value, v_o is the reference phase velocity, and β is the velocity power-law index ($\beta = \nu - \mu$ from the last section).

The fitting of the parameters of the diffusion rate was done by trial and error, by comparing the phase-space density at the pitch angle of maximum f of the calculated distribution function to the same quantity from the observed conic, read from the published plots of Gorney *et al.*[22]. The resulting fit is shown in Fig. 10. The two solid curves are the phase space densities from the observed conic, the two traces being from the contours plotted for $\pm v_\perp$. For this calculation, we began with a population of hydrogen ions traveling up the field line at 2800 km, initially with a Maxwellian velocity distribution of temperature 1 eV. The plotted distribution function was tabulated at the altitude of the satellite, 5700 km, after the ions crossed a region containing auroral hiss turbulence with the parameters: $S_{E0} = (20\text{mV/m})^2/\text{kHz}$, $a_o = 2600$ km, $\alpha = 9$, $v_{min} = 35$ km/s (corresponding to an energy of 6.4 eV), $v_o = 310$ km/s (corresponding to 500 eV), and $\beta = 3$. Note that this value of S_{E0} represents a fairly modest value of the total electric field in the turbulence, whose values have been observed to range up to 50 mV/m or more. The phase velocity of the peak of diffusion, v_o, corresponds to an energy of 500 eV, which is certainly of the right order of magnitude if the turbulence was generated by electron beams of a few keV energy and then subjected to degradation of phase velocity due to propagation and mode coupling effects. The full velocity-space plot of the calculated ion conic distribution is shown in Fig. 11. Note the characteristic folded shape. It is interesting to note that although the model for the diffusion rate decreases monotonically with altitude, the conic shows its peak flux not at a pitch angle corresponding to the minimum altitude of the simulation, but to an intermediate altitude. This altitude corresponds to the point where the ions are at velocities at which they experience the largest transverse heating, that is, $v_\perp \sim v_o$.

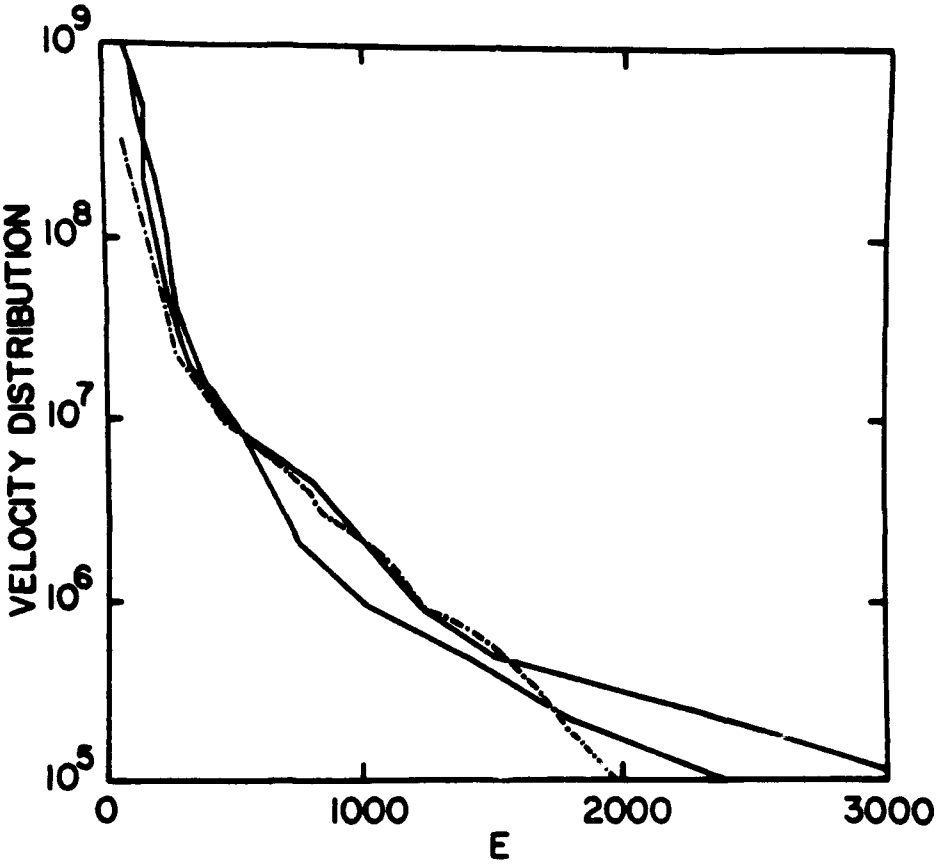

Figure 10. The phase-space density of the S3-3 conic from orbit 718. The solid curves give two measurements of f as a function of energy (in eV) at the pitch angle of maximum f, while the dot-dashed curve gives the fitted theoretical model.

This class of ion conics is distinguished in form from the second class (second only in order of discovery), whose formation is reviewed by Crew and Chang [11], by the behavior of f at small $v_\perp$. In these conics, as $v_\perp$ goes to zero, the parallel velocities of the ions is also found to go to zero, while in the other conic form, the ions of small $v_\perp$ are found with still sizeable values of $v_\parallel$. (Strictly speaking then, the other type of transversely accelerated ion event is not a conic, and is sometimes called an ion bowl, for the shape of its velocity distribution in $v_\perp$-$v_\parallel$ space.) The explanation is that, due to the velocity-dependent resonance condition that low-velocity ions cannot satisfy, the bulk of the ions at low velocities travel up the field lines unaffected by the wave-particle interaction process and serve to anchor the velocity distribution to the origin in velocity space. In the other form of conic, as Crew and Chang [11] describe, the resonance condition is independent of velocity and

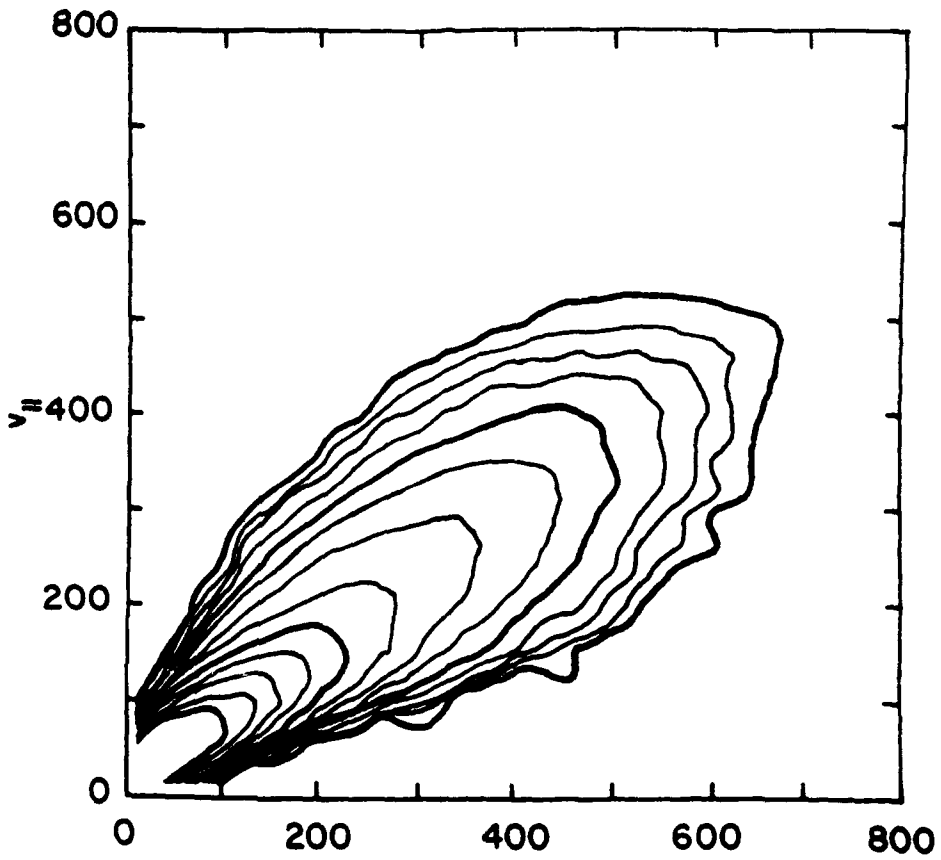

Figure 11. The calculated ion velocity distribution for the S3-3 conic of orbit 718. The velocity distribution as a function of perpendicular (the horizontal axis) and parallel velocities (in km/sec) is presented as a contour plot. The bolder contours are a decade apart.

all ions in the distribution can participate in the wave-particle interaction, which again causes velocity diffusion in the direction perpendicular to the magnetic field. The adiabatic folding effect of the inhomogeneous geomagnetic field acting at the same time serves as a one-way street for the flow of energy, from perpendicular degrees of freedom to the parallel direction. Thus, while the parallel energy of an ion is always increasing, the perpendicular energy is being continually scattered both up and down, and at any time some ions of a given parallel energy will be found with small perpendicular energy.

D. Low Altitude Ion Conic

Our second example will be the ion conic measured during the sounding rocket flight code-named *MARIE*. This rocket campaign over Greenland has provided us with what is probably the most complete and detailed set of observations within the regions of low-altitude transversely accelerated ions yet available [3;45; 46]. The rocket passed through an auroral arc on its upleg and downleg flights; at each crossing a strong correlation was seen between the intensity of the auroral hiss electric fields at frequencies between 3 and 16 kHz and the flux of ions flowing up the field line at energies of 50 to 370 eV, with pitch angles near ninety degrees. The intense fluxes of both waves and particles were observed at altitudes between 500 and 800 kilometers. A mass spectrometer on board determined that the ions were primarily hydrogen, consistent with our expectation that the lighter ions are preferentially heated by auroral hiss turbulence. The noted[46] lack of direct correlation with precipitating electron fluxes probably results because the trajectories of the resonance-cone waves do not follow the geomagnetic field lines like the trajectories of the precipitating electrons do. There is some suggestion of parallel heating of the ambient electron distribution.

To model this event, we first recognize that hydrogen is generally a minority species of the plasma at these altitudes, where the major constituent is expected to be oxygen. Thus the hydrogen ions observed here have probably been drawn down from higher altitudes. This affects the residence time of the ions in the vicinity of the intense turbulence, and thus the energies the ions achieve. Ions traveling down the field line enter the region of intense turbulence and begin to be transversely heated by interaction with the waves. At the same time, the ions's parallel motion slows down (and eventually reverses) as they mirror in the geometry of the geomagnetic field. Thus, the ions spend more time in the region of wave-particle interaction than they would if they were already traveling up the field line,increasing the effectiveness of the heating process. (Another mechanism to note that enhances residence time is effective in regions where the steady parallel electric field is directed to accelerate ions downwards. This electric field causes the ions to bounce repeatedly between the magnetic mirror below and the electrostatic mirror above, until the ions have gained enough energy to pass the electrostatic barrier above. This "pressure-cooker" effect, studied by Gorney *et al.*[47], may be effective in the polar cusp region, where beams of electrons accelerated out of the ionosphere are observed.)

For our simulation of the *MARIE* event, then, we begin with a hydrogen ion species with a temperature of 1 eV at the upper end of the simulated region, from 500 to 800 km altitude. The peak spectral density of the electric field observed in the first pass through the arc, from about 05:29 to 5:31 UT, is around $(7\text{mV/m})^2$ per kHz, averaged over the range from 3 to 16 kHz. Fig. 12 shows the results of the simulation as two contour plots of the ion

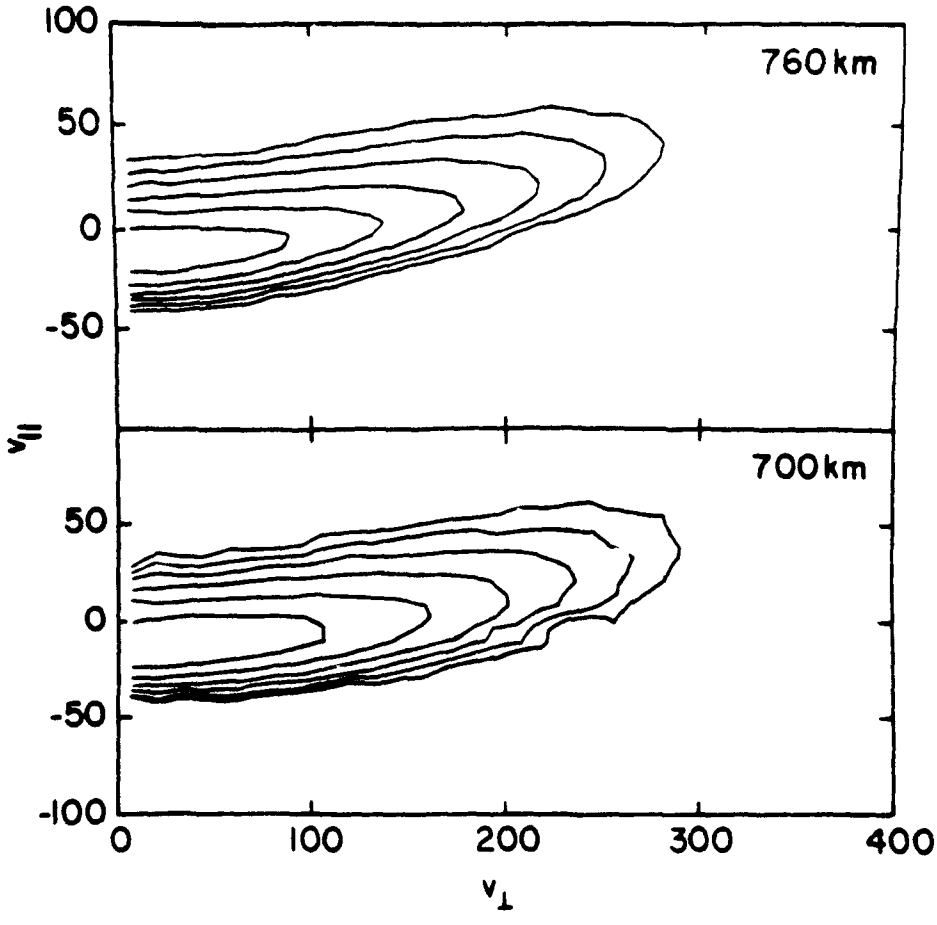

Figure 12. Simulation of the *MARIE* ion conic event. Contour plots of the ion velocity distribution as a function of perpendicular and parallel velocities (in km/sec) at 700 km altitude (bottom) and 760 km (top). The contours are a half decade apart.

phase-space density as a function of $v_{\perp}$ and $v_{\parallel}$ at the altitudes 700 and 760 km. We see in both cases the characteristic near-ninety degree pitch angle of the conic, despite the fact that the heating has occurred over the course of several hundred kilometers. Fig. 13 shows the phase-space density integrated over pitch angle at two altitudes. Yau *et al.* [46] reported that the characteristic energy of the conic was about 22 eV, with a tail emerging from the body of the distribution at around 150 to 200 eV, extending out to a few hundred eV. We see here that in the simulation, the observed level of turbulence was able to produce the heating required to allow the ions to reach these energies.

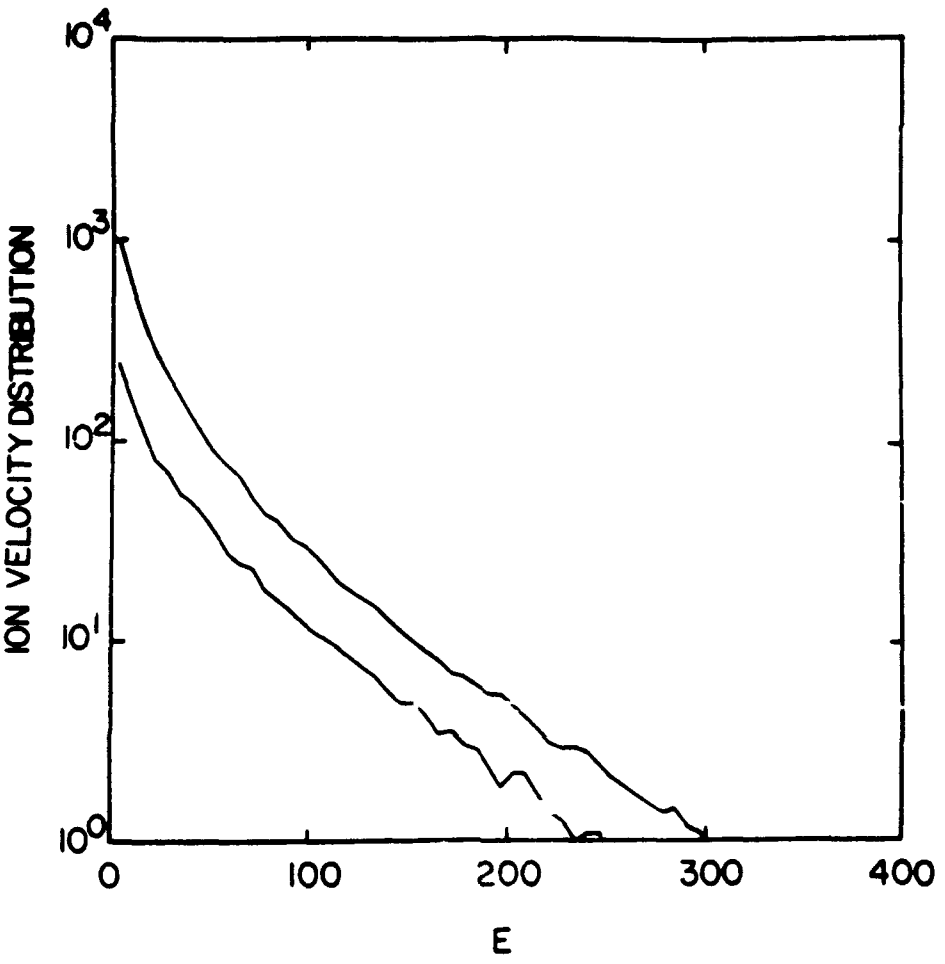

Figure 13. The calculated phase-space density of the *MARIE* conic, integrated over pitch angle. The velocity distribution at the altitudes of 700 and 760 km are plotted as a function of energy (in eV).

The exact shape of the tail distribution could have been fitted by adjusting the spatial and velocity dependences of the diffusion coefficient, which for this run was assumed to be independent of both variables. From our experience with the S3-3 conic, we expect that the phase velocity of the peak spectral density would be the velocity corresponding to an energy above the point where the tails emerge from the body of the velocity distribution, around 200 eV. This energy corresponds to a velocity of about 200 km/s. On the *MARIE* rocket, an electric field interferometer was flown to attempt to measure wavelengths of the observed plasma waves [48]. When the rocket passed through the ion-acceleration region, the electric field interferometer

detected a feature with measureable coherence which at a frequency of 9 kHz had a wavelength of about 20 m. This represents a phase velocity of 180 km/s, in agreement with the phase velocity of the peak spectral density inferred from the ion velocity-distribution measurement.

To summarize the points on which the *MARIE* in-situ plasma and wave measurements agree well with the predictions of the model of ion interaction with intense auroral hiss, we have 1) a strong correlation between VLF wave intensity and energetic ion flux; 2) preferential acceleration of hydrogen over oxygen; 3) enhancements of field-aligned electron fluxes; 4) the frequency spectrum of the VLF turbulence around the lower hybrid frequency shows structure spaced at the hydrogen gyro frequency, suggesting that ion damping of the waves is responsible for the acceleration; 5) the amplitude of the VLF turbulence is several tens of mV/m, strong enough to account for the ion energies; and finally, 6) the form of the ion velocity distribution has the high energy tails that are characteristic of the acceleration observed in the simulation, and the measured phase velocities of the waves match the features of the ion distribution. Many of these points have been observed on other missions and satellites, but never perhaps as convincingly as observed on *MARIE*.

V. DISCUSSION

One of the longlasting controversies in the study of ion conics near auroral arcs has been the question of identifying the mechanism for the transverse ion heating, whether through wave-particle interaction with the lower-hybrid waves reviewed here or with electrostatic ion cyclotron waves [49] or through other mechanisms. Searches for satellite observations of conics of pitch angle near ninety degrees (that were presumably in the process of being accelerated) were inconclusive [50], but suffered because fast velocities and slow spin rates make satellites a poor platform from which to observe transverse ion acceleration near auroral arcs. The advantages of sounding rockets for these observations were demonstrated in the *MARIE* campaign[3], in which the simultaneous observation of transverse ion acceleration and intense lower-hybrid waves provided strong evidence for the lower-hybrid heating mechanism.

To model the observations of ion conics and counter-streaming electrons near auroral arcs requires the consideration of the global evolution of both the particle populations and the wave spectra over ranges of distance and time that stretch our present models. The complete and self-consistent analysis of the fields and particles near auroral arcs remains still only a distant goal of space physics. The origins of the field-aligned potential drops that accelerate the auroral electrons are still poorly understood; our understanding of the spectra of the plasma waves in the arc environment is only beginning to develop. For the calculation of ion conics, in particular, we are

still hampered by the difficulty of measuring the relevant quantities for our theories, and thus considerable uncertainty remains in the empirical estimation of the rate of transverse ion acceleration because of the lack of information on the wave-vector spectrum of the VLF turbulence. Efforts to measure the wavelengths of the plasma waves [48] are most welcome, although such results are still generally limited to the characteristic or dominant wavelength rather than the spectrum of wavelengths that would be needed to calculate wave-particle interaction rates. Such measurements certainly will help elucidate and discriminate among the variety of mechanisms that intervene between the linear excitation of plasma waves in the auroral arc environment and the heating and acceleration of ionospheric ions and electrons. Using the models we have developed, it may be possible to use the form of the ion conic velocity distribution to infer constraints on the spectral shape and magnitude of the VLF turbulence, a great benefit when the acceleration region is localized and remote from the platform observing the accelerated particles.

REFERENCES

[1] D.A. Gurnett, S.D. Shawhan, and R.R. Shaw, Auroral hiss, Z mode radiation, and auroral kilometric radiation in the polar magnetosphere: DE 1 observations, J. Geophys. Res., **88**, pp. 329–340 (1983).

[2] M. Temerin, C. Cattell, R. Lysak, M. Hudson, R.B. Torbert, F.S. Mozer, R.D. Sharp, and P.M. Kintner, The small-scale structure of electrostatic shocks, J. Geophys. Res., **86**, pp. 11278–11298 (1981).

[3] P.M. Kintner, J. LaBelle, W. Scales, A.W. Yau, B.A. Whalen, and Craig Pollock, Observations of plasma waves within regions of perpendicular acceleration, Geophys. Res. Lett., **13**, p. 1113 (1986).

[4] D.M. Klumpar, A digest and comprehensive bibliography on transverse auroral ion acceleration, in *Ion Acceleration in the Magnetosphere and Ionosphere*, Geophysical Monograph Series, Vol. 38, T. Chang, M.K. Hudson, J.R. Jasperse, R.G. Johnson, P.M. Kintner, M. Schulz, and G.B. Crew, eds., p. 389 (American Geophysical Union, Washington, DC, 1986).

[20] M. André, Plasma dispersion surfaces, J. Plasma Phys., **33**, p. 1 (1985).
[21] K. Ronnmark, Computation of the dielectric tensor of a maxwellian plasma, Plasma Phys., **25**, pp. 699–701 (1983), also WHAMP, Kiruna Geophysical Institut Report no. 179, 1982.
[22] D.J. Gorney, S.R. Church, and P.F. Mizera, On ion harmonic structure in auroral zone waves: the effect of ion conic damping of auroral hiss, J. Geophys. Res., **87**, pp. 10479–10486 (1982).
[23] D.S. Evans, Precipitating electron fluxes formed by a magnetic field aligned potential difference, J. Geophys. Res., **79**, pp. 2853–2858 (1974).
[24] K. Papadopoulos and P. Palmadesso, Excitation of lower hybrid waves in a plasma by electron beams, Phys. Fluids, **19**, pp. 605–606 (1976).
[25] W. Lotko and J.E. Maggs, Damping of electrostatic noise by warm auroral electrons, Planet. Space Sci., **27**, pp. 1491–1506 (1979).
[26] W. Calvert, The auroral density cavity, Geophys. Res. Lett., **8**, pp. 919–921 (1981).
[27] J.E. Maggs, Coherent Generation of VLF Hiss, J. Geophys. Res., **81**, pp. 1707–1724 (1976).
[28] J.E. Maggs, Electrostatic noise generated by the auroral electron beam, J. Geophys. Res., **83**, pp. 3173–3188 (1978).
[29] T.H. Stix, Phys. Rev. Lett., **15**, p. 878 (1965).
[30] G.B. Crew, Lower-hybrid wave generation in an electron beam of finite transverse dimension, J. Plasma Phys., **41**, pp. 119–137 (1989).
[31] J.E. Maggs and W. Lotko, Altitude dependent model of the auroral beam and beam-generated electrostatic noise. J.Geophys. Res., **86**, pp. 3439–3447 (1981).
[32] E.A. Bering, J.E. Maggs, and H.R. Anderson, The plasma wave environment of an auroral arc 3. VLF hiss, J. Geophys. Res., **92**, pp. 7581–7605 (1987).
[33] D.B. Melrose and S.M. White, Amplified Cerenkov emission of auroral hiss: limitations implied by quasilinear theory, J. Geophys. Res., **85**, p. 3442 (1980).
[34] J.E. Maggs, Nonlinear evolution of the auroral electron beam, J. Geophys. Res., **94**, pp. 3631–3651 (1989).
[35] R.C. Davidson, *Methods in Nonlinear Plasma Theory* (Academic Press, New York, 1972).
[36] C.K. Birdsall and A.B. Langdon, *Plasma Physics via Computer Simulation* (McGraw-Hill, New York, 1985).
[37] J.B. McBride, E. Ott, J. Boris, and J. Orens, Theory and simulation of turbulent heating by the modified two-stream instability, Phys. Fluids, **15**, p. 2367 (1972).
[38] J.M. Retterer and T. Chang, Plasma simulation of intense VLF turbulence and particle acceleration in the suprauroral region, in *Physics of Space Plasmas (1988)*, SPI Conference Proceedings and Reprint Series,

[5] T. Chang and B. Coppi, Lower hybrid acceleration and ion evolution in the suprauroral region, Geophys. Res. Lett., **8**, p. 1253 (1981).

[6] J.M. Retterer, T. Chang, and J.R. Jasperse, Ion acceleration by lower hybrid waves in the suprauroral region, J. Geophys. Res., **91**, p. 1609 (1986).

[7] C.S. Lin, J.L. Burch, J.D. Winningham, and R.A. Hoffman, DE-1 observations of counterstreaming electrons at high altitudes, Geophys. Res. Lett., **9**, p. 925 (1982).

[8] J.M. Retterer, T. Chang, and J.R. Jasperse, Ion acceleration in the suprauroral region: a Monte Carlo model, Geophys. Res. Lett., **10**, p. 583 (1983).

[9] J.M. Retterer, T. Chang, G.B. Crew, J.R. Jasperse, and J.D. Winningham, Monte Carlo modeling of ionospheric oxygen acceleration by cyclotron resonance with broadband electromagnetic turbulence, Phys. Rev. Lett., **59**, pp. 148–151 (1987).

[10] J.M. Retterer, T. Chang, G.B. Crew, J.R. Jasperse, and J.D. Winningham, Monte Carlo modeling of ionospheric oxygen acceleration by cyclotron resonance with broadband electromagnetic turbulence, in *Physics of Space Plasmas (1985-7)*, SPI Conference Proceedings and Reprint Series, No. 6, Tom Chang, J. Belcher, J.R. Jasperse, and G.B. Crew, eds., p. 97 (Scientific Publishers, Inc., Cambridge, MA, 1987).

[11] G.B. Crew and Tom Chang, Particle acceleration by electromagnetic ion cyclotron turbulence, in *Physics of Space Plasmas (1989)*, SPI Conference Proceedings and Reprint Series, No. 9, Tom Chang, G.B. Crew and J.R. Jasperse, eds., p. 31 (Scientific Publishers, Inc., Cambridge, MA, 1990), (this volume).

[12] R.E. Barrington and J.S. Belrose, Preliminary results from the VLF receiver aboard Canada's Alouette satellite, Nature, **198**, p. 651 (1963).

[13] T. Laaspere, W.C. Johnson, and L.C. Semprebon, Observations of Auroral Hiss, LHR Noise, and Other Phenomena in the Frequency Range 20 Hz - 540 kHz on Ogo 6, J. Geophys. Res., **76**, p. 4477 (1971).

[14] D.A. Gurnett and L.A. Frank, VLF Hiss and related plasma observations in the polar magnetosphere, J. Geophys. Res., **77**, p. 172 (1972).

[15] H.G. James, VLF saucers, J. Geophys. Res., **81**, pp. 501–514 (1976).

[16] C.S. Lin, J.L. Burch, S.D. Shawhan, and D.A. Gurnett, Correlation of auroral hiss and upward electron beams near the polar cusp, J. Geophys. Res., **89**, pp. 925–935 (1984).

[17] T.H. Stix, *The Theory of Plasma Waves* (McGraw-Hill, New York, 1962).

[18] M.A. Temerin, A comment of the source region of VLF suacers, J. Geophys. Res., **84**, p. 6691 (1979).

[19] S. Ichimaru, *Basic Principles of Plasma Physics A Statistical Approach* (W.A. Benjamin, Inc., Reading, MA, 1973).

No. 8, T. Chang, G.B. Crew, and J.R. Jasperse, eds., p. 309 (Scientific Publishers, Inc., Cambridge, MA, 1988).

[39] M. Porkolab, Parametric instabilities due to lower hybrid radio frequency heating of tokamak plasmas, Phys. Fluids, **20**, p. 2058 (1977).

[40] H.E.J. Koskinen, Lower hybrid parametric processes on auroral field lines in the topside ionosphere, J. Geophys. Res., **90**, p. 8361 (1985).

[41] M.V. Goldman, Strong turbulence of plasma waves, Rev. Mod. Phys., **56**, p. 709 (1984).

[42] J.J. Thomson, R. Faehl, and W. Kruer, Mode-coupling saturation of the parametric instability and electron heating, Phys. Rev. Lett., **31**, p. 918 (1973).

[43] G.B. Crew and T. Chang, Asymptotic theory of ion conic distributions, Phys. Fluids, **28**, p. 2382 (1985).

[44] J.G. Roederer, *Dynamics of Geomagnetically Trapped Radiation* (Springer-Verlag, Berlin, 1970), p. 89.

[45] J. LaBelle, P.M. Kintner, A.W. Yau, and B.A. Whalen, Large amplitude wave packets observed in the ionosphere in association with transverse ion acceleration, J. Geophys. Res., **91**, pp. 7113–7118 (1986).

[46] A.W. Yau, B.A. Whalen, F. Creutzberg, and P.M. Kintner, Low altitude transverse ion acceleration: auroral morphology and in-situ plasma observations, in *Physics of Space Plasmas (1985-7)*, SPI Conference Proceedings and Reprint Series, No. 6, T. Chang, J. Belcher, J.R. Jasperse, and G.B. Crew, eds., p. 77 (Scientific Publishers, Inc., Cambridge, MA, 1987).

[47] D.J. Gorney, Y.T. Chiu, and D.R. Croley, Jr., Trapping of ion conics by downward electric fields, J. Geophys. Res., **90**, p. 4205 (1985).

[48] J. LaBelle and P.M. Kintner, The measurement of wavelength in space plasmas, Reviews of Geophysics, **27**, pp. 495–518 (1989).

[49] M. Ashour-Abdalla and H. Okuda, Turbulent heating of heavy ions on auroral field lines, J. Geophys. Res., **89**, p. 2235 (1984).

[50] P.M. Kintner and D.J. Gorney, A search for the plasma processes associated with perpendicular ion heating, J. Geophys. Res., **89**, pp. 937–944 (1984).

4. EQUATORIALLY GENERATED ULF WAVES AS A SOURCE FOR THE TURBULENCE ASSOCIATED WITH ION CONICS

Jay R. Johnson, Tom Chang, G. B. Crew, and Mats André[†]
Center for Space Research
Massachusetts Institute of Technology
Cambridge, Massachusetts 02139

ABSTRACT

Low frequency turbulence present on closed field lines in the central plasma sheet has been used to explain ion heating and conic formation with remarkable success. However, the source of the turbulence has yet to be established, and there are no obvious local sources which could power such a broadband spectrum. Alternatively, observations reveal that ion distributions in the equatorial region are often anisotropic, and such distributions excite waves both above and below the proton gyrofrequency. As these waves propagate to lower altitudes where the magnetic field is stronger, their left–hand circularly polarized component resonates with heavy ions. The presence of a parallel gradient in the magnetic field complicates the details of wave propagation, and as a result, downcoming right–hand circularly polarized waves, which acquire a left–hand circularly polarized component at the crossover frequency, may tunnel through a "stop zone" to altitudes where they resonate with the ions and thus contribute to the observed ion heating.

I. INTRODUCTION

The outflow of ionospheric ions in the form of ion conics into the central plasma sheet (CPS) is often accompanied by a broadband electric field spectrum. This turbulence which exists along closed field lines that emanate from the auroral region can, in fact, account for the ion heating and conic formation via resonant cyclotron heating in the presence of the mirror geometry of the Earth's magnetic field [1–4]. A typical electric field spectral density is shown in Fig. 1. The spectrum is peaked at low frequencies and tends to obey a power law over the range of frequencies which resonantly match the gyrofrequency of the ionospheric ions. Such spectra are commonly observed up to several R_E in altitude. Although the turbulence and conic form are well correlated for the events studied to date [5], the origin and nature of the turbulence remains uncertain.

[†] Permanent address: Swedish Institute of Space Physics, University of Umeå, S901 87 Umeå, Sweden.

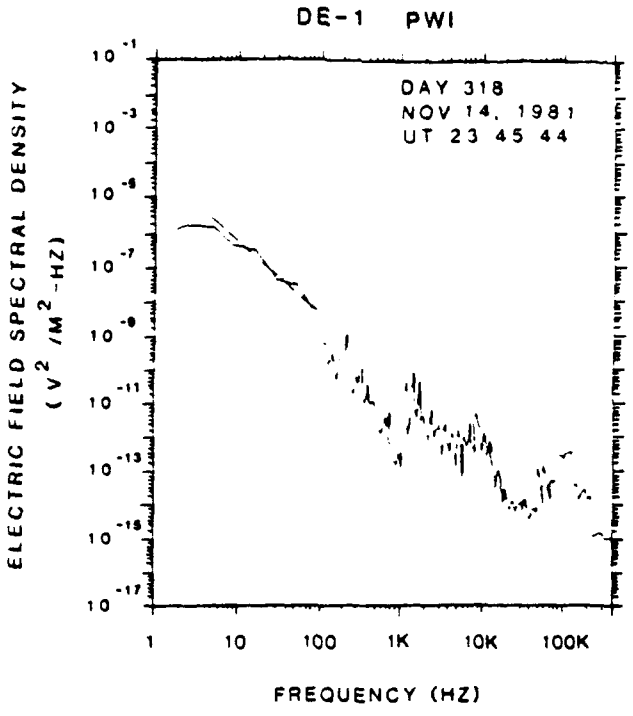

Figure 1. Typical electric field spectral density in the central plasma sheet (l=2.0 R_E, ILAT = 60°), from Ref. [1].

A number of possible sources for the turbulence exist throughout the magnetospheric environment. Of course, the most obvious possibility for a source would be one that is local in nature; however, all of the events scrutinized to date fail to point out any local sources and instead suggest that a more global approach is required [1, 6]. Velocity shears, for example, observed in the cusp region might excite the Kelvin–Helmholtz instability and generate Alfvén waves which might propagate upwards into the heating region. Alternatively, instabilities in the magnetotail associated with reconnection might generate waves which propagate earthward into the central plasma sheet. In this paper, however, we will consider, in particular, the possibility of a nonlocal source emanating from the equatorial region.

II. EQUATORIALLY GENERATED WAVES

Anisotropic ion distributions are often observed in the nightside equatorial region at geosynchronous orbit [7]. As ions are injected earthward from the magnetotail, they drift adiabatically about the Earth along drift shells. Because the shell on which a particle is constrained to move depends on the equatorial pitch angle, initially isotropic distribution functions tend to

develop thermal anisotropies ($T_\perp > T_\parallel$) and acquire anomalous loss cones (enlarged over the 3° atmospheric loss cone) [8, 9]. In addition, the observations reveal that these distributions often contain a large energetic population with 90° pitch angle [7]. Moreover, the proton gyrofrequency near geosynchronous orbit in the equatorial region ($f_{cH^+}^{eq}$) matches the oxygen cyclotron frequency (f_{cO^+}) over the range of altitudes where heating takes place. Below we consider how anisotropic ion distributions can generate waves with frequencies near $f_{cH^+}^{eq}$ in the equatorial region and how these waves may reach the CPS at altitudes ranging from the upper ionosphere to several R_E.

A. Waves with $f < f_{cH^+}^{eq}$

Ion distributions with loss–cones or temperature anisotropies can excite waves below the proton gyrofrequency. Indeed, this instability has been studied comprehensively in the equatorial region in connection with Pc1 ($0.2 < f < 5$ Hz) wave generation and helium heating [10–12]. Waves generated with frequencies below the helium gyrofrequency (typically $f < 1$ Hz) are guided along field lines to the ground [13, 14]. On the other hand, it is believed that waves generated above the helium gyrofrequency but below the hydrogen cyclotron frequency ($1 < f < 5$ Hz), rather than penetrating directly to the ground, travel between geomagnetic conjugate points near the magnetic equator which correspond to the ion–ion hybrid frequency. Although the growth rates for these waves are smaller than those for the waves near the helium gyrofrequency, the power in the waves may be comparable because they amplify as they bounce back and forth through the equatorial plane [13]. Furthermore, when the concentration of helium is low enough, these waves tunnel through the reflection layer to lower altitudes in the right hand circularly polarized (RHCP) mode (see Fig. 6 of Ref. [14]). In fact, ground based instruments often detect both types of waves—an observation which strongly suggests that they contribute to the auroral turbulence [14].

B. Waves with $f > f_{cH^+}^{eq}$

Propagating waves generated below $f_{cH^+}^{eq}$ may explain a significant part of the wave power observed at auroral altitudes, but much of the wave power has $f > 5$ Hz (Fig. 1). Moreover, the initial energization of ionospheric oxygen to magnetospheric energies occurs at low altitudes where f_{cO^+} is larger than Pc1 frequencies. Therefore, it is important to consider the generation and propagation of waves with $f > f_{cH^+}^{eq}$ in the equatorial region.

The measurements taken from GEOS 1 and 2 indicate that ion distributions with loss–cone character ($\partial F/\partial v_\perp > 0$) exist at geosynchronous orbit in the equatorial region and can generate waves at multiples of $f_{cH^+}^{eq}$ [7]. Indeed *Perraut et al.* [7] modeled the hot ion population with a ring distribution and examined the solutions of the linear dispersion relation with $k_\parallel = 0$. They

found that indeed waves are generated at multiples of f_{cH^+}, but the waves have a group velocity perpendicular to the magnetic field which implies that they are confined to the equatorial region.

On the other hand, we have solved the dispersion relation of linear waves using the somewhat more realistic model used by the WHAMP code [15, 16]. In particular, we have included a thermal spread in the hot ion distribution function which we have taken to be of the form

$$f(v_\parallel, v_\perp) = \sum_j n_j(\sqrt{\pi}v_{tj})^{-3}\exp\left[-\frac{v_\parallel^2}{v_{tj}^2}\right]\left\{\frac{\Delta_j}{\alpha_{1j}}\exp\left[-\frac{v_\perp^2}{\alpha_{1j}v_{tj}^2}\right] + \frac{1-\Delta_j}{\alpha_{1j}-\alpha_{2j}}\left[\exp\left[-\frac{v_\perp^2}{\alpha_{1j}v_{tj}^2}\right]-\exp\left[-\frac{v_\perp^2}{\alpha_{2j}v_{tj}^2}\right]\right]\right\} \quad (1)$$

with the parameters listed in Table I. The distribution consists of a cold background plasma with a small energetic proton population which peaks in the perpendicular direction at 7 keV.

Table I. Parameters Used in Eq. (1)

Species	T (keV)	n (cm^{-3})	α_1	α_2	Δ
H^+	0.001	65.0	1.0	0.0	1.0
H^+	1.0	1.6	1.0	0.3	0.0
e^-	0.001	66.6	1.0	0.0	1.0

We find that for $k_\parallel = 0$ electrostatic waves are generated at multiples of f_{cH^+} with group velocity perpendicular to the magnetic field; however, for $k_\parallel\rho_i \geq 10^{-4}$ a broad band of unstable electromagnetic modes arises. In Fig. 2 we plot the dispersion surface of the real frequency in a two dimensional wave vector space, and in addition, we indicate the growth rates for the particular mode with shading. This figure illustrates that for larger $k_\parallel$ the harmonic spectrum at $k_\parallel = 0$ becomes more broadband. In addition, these broadband modes with $k_\parallel \neq 0$ also have $v_{g\parallel}/v_{g\perp} \sim 1$ as is illustrated in Fig. 3. In this figure, we have taken a slice at fixed $k_\perp$ along one band in Fig. 2. We have plotted one curve which corresponds to maximum growth at $k_\parallel = 0$ and another curve which is slightly offset in $k_\perp$ from the first curve. This figure illustrates that although the maximum growth may be in the modes which are electrostatic and propagate perpendicular to the magnetic field, electromagnetic modes, which excite a much larger region of k-space, have comparable growth rates and also have $v_{g\parallel}/v_{g\perp} \sim 1$. Thus, the electromagnetic waves will initially propagate out of the equatorial region. Increasing the temperature and density of the energetic population increases the growth rates as one would expect; however, for sufficiently warm background electrons or ions,

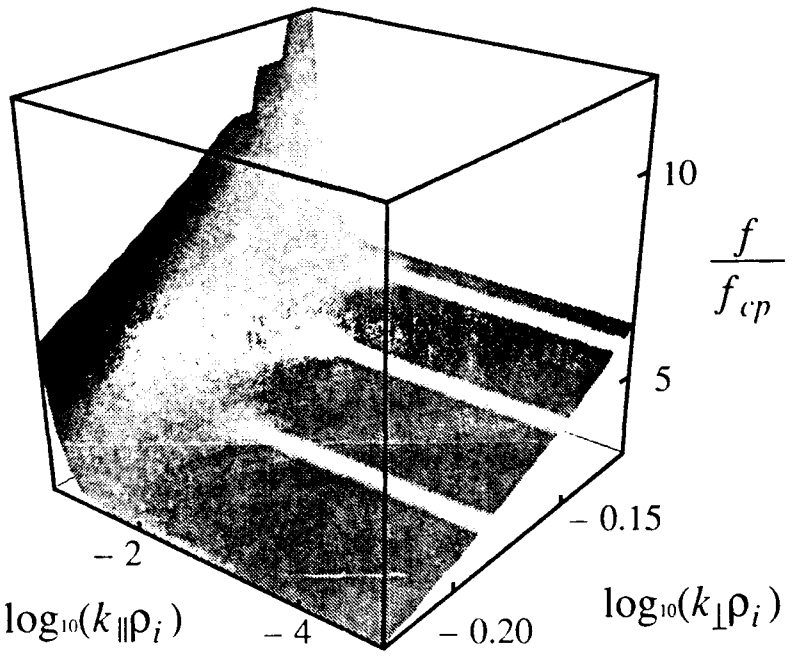

Figure 2. Dispersion relation (ω vs. $\log_{10}(k_{\perp}\rho_i)$, $\log_{10}(k_{\|}\rho_i)$ where ρ_i is the ion gyroradius) using the distribution in Eq. (1) with the parameters listed in Table I. Shading indicates the growth rates (white for growing, dark for damping) for waves on the surface. Notice that electrostatic waves are generated at multiples of f_{cH^+} which are largest at $k_{\|}=0$ whereas the waves at larger $k_{\|}$ tend to be electromagnetic and occupy a much larger region of k-space.

the $k_{\|} \neq 0$ modes become damped.

If we compare the power in the equatorial and auroral waves using the observed wave amplitudes, we may determine whether the free energy in the equatorial region is a viable source for the turbulence. With the assumptions that the auroral waves are essentially Alfvén waves and that the WHAMP results accurately reflect the relationship between the observed magnetic field and the electric field in the equatorial region, we find that the Poynting fluxes are comparable. Although detailed ray tracing calculations will be required to confirm the notion that the auroral turbulence originates in the equatorial plane, this simple comparison elicits some confidence.

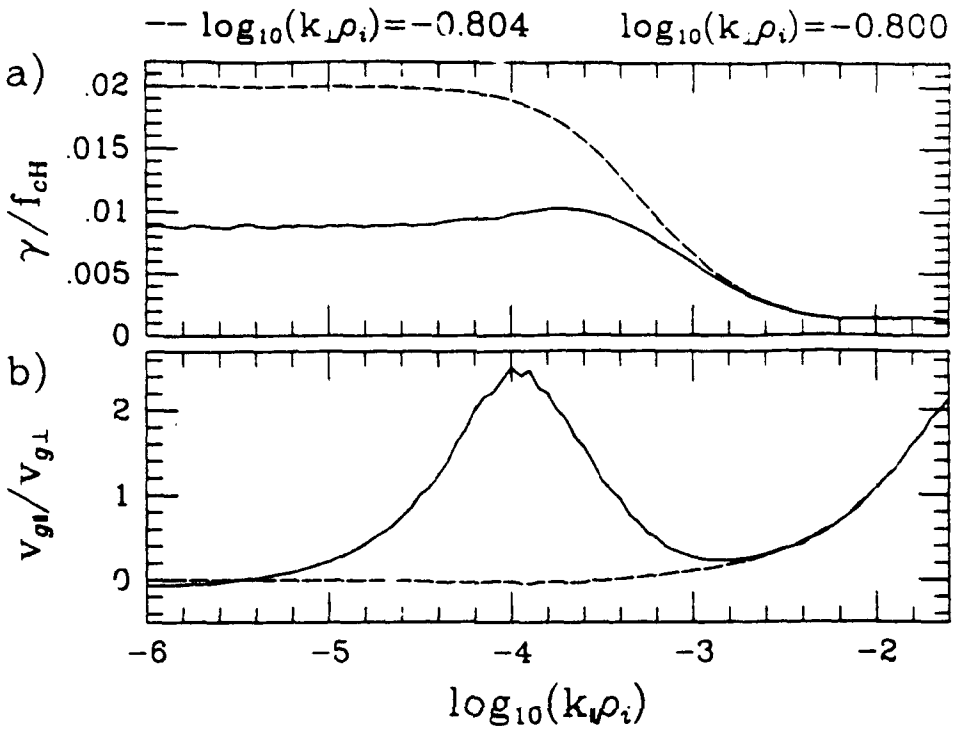

Figure 3. Growth rates (a) and group velocity ratio $v_{g\parallel}/v_{g\perp}$ (b) for a plasma with parameters listed in Table I. The curves are taken at constant $k_\perp\rho_i$ where ρ_i is the ion gyroradius. The dashed curve corresponds to maximum growth for $k_\parallel=0$ modes near the fourth harmonic of the proton gyrofrequency with $\log_{10}(k_\perp\rho_i) = -0.804$. The solid curve corresponds to modes with $\log_{10}(k_\perp\rho_i) = -0.800$ which are slightly offset from maximum growth at $k_\parallel=0$. It is to be noted that these modes have a slightly smaller growth rate, but they also have $v_{g\parallel}/v_{g\perp}>1$.

III. WAVE PROPAGATION

In the previous section we identified an instability in the equatorial region that generates electromagnetic waves which initially propagate earthward. Such an instability would be a likely source for the auroral turbulence observed at lower altitudes. In order to determine whether the auroral region is accessible to these waves, we now consider the characteristics of electromagnetic wave propagation. In a cold plasma only two electromagnetic modes exist at a given frequency. Because only the left hand circularly polarized (LHCP) component of these waves resonates with ions, the waves must contain a non–negligible fraction of LHCP at the local oxygen cyclotron frequency in order for heating to occur. In a cold plasma, however, the

branch which is RHCP for $k_\perp = 0$ contains no LHCP at the ion gyrofrequency even for $k_\perp \neq 0$. The waves that we are considering are generated with $f > f_{cH^+}$ and thus, are most likely RHCP because the LHCP branch is cut off above f_{cH^+}. In order to heat ions, these waves must acquire some fraction of LHCP as they propagate to lower altitudes. Such a transmutation of wave polarization may occur via mode conversion and tunneling.

In order to understand how RHCP waves might gain LHCP as they propagate to auroral altitudes, we consider linear theory for an idealized model consisting of a two ion component plasma as depicted by the dispersion relation in Fig. 4. Because wavelengths are very long and the density does not vary appreciably [17], we assume that the plasma is cold with no variation in density. Furthermore, we assume that the magnetic field varies slowly along itself and that the wavelength $\lambda \ll L_B \equiv [d\ln(B)/dz]^{-1}$. This

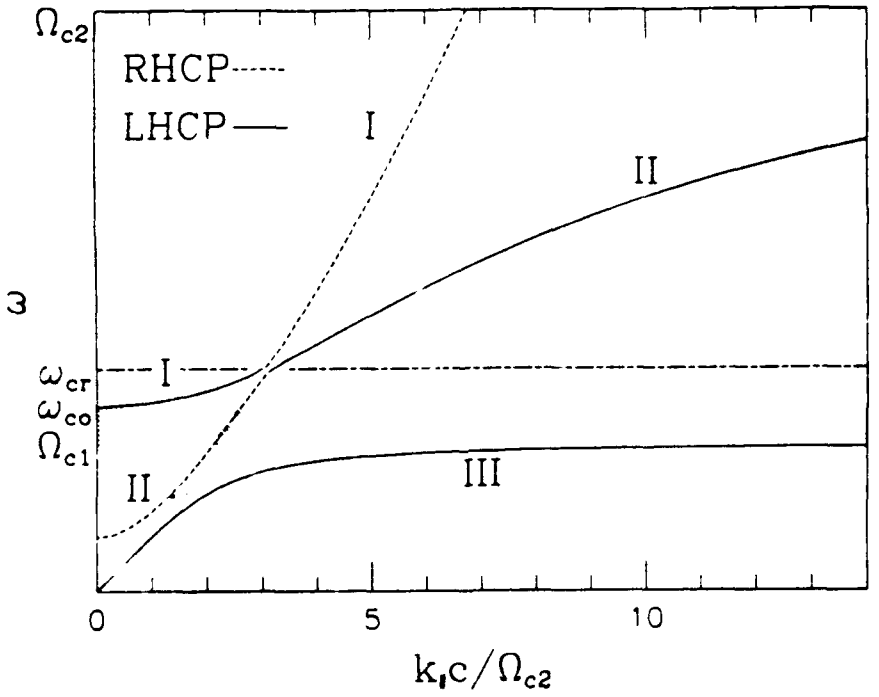

Figure 4. Dispersion relation for a cold two ion component plasma for nonparallel propagation. The various branches are labeled according to their predominate polarization with RHCP dashed and LHCP solid. Coupling occurs at the crossover frequency (ω_{cr}) where the polarization of branches I and II switches abruptly. Tunneling occurs across the shaded "gap" between the cutoff frequency (ω_{co}) and the heavy ion gyrofrequency (Ω_{c1}) from branch I to III.

assumption reduces the problem to one dimension and fixes $k_\perp$.

In the ensuing analysis we consider a particular scenario whereby waves generated with $f > f_{cH^+}$ propagate earthward. The wave initially propagates downward in the RHCP mode (I in Fig. 4). At the crossover frequency (ω_{cr}), where linear theory predicts that the predominate polarization of modes I and II reverses, mode coupling may occur [18]. As the modes couple, some fraction of the wave power will be transferred to mode II and will remain predominately RHCP. For an idealized cold plasma, mode II contains no LHCP at the heavy ion gyrofrequency and thus, this transferred wave power will not heat ions. Nevertheless, the rest of the wave power remains in mode I, which becomes predominately LHCP for $\omega < \omega_{cr}$. As the wave propagates along mode I to lower altitudes, it encounters the cutoff frequency (ω_{co}) where the wave is reflected. However, some of the wave power may tunnel through the evanescent layer to mode III where the waves can resonate with the ions. Below, we calculate the coupling (C), transmission (T), and reflection (R) coefficients where C is the fraction of the wave power that remains in mode I as the wave passes through ω_{cr}, T is the fraction of wave power that tunnels from mode I to mode III at ω_{co}, and R is the fraction of wave power that is reflected back along mode I at ω_{co}.

To proceed with the analysis, Maxwell's equations combined with the continuity and momentum transfer equations yield coupled differential equations for the electric field. Because the waves that we are considering have $E_\parallel \approx 0$ [19] the equations for the electric field components take the simple form

$$\left[\frac{d^2}{dz^2} + \begin{bmatrix} R-\varepsilon & \varepsilon \\ \varepsilon & L-\varepsilon \end{bmatrix} \right] \begin{bmatrix} E_- \\ E_+ \end{bmatrix} = 0 \tag{2}$$

where

$$E_\pm = E_x \pm iE_y \qquad \varepsilon = k_\perp^2 c^2 / 2\omega^2 \tag{3}$$

and

$$\begin{matrix} R \\ L \end{matrix} = 1 - \sum_{species} \frac{\omega_{ps}^2}{\omega^2} \frac{\omega}{\omega \pm \Omega_s} \tag{4}$$

where ω_{ps} and Ω_s are the plasma and cyclotron frequencies for each species s.

A. Coupling at the Crossover Frequency

Because the functions R and L vary slowly in altitude, we may apply the WKB analysis. Therefore, given the boundary conditions (downcoming RHCP wave), the zeroth order (in $\varepsilon \ll 1$) electric fields take the form

$$E_{-}^{(0)} = E^0 [R(z)]^{-1/4} \exp\left(-i \int_h^z [R(s)]^{1/2} ds \right) \; ; \; E_{+}^{(0)} = 0 \tag{5}$$

where h is some suitably chosen reference altitude. The parameter ε couples the two parallel propagating modes so that we may solve for the electric field perturbatively. To first order in ε we obtain the equation for the coupled electric field E_+.

$$\frac{d^2 E_{+}^{(1)}}{dz^2} + L(z) E_{+}^{(1)} = -\varepsilon E_{-}^{(0)} \tag{6}$$

We may solve this equation via variation of parameters to obtain

$$E_{+}^{(1)} = A_{+}\phi_{+} + A_{-}\phi_{-} \tag{7}$$

where

$$A_{\pm}(z) = \frac{1}{2i} \int_h^z ds \; [L(s) R(s)]^{-1/4} \times \tag{8}$$

$$\exp\left(-i \int_h^z \left([R(q)]^{1/2} \pm [L(q)]^{1/2} \right) dq \right)$$

and

$$\phi_{\pm}(z) = E^0 [L(z)]^{-1/4} \exp\left(\pm i \int_h^z [L(s)]^{1/2} ds \right) \tag{9}$$

The amplitude of the downgoing coupled wave A_- involves a phase integral over an oscillating function which becomes stationary at the crossover frequency

$$\omega_{cr} = \frac{n_1 \Omega_{c2}^2 + n_2 \Omega_{c1}^2}{n_1 + n_2} \tag{10}$$

defined by $D = (R - L)/2 = 0$. Because the contribution to the overall integral in (8) is exponentially small except at the stationary point, we may expand the integral in the integrand of (8) about the stationary point. We may then extend the limits of the overall integration to be $\pm\infty$ which introduces only exponentially small errors. Then we find that the coupling coefficient is, up to an unimportant phase, given by

$$A_{-}(-\infty) = \frac{1}{2\,[R(\omega_{cr})]^{1/2}} \int_{-\infty}^{+\infty} ds \exp\left(\frac{-i\, D'(\omega_{cr})\, s^2}{2\,[R(\omega_{cr})]^{1/2}} \right) \tag{11}$$

where

$$D'(\omega = \omega_{cr}) = -\frac{2c}{L_B} \omega_{cr}^2 \frac{(\omega_{p1}^2/\Omega_{c1} + \omega_{p2}^2/\Omega_{c2})}{(\Omega_{c1}^2 - \Omega_{c2}^2)^2} \frac{(n_1+n_2)^2}{n_1 n_2} \tag{12}$$

We may then rotate the path of integration to evaluate the trivial Gaussian integral in (11). By comparing the Poynting's flux of the incident wave above the coupling region (mode I, RHCP) to that of the coupled wave below the coupling region (mode I, LHCP) we may obtain the coupling coefficient

$$C \equiv \left| \frac{\vec{S}_{below}}{\vec{S}_{above}} \right| = -\frac{\pi}{2} \frac{\epsilon^2}{\sqrt{R}\, D'} \Big|_{\omega=\omega_{cr}} \sim \frac{k_\perp^4}{k_\parallel^4} L_B\, k_\parallel \tag{13}$$

Thus, although the dispersion curves appear to be continuous and separate for modes I and II, the presence of a gradient does introduce coupling. At small angles of propagation most of the wave power is transferred from mode I to II in which case the waves remain RHCP, while at larger angles of propagation much of the wave power remains in mode I, which is predominately LHCP below ω_{cr}.

B. Tunneling Through the Evanescent Layer

Once the downcoming RHCP wave has gained some LHCP at the crossover frequency, the wave encounters the cutoff–resonance pair of frequencies. At this point, intermode coupling is small so that we neglect ϵ in the ensuing calculations. We are now concerned with the lower component of equations (1) which may be written

$$\frac{d^2 E_+}{dz^2} = \frac{\omega^2}{v_A{}^2} \frac{\Omega_{c1}\Omega_{c2}}{\omega_{co}} \frac{\omega - \omega_{co}}{(\omega - \Omega_{c1})(\omega - \Omega_{c2})} E_+ \tag{14}$$

where

$$\omega_{co} = \frac{n_1\Omega_{c2} + n_2\Omega_{c1}}{n_1 + n_2} \qquad \frac{v_A{}^2}{c^2} = \sum_{species} \frac{4\pi n_s m_s}{B^2} \tag{15}$$

If we linearize about Ω_{c1} we find that this equation is of the Budden form [20]. The transmission and reflection coefficients are then given by

$$T = \exp(-\pi\beta) \qquad R = (1 - \exp(-\pi\beta))^2 \tag{16}$$

where

$$\beta = \frac{\Omega_{c1}}{v_A} L_B \frac{(1-m_2/m_1)^{1/2}}{(1+n_2 m_2/n_1 m_1)} \tag{17}$$

As is characteristic of Budden Tunneling $R+T \neq 1$, and the missing wave flux is absorbed by the medium. The absorption typically occurs because wave power is converted to a thermal branch which heats the ions [20].

C. Numerical Results

We consider an O^+–H^+ plasma in the auroral region at 2 R_E along a field line with invariant latitude 60°. If we take parameters typical of this region: n = 100cm^{-3}, B = 0.05 G, f_{cH^+} = 80 Hz, f_{O^+} = 5 Hz, L_B = 1 R_E, we find that for sufficiently low concentrations of O^+ a few percent LHCP is obtained at the heavy ion gyrofrequency via mode conversion and tunneling as indicated in Table II. These results are consistent with ion heating theory, which required only a small fraction of the waves to be LHCP [2].

Table II. Transmission and Coupling Coefficients

n_{O^+}/n_{H^+}	$\tan^{-1}(k_\perp/k_\parallel)$	C	T	R
0.05	18°	10%	0	100%
0.01	27°	10%	18%	67%

IV. DISCUSSION

In this paper we have identified a plausible source region for the turbulence associated with ion conics. It is evident that equatorially generated low frequency ($f < f_{cH^+}^{eq}$) waves do propagate to low altitudes where they may contain sufficient LHCP to heat the ions. In addition, we have determined that waves at higher frequencies may also be generated in the equatorial region, where they initially propagate earthward. Careful ray tracing will demonstrate whether these waves do indeed propagate to auroral altitudes.

The high frequency waves ($f > f_{cH^+}^{eq}$) are important because they may be responsible for extracting oxygen from the ionosphere where $f_{cO^+} > f_{cH^+}^{eq}$. Although the wave power at high frequencies provides a resonant mechanism whereby a small fraction of the ionospheric ions may be accelerated to magnetospheric energies, at low altitudes where the oxygen cyclotron frequency is increased, the power available to heat the ions is diminished by several orders of magnitude. On the other hand, the spectral density seems to be peaked at the lowest frequencies. This fact elicits the question of whether at some altitude, non–resonant heating, resulting from small fluctuations in the fields, might become important [21, 22].

We have also demonstrated that the effects of mode conversion and tunneling become significant in the presence of parallel magnetic field gradients. In the special case that we considered, we found that at the crossover frequency, power in the RHCP branch may be transferred to the LHCP branch, and at lower altitudes, the waves tunnel through an evanescent layer and resonate with the ions. Of course, a similar analysis would apply to waves generated in the LHCP mode. Furthermore, the addition of another ion species would complicate wave propagation further and introduce another crossover frequency and resonance.

Consideration should also be given to other effects which might effect wave propagation and heating. Although the inclusion of finite temperature should not affect the crossover coupling, it will affect the resonance–cutoff tunneling by introducing higher order derivatives which become important at the singularity of the differential equation (7). However, careful consideration of the effects of finite temperature typically demonstrates that the missing wave flux goes into a thermal branch which ends up heating the plasma. In addition, nonlinear coupling of the turbulence may allow more heating to take place near the gyrofrequency.

In conclusion, the notion that the CPS turbulence arises in the equatorial region appears to be a very promising possibility, and the details of wave propagation from this region to auroral altitudes will be the subject of further investigation.

REFERENCES

[1] Tom Chang, G. B. Crew, N. Hershkowitz, J. R. Jasperse, J. M. Retterer, and J. D. Winningham, Transverse acceleration of oxygen ions by electromagnetic ion cyclotron resonance with broad band left-hand polarized waves, Geophys. Res. Lett., **13**, pp. 636–639 (1986).

[2] John M. Retterer, Tom Chang, G. B. Crew, J. R. Jasperse, and J. D. Winningham, Monte Carlo modeling of ionospheric oxygen acceleration by cyclotron resonance with broadband electromagnetic turbulence, Phys. Rev. Lett., **59**, pp. 148–151 (1987).

[3] G. B. Crew and Tom Chang, Path-integral formulation of ion conic heating, Phys. Fluids, **31**, pp. 3425–3439 (1988).

[4] G. B. Crew and T. Chang, Particle acceleration by electromagnetic ion cyclotron turbulence, in *Physics of Space Plasmas (1989), SPI Conference Proceedings and Reprint Series, Number 9*, Jack Jasperse ed., pp. 31–31 (Scientific Publishers, Inc., Cambridge, MA, 1990).

[5] G. B. Crew, Tom Chang, J. M. Retterer, W. K. Peterson, D. A. Gurnett, and R. L. Huff, Ion cyclotron resonance heated conics: theory and observations, J. Geophys. Res., **94** (1989), submitted.

[6] D. A. Gurnett, R. L. Huff, J. D. Menietti, J. L. Burch, J. D. Winningham, and S. D. Shawhan, Correlated low-frequency electric and magnetic noise along the auroral field lines, J. Geophys. Res., **89**, pp. 8971–8985 (1984).

[7] S. Perraut, A. Roux, P. Robert, R. Gendrin, J. Sauvaud, J. Bosqued, G. Kremser, and A. Korth, A Systematic study of ULF waves above F_H from GEOS 1 and 2 measurements and their relationships with proton ring distributions, J. Geophys. Res., **87**, pp. 6219–6236 (1982).

[8] M. Ashour-Abdalla and S. W. H. Cowley, Wave-particle interactions near the geostationary orbit, in *Magnetospheric Physics*, B. M. McCormac ed., pp. 241–270 (D. Reidel, Hingham, MA, 1974).

[9] D. G. Sibeck, R. W. McEntire, A. T. Y. Lui, R. E. Lopez, and S. M. Krimigis, Magnetic field drift shell splitting: cause of unusual dayside particle pitch angle distributions during storms and substorms, J. Geophys. Res., **92**, pp. 13,485–13,497 (1987).

[10] D. T. Young, S. Perraut, A. Roux, C. de Villedary, R. Gendrin, A. Korth, G. Kremser, and D. Jones, Wave-particle interactions near Ω_{He} observed on GEOS 1 and 2 1. propagation of ion cyclotron waves in He^+-rich plasma, J. Geophys. Res., **86**, pp. 6755–6772 (1981).

[11] A. Roux, S. Perraut, J. L Rauch, C. de Villedary, G. Kremser, A. Korth, and D. T. Young, Wave-particle interactions near Ω_{He} observed on GEOS 1 and 2 2. generation of ion cyclotron waves and heating of He^+ ions, J. Geophys. Res., **87**, pp. 8174–8190 (1982).

[12] T. Oscarsson and Mats André, Waves with frequencies below the proton gyrofrequency in a multicomponent plasma, Annales Geophysicae, **4**, pp. 319–326 (1986).

[13] J. L. Rauch and A. Roux, Ray tracing of ULF waves in a multicomponent magnetospheric plasma: consequences for the generation mechanism of ion cyclotron waves, J. Geophys. Res., **87**, pp. 8191–8198 (1982).

[14] S. Perraut, R. Gendrin, A. Roux, and C. de Villedary, Ion cyclotron waves: direct comparison between ground-based measurements and observations in the source region, J. Geophys. Res., **89**, pp. 195–202 (1984).

[15] K. Rönnmark, "WHAMP—waves in homogeneous, anisotropic multicomponent plasmas," Rep 179, Kiruna Geophys. Inst., Umeå, Sweden (1982).

[16] K. Rönnmark, Computation of the dielectric tensor of a Maxwellian plasma, Plasma Phys., **25**, pp. 699–701 (1983).

[17] T. E. Moore, D. L. Gallagher, J. L. Horwitz, and R. H. Comfort, MHD wave breaking in the outer plasmasphere, Geophys. Res. Lett., pp. 1007–1010 (1987).

[18] D. A. Gurnett, S. D. Shawhan, N. M. Brice, and R. L. Smith, Ion cyclotron whistlers, J. Geophys. Res., **70**, pp. 1665–1688 (1965).

[19] T. H. Stix, *The Theory of Plasma Waves* (McGraw-Hill, New York, 1962), § 2.5.

[20] K. G. Budden, *The Propagation of Radio Waves* (Cambridge University Press, 1985), 669 pp., §§ 19.5,19.6.

[21] Setsuo Ichimaru, Theory of plasma heating by fluctuating electric fields—effects of correlation times, J. Phys. Soc. Japan, **39**, pp. 1373–1377 (1975).

[22] Rickard Lundin and Bengt Hultqvist, Ionospheric plasma escape by high-altitude electric fields: magnetic moment "pumping", J. Geophys. Res., **94**, pp. 6665–6680 (1989).

5. 3D MODEL OF DOUBLE LAYER FORMATION ON AURORAL FIELD LINES

David Tetreault
Massachusetts Institute of Technology Cambridge, MA 02139

ABSTRACT

The one dimensional, nonlinear ion hole model of double layer formation on auroral field lines is modified to include three dimensional effects. In this expanded model, the hole potential drives electrostatic ion cyclotron waves in the background plasma, much as in a discrete particle model. The field aligned dynamics (trapping) which result in hole/double layer formation are retained as in the one dimensional model. The three dimensional hole/double layer structure has parallel and perpendicular scale lengths in agreement with Viking satellite data.

I. INTRODUCTION

Nonlinear ion hole/clump instability [1, 2] has been proposed as the cause of double layers observed in the auroral particle acceleration region [3]. An ion hole is a localized depletion in the ion phase space density. Because of the neutralizing charge density of the plasma electrons, ions become trapped in the hole's negative potential. Such a self-trapped, virialized phase space structure is a BGK mode.

A novel feature of the instability is that the holes can form and grow in linearly stable plasma where (for example), for weak currents and $T_e \approx T_i$, ion acoustic waves can not grow. An ion hole grows as electrons are resonantly reflected by the ion hole's negative potential. In a drifting plasma, the electron reflection gives the ion hole a double layer potential structure, and causes the hole to accelerate through the ion distribution function. As a result, the plasma, in its fully developed turbulent state, is composed of an intermittent distribution of colliding, growing hole fluctuations (clumps). Though the hole/clump model of Refs. [1–3] is one dimensional, its predictions agree well with double layer observations from the S3-3 and Viking satellites. This agreement results from the fact that, in a strongly magnetized plasma, the magnetic field restricts the particle trapping to one dimension (the component of velocity along the magnetic field).

However, the satellite data indicates that the double layers have three dimensional structure, the perpendicular scale of the double layer being somewhat larger than the field aligned dimension [4–7] In addition, the data reveals the presense of electrostatic ion cyclotron (EIC) waves. We show here how the model of Ref. [3] can be extended to three dimensions. A fully 3D model of double layer formation in a magnetic field requires a fully nonlinear

treatment of hole dynamics in three dimensions. As in the nonlinear hole dynamics in 1D, a fully three dimensional hole model requires an extensive investigation of hole dynamics from first principles. The resulting model becomes significantly more complex than in the 1D case. For example, in three dimensional geometry with a magnetic field, it is possible for groups ("clumps") of ions to become correlated along their gyro orbits. Each such clump of ions ("gyro-clump") will gyrate ballistically around a magnetic field line. Conceptually, we would expect such nonlinearly enhanced particle correlations to effect the perpendicular scale of the holes. In addition, ion cyclotron wave emmision would be nonlinearly enhanced. The mathematical evaluation of these collective, nonlinear effects from the gyro-kinetic Vlasov equation is formidable.

Here, we present a more modest, but certainly not trivial, extension of the 1D model. In this, the 1D dynamics of ion trapping along the field lines is fully nonlinear. However, the perpendicular dynamics is treated linearly. We show that the essential hole dynamics of Ref. [3] carry over to the 3D case, but with the hole linear dielectric function generalized to the appropriate 3D analogue. The model allows for the existence of both parallel ion (velocity space) trapping along the field lines (ion hole formation as in Refs. [1–3]) and ion cyclotron motion perpendicular to the field lines (3D double layer structure as well as the generation of EIC waves). In this way, we show that the double layers and EIC waves can be integrated naturally into the same nonlinear model. The model demonstates that hole/clump fluctuations are nonlinearly unstable to growth in a 3D plasma with strong magnetic field. Specifically, we find that the double layers can be the source for EIC waves, much as in the Cerenkov emission of waves by discrete particles. Of course, as we have just noted above, the nonlinear formation of gyro-clumps will enhance this Cerenkov emission. However, preliminary investigation shows that these enhancements appear to make quantatative (of order unity) rather than qualitative changes in the model we present here.

II. THREE DIMENSIONAL MODEL

We invoke the disparity between the ion dynamics parallel and perpendicular to the magnetic field. The characteristic time for the parallel ion motion is the trapping time ($\Delta x_\parallel/\Delta v_i$) of an ion that is trapped in the negative potential (ϕ) of an ion phase space hole. The ion gyro frequency (Ω_i) characterizes the ion perpendicular dynamics. We note that

$$\frac{\Delta v_i/\Delta x_\parallel}{\Omega_i} \sim \left[\frac{\Delta v_i}{v_i}\right]\left[\frac{\rho_i}{\Delta x_\parallel}\right] \sim \left[\frac{e\phi}{T_e}\right]^{1/2}\left[\frac{\rho_i}{\Delta x_\parallel}\right] < 1 , \qquad (1)$$

where v_i and ρ_i are the ion thermal velocity and gyro radius, and we have assumed that $T_e = T_i$. With this disparity in time scales, the Vlasov equation

splits up into a response, $\delta f_{\parallel}^{i}$, for parallel ion motion, and a response, $\delta f_{\perp}^{i}$, for perpendicular ion motion. The ion hole can thus be thought of forming in a background plasma of gyrating ions.

Assuming that the perpendicular ion dynamics are linear, the Fourier transform of $\delta f_{\perp}^{i}$ is given by the usual linear response,

$$\delta f_{\perp}^{i}(\mathbf{k},\omega) = \frac{1}{4\pi e}\frac{\omega_{pi}^{2}k_{\perp}^{2}}{\omega^{2}-\Omega_{i}^{2}} f_{0i}\,\phi(\mathbf{k},\omega) \,. \tag{2}$$

Poission's equation is

$$\frac{1}{4\pi e}\nabla^{2}\phi = \int dv_{\parallel}\frac{e}{T} f_{0i}\,\phi - \int dv_{\parallel}\delta f_{\parallel}^{i} - \int dv_{\perp}\delta f_{\perp}^{i} \,, \tag{3}$$

where the first term on the RHS is the electron response. With (2), the Fourier transform of (3) can be written as

$$\phi(\mathbf{k},\omega) = \frac{\tilde{\phi}(\mathbf{k},\omega)}{\varepsilon(\mathbf{k},\omega)} \,, \tag{4}$$

where

$$\tilde{\phi}(\mathbf{k},\omega) = \frac{4\pi e}{k^{2}}\int dv_{\parallel}\delta f_{\parallel}^{i} \tag{5}$$

is the ion hole potential and, with $k^{2} = k_{\parallel}^{2}+k_{\perp}^{2}$,

$$\varepsilon(\mathbf{k},\omega) = 1 + \frac{1}{k^{2}\lambda_{D}^{2}} - \frac{1}{k^{2}}\frac{\omega_{pi}^{2}k_{\perp}^{2}}{\omega^{2}-\Omega_{i}^{2}} \tag{6}$$

is the linear dielectric function for EIC waves. Accordingly, (4) describes the shielding of the hole/double layer potential by the background plasma. The double layer potential can excite EIC waves in the background plasma, much as in a discrete particle model. The parallel (trapping) dynamics of the double layer is as described in Ref. [3], and enters the 3D model here via (5) in the numerator of (4). The perpendicular dynamics enters through the dielectric function in the denominator of (4). While the existence of EIC waves in the auroral acceleration region may also be do to other dynamical mechanisims than the Cerenkov emission model (4), the 3D model presented here shows that the hole/double layers can form and grow in a background plasma containing EIC waves.

The hole/double layers are described by the low frequency ($\omega \simeq k_{\parallel}\Delta v_{i} < \Omega_{i}$) portion of (4). For this frequency range, we revert back to perpendicular position and, using (5) and (6), write (4) as

$$\left[-(1 + \frac{\omega_{pi}^2}{\Omega_i^2})\frac{\partial^2}{\partial x_\perp^2} + k_\parallel^2 + \frac{1}{\lambda_D^2} \right] \phi(x_\perp, k_\parallel, \omega) \tag{7}$$
$$= 4\pi e \int dv_\parallel \delta f_\parallel^i (x_\perp, k_\parallel, \omega)$$

From (7), the ratio of perpendicular to parallel scale length for a 3D double layer fluctuation is

$$\left[\frac{\Delta x_\parallel}{\Delta x_\perp}\right]^2 \sim \frac{1+(k_\parallel \lambda_D)^{-2}}{1+(\rho_i/\lambda_D)^2} \tag{8}$$

This ratio is on the order of unity or less for typical parameters and is consistent with the satellite measurements [4-6].

REFERENCES

[1] T. Dupree, Growth of phase space holes, Phys. Fluids, **26**, p. 2460 (1983).

[2] D. Tetreault, Growth rate of the clump instability, Phys. Fluids, **26**, p. 3247 (1983).

[3] D. Tetreault, Growing ion holes as the cause of auroral double layers, Geophysical Research Letters, **15**, p. 164 (1988).

[4] M. Temerin, K. Cerny, W. Lotko, and F. S. Mozer, Observations of double layers and solitary waves in auroral plasma, Phys. Rev. Lett., **48**, p. 1175 (1982).

[5] R. Bostrom, G. Gustafsson, B. Holback, G. Holmgren, H. E. J. Koskinen, and P. Kintner, Characteristics of solitary waves and weak double layers in the magnetospheric plasma, Phys. Rev. Lett., **61**, p. 82 (1988).

[6] H. E. J. Koskinen, R. Bostrom, and B. Holback, Viking observations of solitary waves and weak double layers on auroral field lines, in *Physics of Space Plasmas (1987), SPI Conference Proceedings and Reprint Series, Number 7*, T. Chang, G. B. Crew, and J. R. Jasperse, eds., p. 147 (Scientific Publishers, Cambridge, Mass., 1987).

[7] R. Boström, B. Holback, G. Holmgren, and H. E. J. Koskinen, Solitary structures in the magnetospheric plasma observed by Viking, Physica Scripta, **39**, pp. 782–786 (1989).

6. LIST OF SCIENTIFIC PUBLICATIONS

1. "Nonlocal Analysis of Finite Beam-Driven Instabilities", C.T. Dum and Y. Serizawa, Phys. Fluids, 1991, to be published.

2. "Wave Observations and Their Relation to "Nonresonant" Ion Heating in a "Weakly Turbulent" Plasma Model", J. Johnson, L. Ball and M. Andre, Annales Physicae, 1991, to be published.

3. "Critical Points in the 16-Moment Approximation", F. Yasseen and J.M. Retterer, J. Geophys. Res., 96, 1827, 1991.

4. "Theory of Electric Fields in the Auroral Acceleration Region", D. Tetreault, J. Geophys. Res., 96, 3549, 1991.

5. "Ion Cyclotron Resonance Heated Conics: Theory and Observations," G.B. Crew, T. Chang, J.M. Retterer, W.K. Peterson, D.A. Gurnett and R.L. Huff, J. Geophys. Res., 94, 3959, 1990.

6. "Particle Acceleration by Electromagnetic Ion Cyclotron Turbulence", G.B. Crew and T. Chang, Physics of Space Plasmas, 9, 31, 1990.

7. "Particle Acceleration by Intense Auroral VLF Turbulence", J.M. Retterer, T. Chang and J.R. Jasperse, 9, 119, 1990.

8. "Turbulent Relaxation in Magnetohydrodynamic Plasma", D. Tetreault, Phys. Fluids B, 2, 53, 1990.

9. "Heating of Thermal Ions Near the Equatorward Boundary of the Mid-Altitude Polar Cleft", W.K. Peterson, M. Andre, G.B. Crew, A.M. Persoon, M.J. Engebretson, C.J. Pollock and M. Temerin, Electromagnetic Coupling in the Polar Clefts and Caps, NATO ASI Series C: Mathematical and Physical Sciences, P.E. Sandhold and A. Egeland, eds., Kluwer Academic Publishers, 278, 103, 1989.

10. "Equatorially Generrated ULF Waves as a Source for the Turbulence Associated with Ion Conics", J. Johnson, T. Chang, G.B. Crew, M. Andre, Geophys. Res. Lett., 16, 1469, 1989.

11. "Monte-Carlo Modeling of Polar Wind Eleectron Distributions with Anomalous Heat Flux", F. Yasseen, J.M. Retterer, T. Chang and J.D. Winningham, Geophys. Res. Lett., 16, 1023, 1989.

12. "Ion Conics and Counterstreaming Electrons Generated by Lower Hybrid Waves in Earth's Magnetosphere", T. Chang, G.B. Crew, J.M. Retterer and J.R. Jasperse, IEEE Transactions on Plasma Science, 17, 186, 1989.

13. "Electromagnetic Tornadoes in Earth's Ionosphere and Magnetosphere", T. Chang, G.B. Crew and J.M. Retterer, Eringen Symposium Volume, Recent Advances in Engineering Science, Springer-Verlag, 39, 12 1989.

14. "Lower Hybrid Wave Generation in an Electron Beam of Finite Transverse Dimension", G.B. Crew, J. Plasma Phys., 41, 119, 1989.

15. "Exact Dielectric Tensor for Relativistic Magnetized Anisotropic Plasma", P. Yoon and T. Chang, J. Plasma Phys., 42, 193, 1989.

16. "Path Integral Formulation of Ion Heating", G.B. Crew and T. Chang, Phys. Fluids, 31, 3425, 1988.

17. "Electromagnetic Tornadoes in Space: Ion Conics along Auroral Field Lines Generated by Lower Hybrid Waves and Electromagnetic Turbulence in the Ion Cyclotron Range of Frequencies", T. Chang, G.B. Crew and J.M. Retterer, Computer Phys. Comm., 49, 61, 1988.

18. "Growing Ion Holes as the Cause of Auroral Double Layers", D. Tetreault, Geophys. Res. Lett., 15, 164, 1988.

19. "Kinetic Treatment of Oxygen Conic Formation in the Central Plasma Sheet by Broadband Waves", G.B. Crew and T. Chang, Modeling Magnetospheric Plasma, AGU Geophysical Monograph Series, 44, 159, 1988.

20. "Monte Carlo Modeling of Large-Scale Ion-Conic Generation", J.M. Retterer, T. Chang, G.B. Crew, J.R. Jasperse and J.D. Winningham, Modeling Magnetospheric Plasma, AGU Geophysical Monograph Series, 44, 185, 1988.

21. "Monte Carlo Modeling of Ionospheric Oxygen Acceleration by Cyclotron Resonance with Broad-Band Electromagnetic Turbulence", J.M. Retterer, T. Chang, G.B. Crew, J.R. Jasperse and J.D. Winningham, Phys. Rev. Lett., 59, 151, 1987.

22. "Lower Hybrid Ion Conics", G.B. Crew and T. Chang, Physics of Space Plasmas, 6, 55, 1987.

23. "Monte Carlo Modeling of Oxygen Ion Conic Acceleration by Cyclotron Resonance with Broadband Electromagnetic Turbulence", J.M. Retterer, T. Chang, G.B. Crew, J.R. Jasperse and J.D. Winningham, Physics of Space Plasmas, 6, 97, 1987.

24. "Simulation of Oxygen Conic Formation", G.B. Crew, T. Chang, J.M. Retterer and J.R. Jasperse, ISS-3, Part 2, 22, 1987.

25. "Two-D Simulation and Theory of Ion and Electron Acceleration by VLF Turbulence in the Suprauroral Region", J.M. Retterer, T. Chang and J.R. Jasperse, ISSS-3, Part 2, 22, 1987.

26. "Ion Acceleration by Lower Hybrid Waves in the Suprauroral Region", J.M. Retterer, T. Chang and J.R. Jasperse, J. Geophys. Res. 91, 1609, 1986.

27. "Transverse Acceleration of Oxygen Ions by Electromagnetic Ion Cyclotron Resonance with Broad Band Left-Hand Polarized Waves", J.M. Retterer, T. Chang, G.B. Crew, N. Hershkowitz, J.R. Jasperse and J.D. Winningham, Geophys. Res. Lett., 13, 636, 1986.

28. "Analytic Ion Conic in the Magnetosphere", Ion Acceleration in the Magnetosphere and Ionosphere, G.B. Crew, T. Chang, J.M. Retterer and J.R. Jasperse, AGU Geophysical Monograph Series, 38, 286, 1986.

29. "Plasma Simulation of Ion Acceleration by Lower Hybrid Waves in the Suprauroral Region", J.M. Retterer, T. Chang and J.R. Jasperse, Ion Acceleration in the Magnetosphere and Ionosphere, AGU Geophysical Monograph Series, 38, 282, 1986.

30. "Parametric Processes of Lower Hybrid Waves in Multicomponent Auroral Plasmas", H.E.J. Koskinen, Ion Acceleration in the Magnetosphere and Ionosphere, AGU Geophysical Monograph Series, 38, 291, 1986.

7. PUBLISHED BOOKS OF CONFERENCE PROCEEDINGS

1. "Physics of Space Plasmas (1990): Magnetic Fluctuations, Diffusion and Transport", SPI Conference Proceedings and Reprint Series, Vol. 10, T. Chang, G.B. Crew and J.R. Jasperse, eds., Scientific Publishers, Inc., Cambridge, MA, 1991.

2. "Physics of Space Plasma (1989): Wave-Particle Interaction Phenomena in Geoplasmas", SPI Conference Proceedings and Reprint Series, Vol. 9, T. Chang, G.B. Crew and J.R. Jasperse, eds., Scientific Publishers, Inc., Cambridge, MA, 1990.

3. "Physics of Space Plasmas (1988): Polar Cap Dynamics and High-Latitude Ionospheric Turbulence", SPI Conference Proceedings and Reprint Series Vol. 8, T. Chang, G.B. Crew and J.R. Jasperse, eds., Scientific Publishers, Inc., Cambridge, MA, 1989.

4. "Physics of Space Plasmas (1987): Ionosphere-Magnetosphere-Solar Wind Coupling Processes", SPI Conference Proceedings and Reprint Series, Vol. 7, T. Chang, G.B. Crew and J.R. Jasperse, eds., Scientific Publishers, Inc., Cambridge, MA, 1987.

5. "Physics of Space Plasmas (1985-87)" SPI Conference Proceedings and Reprint Series, Vol. 6, T. Chang, J. Belcher, J.R. Jasperse and G.B. Crew, eds., Scientific Publishers, Inc., Cambridge, MA, 1986.

6. "Ion Acceleration in the Magnetosphere and Ionosphere", AGU Geophysical Monograph Series, Vol. 38, T. Chang, M.K. Hudson, J.R. Jasperse, R.G. Johnson, P.M. Kintner, M. Schulz and G.B. Crew, eds., American Geophysical Union. Washington, D.C., 1986.